



HAL
open science

Automation and integration of a bioreactor for continuous cell culture

Fabien Abeille

► **To cite this version:**

Fabien Abeille. Automation and integration of a bioreactor for continuous cell culture. Biotechnology. Université de Grenoble, 2014. English. NNT : 2014GRENS036 . tel-01556082

HAL Id: tel-01556082

<https://theses.hal.science/tel-01556082>

Submitted on 4 Jul 2017

HAL is a multi-disciplinary open access archive for the deposit and dissemination of scientific research documents, whether they are published or not. The documents may come from teaching and research institutions in France or abroad, or from public or private research centers.

L'archive ouverte pluridisciplinaire **HAL**, est destinée au dépôt et à la diffusion de documents scientifiques de niveau recherche, publiés ou non, émanant des établissements d'enseignement et de recherche français ou étrangers, des laboratoires publics ou privés.



IRTSV

UNIVERSITÉ
GRENOBLE
ALPES



THÈSE

Pour obtenir le grade de

DOCTEUR DE L'UNIVERSITÉ DE GRENOBLE

Spécialité : **Biotechnologie, instrumentation, signal et imagerie pour la biologie, la médecine et l'environnement (BIS)**

Arrêté ministériel : 7 août 2006

Présentée par

Fabien ABEILLE

Thèse dirigée par **Nathalie PICOLLET-D'HAHAN**
codirigée par **Vincent AGACHE**

préparée au sein du **CEA-LETI, Laboratoire Bio-Chip et bio-Packaging (LBCP)**
en collaboration avec **BGE, équipe Biomics, IRTSV, CEA**
dans **l'École Doctorale Ingénierie pour la Santé, la Cognition et l'Environnement (EDISCE)**

Automatisation et intégration d'un réacteur de culture cellulaire pour un fonctionnement en continu

Thèse soutenue publiquement le **25 Novembre 2014**
devant le jury composé de :

M. Eric LECLERC

Chercheur à l'Université de Technologie Compiègne (UTC), Président

Mme Elisabeth M. J. VERPOORTE

Professeur à l'Université de Groningen (RUG), Rapporteur

Mme Rosaria FERRIGNO

Professeur à l'Université Claude Bernard Lyon (UCBL), Rapporteur

M. Donald K. MARTIN

Professeur à l'Université Joseph Fourier (UJF), Examineur

M. Olivier THEODOLY

Chercheur à l'Université Aix-Marseille (AMU), Examineur

Mme Nathalie PICOLLET-D'HAHAN

Ingénieure-Chercheur au CEA, Directrice de thèse

M. Agache Vincent

Ingénieur-Chercheur au CEA-LETI, Co-encadrant

Table of contents

Remerciements	5
1 Introduction.....	7
1.1 Motivations	7
1.2 Context	8
1.3 Aim of the work.....	8
1.4 Cell culture.....	9
1.4.1 Cell models & applications	9
1.4.2 Standard cell culture.....	10
1.4.3 Industrial cell culture.....	17
1.4.4 Microfluidic systems for cell culture	27
1.5 Conclusion	41
2 Thesis objectives.....	43
3 Microbioreactor design and fabrication.....	45
3.1 Microbioreactor overview.....	45
3.2 Cartridge design.....	46
3.3 Perfusion integration.....	47
3.3.1 Perfusion strategy	47
3.3.2 Type of membrane	49
3.3.3 Bonding.....	50
3.3.4 Glue biocompatibility	55
3.3.5 Leakage tests	57
3.3.6 Optical considerations/cell visualization enhancement.....	58
3.3.7 Conclusions.....	59
4 Cell proliferation.....	60
4.1 Control and monitoring of the cell environment	60
4.1.1 Porous-membrane-based perfusion	60
4.1.2 Thermal management	67
4.1.3 pH regulation.....	72
4.2 Microcarrier-based cell culture	77
4.2.1 Microcarrier preparation.....	77
4.2.2 Standard microcarrier cell culture.....	77

4.2.3	Bioreactor (microcarrier) cell culture	81
4.3	Conclusion.....	83
5	Cell harvest.....	85
5.1	The different strategies for cell harvest.....	85
5.2	Thermally-mediated cell harvest	88
5.2.1	Poly(N-isopropylacrylamide).....	88
5.2.2	Materials and methods	91
5.2.3	Physical characterization of PNIPAM-coated substrates.....	100
5.2.4	Biological characterization of PNIPAM-coated substrates	100
5.2.5	Discussion.....	104
5.2.6	Conclusion.....	108
5.3	Microcarrier dissolution.....	109
5.4	Bead-to-bead cell transfer for subculture	111
5.5	Conclusion.....	112
6	General conclusion.....	113
7	Perspectives and future work	115
	Appendix A.....	117
	Appendix B.....	118
	Appendix C	120
	Appendix D.....	121
	Appendix E	123
	Appendix F	125
	Appendix G.....	128
	Appendix H.....	131
	Appendix I	132
	Bibliography	133

Remerciements

Je tiens à remercier le CEA pour avoir financé cette thèse. Je remercie aussi le Département des micro-Technologies pour la Biologie et la Santé et son Service Bio-Systems on Chip, et l'Institut de Recherche en Technologies et Sciences pour le Vivant de m'avoir accueilli dans leurs laboratoires, d'avoir investi leur confiance en moi et de m'avoir soutenu matériellement et financièrement pour la réalisation de cette thèse.

Cette thèse n'aurait pas pu être aussi riche en résultats, développement professionnel et personnel sans un grand nombre de personnes des laboratoires LBCP, LBAM, LCM, Biomics, LISA, LIPhy et bien d'autres encore. Les rencontres et les collaborations ont été essentielles pour mes recherches ainsi que pour ma construction en tant que jeune chercheur. Elles ont aussi été sources de motivations et de créativité. Certaines d'entre elles ont même donné naissance à des amitiés, qui je l'espère dureront par la suite.

Je tiens vivement à remercier les différents chefs des laboratoires LBCP, LBAM, LCM et Biomics. Christine Louis et Béatrice Icard, chefs qui se sont succédées au LBCP, ont toujours prêté une oreille attentive à mes besoins. J'ai beaucoup apprécié l'intérêt de Béatrice pour ma thématique. Je suis reconnaissant envers Guillaume Delapierre, chef du LBAM, qui m'a généreusement permis de présenter mes travaux et d'échanger avec ses équipes. Je remercie également, Gilles Marchand, chef du LCM, qui m'a ouvert les portes de son laboratoire et m'a donné de précieux contacts pour résoudre certains des problèmes techniques que j'ai pu rencontrer. Xavier Gidrol, chef du laboratoire Biomics, a toujours su être présent pour donner une opinion utile à l'avancée de cette thèse.

J'exprime une profonde gratitude envers tous les ingénieurs-chercheurs du CEA qui m'ont apporté de nombreux conseils scientifiques, leur aide et leur soutien pendant ces 3 ans de thèse. Je remercie tout particulièrement Fabrice Navarro, Florence Rivera, Guillaume Nonglaton, Pascal Maillet, Cédric Goyer, Jean Bertier, Jean-Maxime Roux, Nicolas Verplanck, Anthony Corfa, Cédric Allier, Ruth Griffin-Shea, François Baleras, Frédéric Bottausci, Cédric Poulain, Antoine Hoang, Tarek Fathallah, Eric Sulpice, Vincent Haguët, Amandine Pitaval, Danielle Gulino et Yoann Roupioz.

Je remercie mon collaborateur du LIPhy, Lionel Bureau, qui a généreusement accepté de travailler avec moi et qui a pris du temps pour me transmettre son savoir et ses techniques.

De nombreuses réalisations et la maîtrise de plusieurs techniques n'auraient été possibles sans les techniciens des différents laboratoires. Je les remercie pour le temps, la patience et la conciliation dont ils ont su faire preuve à mon égard. J'ai une pensée particulière pour Mathilde Menneteau, François Boizot, Manuel Alessio, Martine Cochet, Marie Escude, Frédérique Kermarrec, Nadine David, Patricia Obeid, Sophie Gerbaud, Frédérique Mittler, Guillaume Costa, Thomas Bordy et Jean-Guillaume Coutard.

Je remercie les post-doc et thésards que j'ai pu rencontrer lors de mon séjour au CEA. Ils ont été sources de réconfort, de joies et autres bons moments passés ensemble. Merci à Monika Dolega, Guillaume Laffite, Jonathan Bruniaux, Thomas Courant, David Lefebvre, Emilie Bisceglia, Prisca Dalle, Rapahél Renaudot, Pierre-Henri Cazorla, Jessica Morlieras, Srikanth Vinjimore Kesavan, Frédéric Fantoni, Marjorie Vrignaud, Johannes Theisen, Claire Authesserre, Lisa Racine, Alan Hibbitts, Aurélie Jacquart, Anthony Daures.

Je voudrais chaleureusement remercier mes encadrants de thèse avec qui j'ai beaucoup appris de leur personnalité et de leurs méthodes. Ils ont su tirer le meilleur de moi-même. Grâce à Patrick Pouteau j'ai pu développer mon autonomie, mon assurance et mes capacités de communication. Je suis profondément reconnaissant envers Vincent Agache d'avoir accepté l'encadrement de ma thèse suite au départ de Patrick Pouteau. Un grand merci à Nathalie Picollet-D'ahan qui m'a guidé du début jusqu'à la fin. Nathalie et Vincent ont su être des encadrants particulièrement humains, attentifs, à l'écoute et source de motivation.

Je voudrais remercier les enseignant-chercheurs du Master Nanotech (PHELMA-INPG) pour la formation de qualité que j'ai pu recevoir et qui m'a conduit à faire cette thèse.

Je remercie aussi mes amis, ma famille et ma belle-famille pour leur soutien.

Pour finir, je remercie de tout mon cœur ma partenaire de vie, Zuza, pour sa patience et tous ces moments de bonheur qui permettent de surmonter les inquiétudes et le stress que peut donner une thèse. Je lui dédicace cette thèse.

1 Introduction

1.1 Motivations

Cell culture is a simple process used to produce cells and cell products. It requires many manual steps such as subculture (or reseeding), each two or three days associated with lots of manipulations, a periodic renewal of the culture medium and a control over the cell environment (temperature, humidity, CO₂/pH, O₂). These operations often lead to variability and contamination.

In order to improve the consistency of the cell culture process and to reduce the risks of contamination, bio-industries have developed automated cell culture systems. Automation of bioreactors has improved the productivity and the quality of cell lines. However industrial bio-production remains a cumbersome, lengthy and costly process. Microbioreactors are expected to provide solutions to ease, shorten and reduce the costs of some of the steps involved in bioprocessing. For instance, enhancement of the clone or strain selection step and the media optimization step will be possible by the capacity of automated microbioreactors to perform higher throughput tests and to better address the cell microenvironment compared to the use of standard flasks or well plates.

Another example concerns the scaling-up phase during bioprocessing. The previously selected clones or strains can behave differently with the increasing culture volume of the bioreactors. Therefore, there is a need to perform more reliable upscaling cultures using bioreactors that better reproduce the full-scale cultivation.

Expectations are also rising on the side of research which strives to develop culture models closer to the *in-vivo*. Indeed, conventional methods (e.g. 2D cell culture, spheroids culture, use of animal models) have become questionable either on an ethical point of view or because the cell behavior can significantly differ from the one in the human body. As mentioned, microbioreactors are able to provide controlled microenvironments that can be used to create more relevant culture models. Their parallelization can allow obtaining large amount of quantitative data.

Microscale culture systems appear as promising tools to solve many shortcomings for both industrial bio-production and research. Based on these considerations, a microbioreactor has been developed during this thesis.

1.2 Context

This thesis project was done in collaboration between two labs both part of the French Alternative Energies and Atomic Energy Commission (CEA): the Biomics lab, led by Ph. D. Xavier GIDROL and the BioChip and BioPackaging lab led by Ph. D. Béatrice ICARD.

The Biomics lab relies on micro-technologies, microfluidics, micromanufacturing and MEMS (MicroElectroMechanical Systems) to identify genetic and microenvironmental determinants that control the proliferation/differentiation balance and carcinogenesis using cell prostate cancer models.

The BioChip and BioPackaging lab designs, manufactures and packages components for microfluidic devices with chemical/biological reagents and for implanted and embedded medical devices (electrodes).

1.3 Aim of the work

The aim of this collaborative project was to:

- initiate, in the host laboratory, the development a microfluidic system to perform continuous cell culture of anchorage-dependent mammalian cells
- provide novel tools to automate and simplify the steps involved in cell culture
- control the culture conditions by the integration of means to monitor and regulate the cell environment
- study the culture of cellular models under conditions not yet described

1.4 Cell culture

This section intends to give a general description of the state of the art of cell culture at a laboratory and industrial level. Through this description, the limitations of the standard cultures are highlighted in order to introduce the advantages that microfluidic bioreactors could offer to address the remaining challenges.

1.4.1 Cell models & applications

Cell culture is defined as the process by which dispersed cells are grown under controlled conditions in order to produce cells or cell products[1]. It has been used since the ancient times by many civilizations for the production of alcoholic beverages, cheese, yogurt, etc., although they were not aware of it[2]. Such culture leading to fermentation involves yeasts and bacteria. The implication of these organism cultures was only discovered by Louis Pasteur in 1857[3]. Later, in the early 20th century, the tissue culture of plants and animal cells started to develop with their respective pioneer Gottlieb Haberlandt[4] and Granville Harrison[1]. Tissue culture consists in the study of non-disaggregated cells from a tissue fragment. Coming from this type of culture, cell culture soon appeared when cells could be disaggregated cells from tissues with the use of a proteolytic enzyme, called trypsin[5]. This major discovery was one of the many that contributes in popularizing cell culture. The other main breakthroughs were the development of the first continuous cell line (HeLa)[6] which lead to the development of other cell lines and cell line banks, the introduction of antibiotics to preserve cell culture from microbial contamination and the development of chemically defined media to specifically support the growth of cell lines. Cell culture of various cell types can be achieved currently; however, the meaning of the words “cell culture” is often reduced to the culture of eukaryotes and more particularly to the culture of animal cells. The culture of bacteria, yeasts, fungi and protozoa is often referenced as “microbiological culture”, while the culture of cell plants is referenced as “tissue plant cell culture”. This classification of the different types of cell culture is not related to the conventional classifications of cells[7] but, seems instead, coming from the different fields of microbiology, botany and sciences related to medicine, existing in the late 19th before cell culture emerged. The applications of cell culture are numerous and diverse and are summarized in Figure 1.

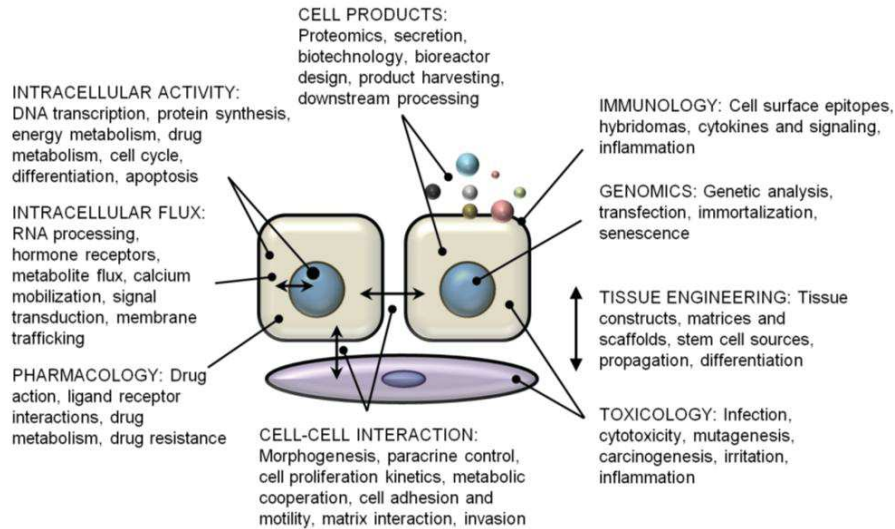


Figure 1. Cell culture applications. Reprinted from[1].

1.4.2 Standard cell culture

1.4.2.1 The cell culture process

The following description of the cell culture process stands for any type of cells. The process of cell culture can be divided into 3 consecutive steps: seeding, proliferation and subculture. These phases are synchronized according to the growth kinetics of the cell type being cultured (Figure 2). To initiate a culture, a small population of cells is placed in a controlled environment: this is the seeding step. The cells comes usually from the cell bank (from the laboratory or an external one: ATCC for the U.S.A, ECACC for Europe...) or from a donor tissue. Then, follows the step of proliferation: the cell population remains stable the time to adapt to their new environment[8] (lag phase) and then starts to increase as the cells divide (exponential phase). If there is no human intervention, the cell growth rate eventually slows until becoming null. The plateau phase is either:

- The result of a lack of space available for the cells to keep on dividing. Indeed, in cell culture two categories of cells exist: adhering cells which need a substrate to adhere to in order to divide, and floating cells which can be cultured in suspension. After multiple divisions, anchorage-dependent cells will occupy the entire available space forming a monolayer, this state is called confluence. At this point, cells usually lose their ability to divide due to contact inhibition[9].
- the consequence of the depletion of a nutrient
- due to the accumulation of cell wastes.

Generally, the plateau phase is preferably avoided since it can later alter the cell phenotype[10], lower their growth rate and initiate cell death. Moreover, cell populations in the exponential

phase are more consistent and uniform, which is important to obtain reproducible cell culture tests. The subculture step, also often referred as “passage”, is required before reaching this phase. During this step, cells are harvested and a fraction of them are seeded in a new controlled environment to propagate and divide again. The remaining cells are either used for experiments or simply discarded.

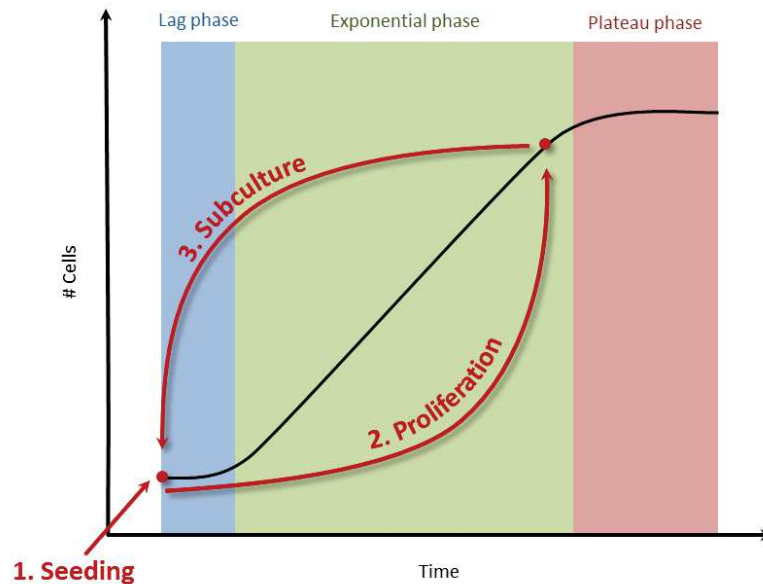


Figure 2. Cell growth kinetics driving the cell culture process. Cell culture is initiated by seeding a small number of cells in a new environment. The cells first adapt to their environment (lag phase), then they proliferate (exponential phase) and their number increases. Eventually, before reaching a critical number of cells, after which cells will not proliferate properly and die (plateau phase), subculture is performed. A part of the cells will be used for experiments while others will be used to perform another seeding and starts a new cell culture cycle.

All cells are characterized by a sigmoidal growth curve. However, each cell type exhibits specific growth kinetics. The exponential phase, the major phase of the growth kinetics, is related to the speed with which cells can divide, in other words their doubling time (time needed to increase the cell number twofold in the exponential phase). The doubling time corresponds to the cell cycle duration which is specific to a cell line or strain. For instance, bacteria have a doubling time, or cell cycle duration, of about 1 h[11] while mammalian cells have a doubling time of about 24 h[12]. The environmental conditions in which cells are cultured can vary this cell cycle duration and even block it[13]. Therefore, optimal growth requires optimal culture conditions.

1.4.2.2 Cell culture duration

There are many ways to classify cells in cell culture. Of these, only two will be described for the purpose of a general understanding. One, already mentioned, classifies cells according to their dependence to adhere or not to a substrate in order to proliferate: anchorage-dependent cells are called adhering cells and anchorage-independent cells are called floating cells.

The other classification separates cells into two groups:

- Finite cell line, which refers to a uniform population of cells that has been obtained after the subculture of primary cells (i.e. cells taken from a living tissue). These cells naturally die after a finite number of cell divisions due to senescence (i.e. naturally programmed cell death within cell genes)
- Continuous cell line, which corresponds to a cell line that has become immortal through *in vitro* transformation. Such a transformation can be spontaneous or physically, chemically or virally induced, and allows cells to escape senescence.

From these definitions, one can understand that the culture of continuous cell lines can be indefinite. However, the culture of continuous cell lines is commonly performed a finite number of passages. After many passages, continuous cell lines are likely to undergo selective pressures that may induce genotypic or phenotypic variations, impacting result reproducibility and consistency[14]. The limit of passages to consider before stopping the culture of a continuous cell line depends on the cell line itself and the phenotype that must be preserved[15]. As a rule of thumb, the American cell bank ATCC recommends not to use continuous cell lines after 5 consecutive passages. The limit of passages for the culture of an animal cell line before senescence also varies according to the cell type and specie[16,17]. In fact, any eukaryote cell will undergo senescence[18] as well as prokaryote cells[19]. However, prokaryote cell cultures are usually limited for the same reasons as for continuous cell lines[20].

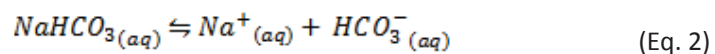
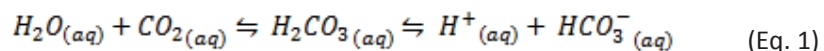
1.4.2.3 Laboratory cell culture: a practical example of mammalian cell culture

After detailing the general process of cell culture, it is interesting to have a practical insight into the culture performed routinely in research laboratories. The given example will describe how the culture of mammalian cells is performed since it will be the main concern in this thesis. However, the procedure remains analogous for any type of other cell culture except for a few minor variations.

To initiate a culture, cells stored in a frozen vial are thawed. Then, they are seeded in a specific liquid culture medium (Figure 3.A) in a Petri dish or a culture flask (Figure 3.B). This gas permeable container is then stored in an incubator. The medium and the incubator (Figure 3.C) ensure that adequate conditions are provided to promote cell proliferation, which includes:

- Nutrients: The media contains, among other components, the nutrients required for the cell metabolism needs (see Appendix A for an example of the complete formulation of a culture medium). The more complex is the organism metabolism to be cultured, the more nutrients types are needed, which is the case for mammalian cells that have high nutritional needs. Their culture requires the presence of:

- Amino acids, the basic materials for cells to synthesize proteins
- Vitamins, which assist biochemical transformation through enzymatic activity
- Glucose, which is a source of energy
- Inorganic ions, which play a role in cellular adhesion, cell signaling and the regulation of membrane potential and intracellular charges
- Metal traces are involved in the enzymatic activity of the cells
- Serum: serum is a complex mixture usually supplemented in the media. It is composed of hormones (regulating the uptake of glucose and amino acids), growth factors (having a beneficial impact on cell growth), proteins (acting as carriers for minerals, fatty acids and hormones) and other lipids, minerals and amino acids. The use of serum to supplement culture media is sometimes avoided as serum composition is variable and poorly defined from batch to batch, introducing potential cell culture results[21].
- Osmolality: Osmolality is mainly regulated by the salts, the glucose and the amino acids present in the media. Osmolalities between 260 mosmol/kg and 320 mosmol/kg are acceptable for mammalian cell culture. Higher or lower osmotic pressure will affect the cell membrane integrity and respectively induce the collapse or the explosion of the cells[22].
- Temperature: temperature is regulated by the incubator. The adequate cell culture temperature depends on the body temperature of the animal tissue (or the host for microbes). The target temperature is 37°C for most of the mammalian cells. Although mammalian cells can tolerate substantial drops in temperature, survive several days at 4°C, and be frozen to -196°C; they cannot endure more than about 2°C above normal for more than a few hours and will die quite rapidly at 40°C and over[23].
- pH: pH is regulated by the CO₂ level in the incubator atmosphere and the hydrogen carbonate ions contained in the media through acid-base equilibriums.



The bicarbonate salt balances the dissolution of CO₂ from the incubator atmosphere. The CO₂ partial pressure of the incubator is commonly regulated at 5% and the concentration in bicarbonate is adapted to provide a buffering capacity to the media between pH 7.0 and 7.4. Some cell types may be best cultured slightly outside this range, and cells surely differ widely in their ability to tolerate significant deviations from

this level. Slow changes in pH are better tolerated than rapid changes that lead to apoptotic cell death. Most cells will tolerate a medium pH in the range of 6.5 to 7.8, but media much outside this range can degrade cell viability[22]. The buffer also compensates to some extent for any change in pH that would be induced by the wastes that cell produce such as lactic acid, CO₂ or ammonia.

- Oxygen: more precisely dioxygen is needed for the respiratory system of the cells, even though some cells can be cultured in anaerobic conditions (i.e. deprived of oxygen). Mammalian cells have an oxygen dependent metabolism. The level of oxygen can be regulated in the incubator with the addition of an inert gas, such as nitrogen. Usually for mammalian cell culture, the level of CO₂ in the incubator defines the level of oxygen. For 5% of CO₂, the incubator atmosphere contains 18% of O₂. However, the partial pressure of O₂ can also be actively regulated. The medium height is adapted to modulate the diffusion of dioxygen according to the cell need[22]. Cells having high O₂ requirement are cultured in shallow media while cell with low O₂ requirement are cultured in deep media.
- Antibiotics are often added to prevent the cultures from being contaminated by other microorganisms. The most common is to use a combination of penicillin and streptomycin.

All requirements for cell culture are cell line and cell type specific. They have to be adapted accordingly.



Figure 3. The different components and equipment used for cell culture. A) Non supplemented culture medium (left) and serum (right) for cell culture. B) Vented flasks filled with culture medium. C) Incubator containing cell culture flasks. D) Operator working under a safety cabinet for cell culture.

As cells proliferate, they consume some of the medium constituents and release wastes, such as lactic acid, ammonia and CO_2 , proportionally to their density. Without human intervention, cells will soon starve because of nutrient depletion and suffer from a drift of the pH due to the accumulation of cell wastes. Therefore, during proliferation, the medium is changed frequently (every 2 or 3 days for mammalian cells) depending on the cell metabolism and density.

Eventually, subculture is performed upon reaching a critical cell density. For adherent cells, cell harvest is achieved by enzymatic, chemical or mechanical action. The most common technique relies on the use of trypsin, a proteolytic enzyme that digests the cell membrane proteins involved in cellular adhesion. Floating cells are harvested simply by collection of the media in which they reside. A portion of the harvested cells are then placed in a new vessel containing medium and placed back into the incubator for proliferation. The remaining cells are used for experiments or are discarded.

The aforementioned steps of thawing, seeding, media change and subculture are all accomplished by an operator in a special outfit and under a laminar hood (Figure 3.D) to limit possible contaminations of the cells and the operator.

1.4.2.4 Manual laboratory cell culture limits

Cell culture is originally a manual laboratory practice extensively used in research that faces inherent challenges and limitations. As a manual technique, it is prone to human errors. Even if cell culture is performed by highly qualified operators with great care in order to preserve sterility, there is a non negligible risk for contamination due to repeated manipulations. Every cell culture laboratory has already experienced a microbial contamination.

Besides the frequent handling, media renewal and subculture expose cells to important environmental variations, such as thermal variations or dissolved species concentration variations. Indeed, cells need to be taken out of incubators for observation or to perform media exchange, exposing them to room temperature (20-25°C). Additional environmental variations may arise due to evaporation. Incubators are water vapor-saturated to limit media evaporation, but it still occurs. A reduction of the culture volume induces an increase in the concentration of salts and ions leading to osmolarity and pH drifts. All of these variations are not controlled in term of frequency and amplitude. It is established that they are likely to affect the cell phenotypes and to impact on the reproducibility of cell culture experiments[1,22].

Additionally, manual laboratory cell culture can hardly achieve mass production of cell or cell products. It also gives little and poor monitoring of the culture state (cell density, temperature, O₂, pH, glucose, lactate, ammonia...).

As a consequence of the highlighted drawbacks, some laboratories and industries have turned to automated cell culture systems. These systems provide better sterile environment and reduce human intervention. They are usually coupled to a large number of probes that can regularly monitor the diverse culture parameters. Therefore, they can maintain the cell environment more accurately. Automated systems render cell culture less labor intensive and time consuming with the possibility to produce large amounts of cells and cell products[24]. Different classes of culture-automated systems exist. Some solely intend to provide cells to scientist for their research while others, called bioreactors or fermentors, aim at producing biomass or bioproducts. The next section will rather concentrate on the latter systems.

1.4.3 Industrial cell culture

1.4.3.1 Applications

Industrial cell culture concerns mammalian, microbial (meaning bacteria, yeast, fungi and some algae) and plant cells. The application of these cultures is diverse. They play a major role in:

- The food and the beverage industry with the production of food additives, food preservatives, alcohols...
- The chemical industry with the production of biopolymers, solvents, biofuels...
- The pharmaceutical industry with the production of recombinant products such as monoclonal antibodies, drugs, vitamins, hormones

Table 1 gives a non-exhaustive list of product types synthesized by cells and used in the different industries.

Table 1. Specific use of cells in industries

Industry Cell culture	Pharmaceutical	Food & Beverages	Chemical	Agri-food	Ref.
Microbial	Monoclonal antibodies Hormones Vitamins Other drugs Other recombinant protein	Food additives Food conservative Alcohols Vitamins Foodstuffs	Biofuels Biopolymers Solvents Alcohols Acids		[25,26]
Mammalian	Monoclonal antibodies Hormones Vitamins Other Drugs Other recombinant protein				[27]
Plant	Monoclonal antibodies Vitamins Other drugs Other recombinant proteins Narcotics Stimulants Nutraceuticals	Food additives Flavors	Perfume Aromas	Insecticides	[28]

The main industry driving cell culture is the pharmaceutical industry[26] with global sales over US\$120 billion per year, within which the production of monoclonal antibodies production represents a fifth of the sales with a growing trend[29].

Microbial cell culture dominates industrial cell culture because these cells are less sensitive to culture conditions, have simpler needs to grow, grow rapidly and produce in high yield (3-fold more than mammalian cells[30]).

However, plant and mammalian cells possess a higher level of expression which makes them capable of producing valuable pharmaceutical products that microbial cell culture cannot

achieve[26,31]. Although mammalian cells have been for a long time the most desired expression system to produce human compatible products[32], plant cell cultures are gaining interest and may provide in the future a more economical way to produce such human-like products[33,34].

Cells themselves can be produced as the end-product. For instance, microbial cells are used in wastewater treatment. Another example is stem cells, which are expected to impact medicine, healthcare and clinical applications for drug testing, tissue and organ repair and human disease curability[35].

1.4.3.2 Bioreactor culture modes

For the production of bioproducts, industrial cell culture relies on large-scale bioreactors. Higher volumes of culture mean higher number of cells and therefore higher quantity of product. Industrial bioreactors can be run in different ways. Four main operating modes exist and are from the least to the most complex to operate as follows: batch and semi-continuous batch, fed-batch, continuous, perfusion (Figure 4).

- Batch: Any culture mode is initiated with a batch culture. Cells and medium are dispensed inside the bioreactor and the culture volume remains constant over time. During the culture the cell population follows a sigmoid curve as described earlier in Figure 2. The medium nutrients, byproducts and products concentrations vary in time. The stability or the accumulation kinetics of the targeted product inside the bioreactor drive the time of harvest.

A variant of the batch is the semi-continuous batch which consists in repeated batch culture. Between two consecutive batches, a portion of the culture is kept to serve as an inoculum and fresh medium is added. This method presents the advantage to reduce the time and cost associated with cleaning, sterilization and re-seeding of the bioreactor. Runs over several months have been reported for the production of a monoclonal antibody using mammalian cells[36].

- Fed-batch: fed-batch culture is a batch culture during which the culture volume is continuously or periodically increased in time. The starting volume represents about 10% of the final volume reached at the end of the culture[37]. During this process, cells, nutrients, products and byproducts vary in time. This strategy aims at feeding the appropriate nutrients in order to maximize growth and product formation and lower the formation of toxic products such as ammonia or lactate. Fed-batch feeding strategies imply a good understanding of the cell metabolism and the rate of utilization by the cells of the nutrients. Complex organisms such as mammalian cells require more complex

mechanistic models of cell growth to provide the adequate feeding[38]. Higher cell densities ($\sim 2 \cdot 10^7$ cells/mL) than in batch culture can be achieved as well as 10 to 50-fold higher titer (i.e. product concentration)[39].

- Continuous: In this mode there is constant flow in and out of the same amount of medium. Cell population, concentration of nutrients, product and byproduct remain constant during the culture. The feeding rate can be adjusted by controlling and measuring the biomass concentration; such bioreactors are called turbidostat. However, the most common type of continuous culture is the chemostat where the feeding of a limiting substrate regulates the biomass concentration. Other systems such as auxostats regulate the biomass concentration through a feedback loop based on the measurement of the pH, the dissolved oxygen tension or the product concentration (e.g. ethanol, sugar).
- Perfusion: As for continuous cultures, perfusion cultures are characterized by a constant supply and draw off of medium. Cells, nutrients, byproducts and products remain constant during the culture. The difference with the previous process is that cells are retained in the bioreactor. Perfusion process provides the highest volumetric productivities of all processes enhanced by about 10-fold compared to batch and fed-batch volumetric productions[40].

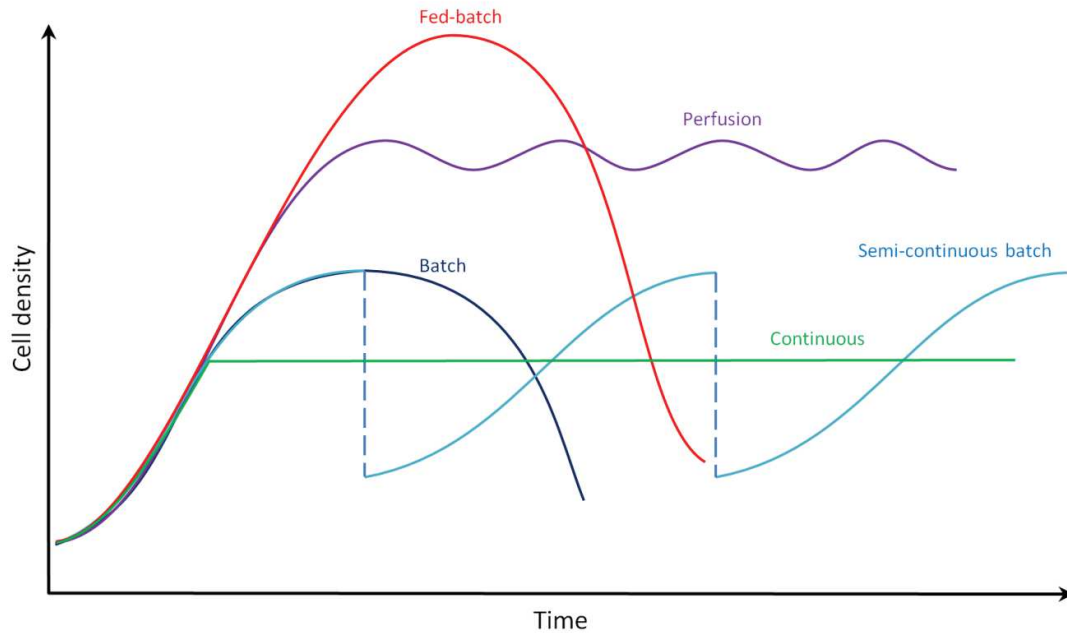


Figure 4. Evolution of cell density in time according to bioreactor culture modes. Adapted from[41]. Batch mode: fixed volume, no feeding. Fed-batch mode: gradual feeding until filling the entire bioreactor volume. Continuous mode: constant feeding, adjusted to keep a constant cell population. Semi-continuous mode: repetitive batch cultures operated from the same inoculum. Perfusion mode: continuous feeding, cells are retained in the bioreactor.

The choice of the culture mode depends on the experience of the companies, the type and the stability of the product to be produced and ultimately on process economics[25,37,39,42]. As mentioned, fed-batch, continuous and perfusion cultures are more complex and require a good understanding of the cell needs and metabolism as well as developed regulation systems based on complex mechanistic models. Microbial batch or fed-batch processes are preferred in the biopharmaceutical field since the producing organisms are highly mutated and tend to be replaced by fast growing and less effective producing organisms over long-term cultures. Besides, due to the low residence time in the bioreactor compared to batch and fed-batch, perfusion process offers advantages for the production of less stable products by improving their quality. To date, continuous processes have not been applied to the industrial culture of mammalian cells. Eventually, continuous and perfusion cultures requires smaller volume and less time to achieve comparable batch or fed-batch productivity but are more subjected to contamination and equipment failure.

1.4.3.3 Bioreactor designs

A wide diversity of bioreactors exists under different scales. For production, large-scale reactors are used and can reach up to 20,000 L[39]. Most of them can be operated in any of the modes described in the previous section and can cultivate any type of cells. The commercial systems

have been widely reviewed[39,43,44,45,46] and can be classified into five categories: stirred bioreactor, pneumatic bioreactor, fixed or fluidized bed bioreactor, dialysis bioreactor and shaken bioreactor. Among them, the stirred bioreactor, in the first place, and then the airlift bioreactor are the most common for production. This is principally due to the historical know-how acquired over the past decades and the ease with which these reactors can be scaled up[44]. A schematic representation of these bioreactors is given in Figure 5.

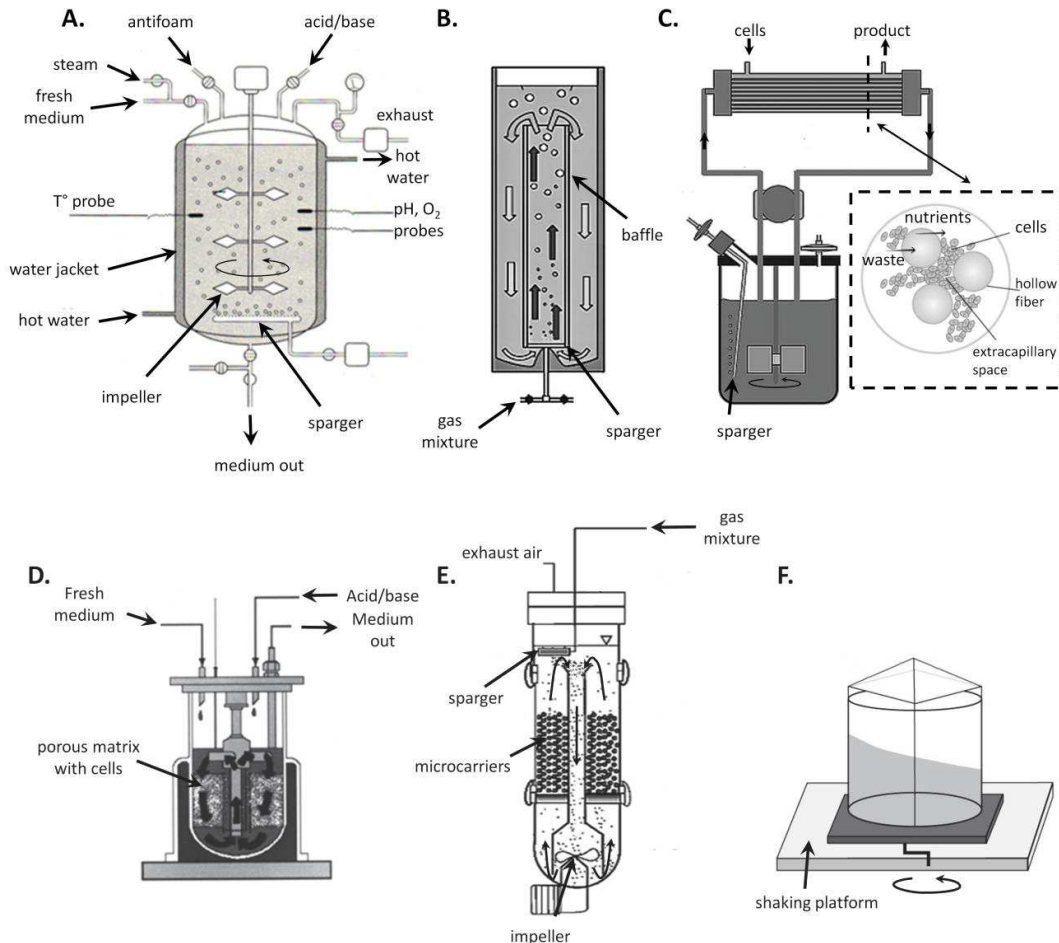


Figure 5. Schematic representation of bioreactors. A) Stirred bioreactor. B) Pneumatic bioreactor: airlift bioreactor[44]. C) Dialysis bioreactor: Hollow fiber bioreactor[44]. D) Fixed bed bioreactor. E) Fluidized bed bioreactor[44]. F) Shaken bioreactor: Orbital shaken bioreactor[47].

Despite the diversity of bioreactor designs, they all strive to provide the most homogeneous environment and fulfill the nutritional cell need in order to achieve robust and maximal cell growth and productivity in sterile conditions. Providing a homogeneous environment is a real challenge at large-scale. Indeed, large-volumes reactors require a mean by which mix the medium to maximize mass transport and avoid cell aggregation[35]. However, when medium is set in motion a shear stress is applied to the cells to which they may be sensitive, leading to their

death. Shear stress sensitivity depends on the type of microorganism: mammalian cells are extremely sensitive to shear stress, plants cells highly sensitive while microbial cells are poorly sensitive[48]. Strategies to provide good mixing with lower shear stress rely on impeller design and stirring rate optimization[49] (stirred bioreactor), shake rate optimization of the bioreactor[50] (shaken bioreactor), utilization of membranes (dialysis and fluidized bed bioreactor) or packing the cells in a porous matrix (fixed bed bioreactor)[44].

Bioreactor designs integrate engineered solutions to monitor and control the culture conditions as they impact on the process productivity and quality[44]. Figure 6 shows the influence of process operating strategies and parameters on the environmental conditions with their subsequent influence on process performance.

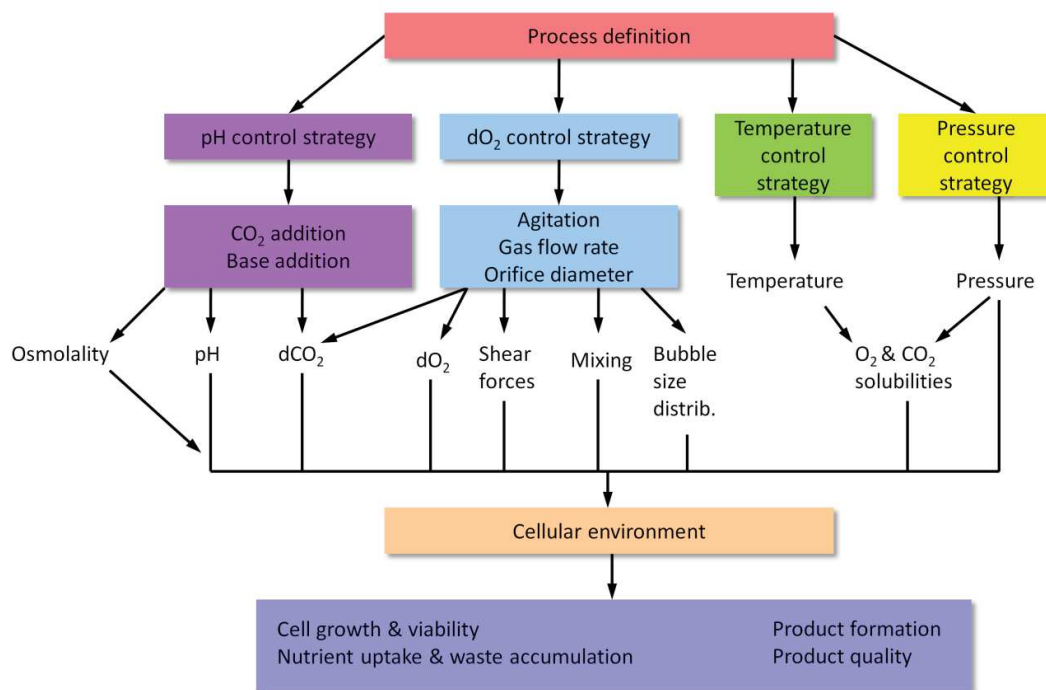


Figure 6. Diagram showing the influence of process operating strategy and parameters on process performance[51].

The maintenance of the cell environment (T° , pH, pO_2 , pCO_2 , osmolality, nutrient concentrations) is usually performed inside the culture vessel, except for dialysis bioreactors and some fixed bed bioreactor designs which externalize their regulation in another vessel. In the latter case, controlling the environment is more challenging[52]. Sensors are inserted inside the regulated vessel to monitor the different culture parameters and also obtain more information on the culture with respect to metabolite concentrations, cell density and cell viability... Common strategies are shared by bioreactors to regulate the cell environment. Temperature is regulated using a water jacket or a heating element around the bioreactor[53]. Regulation of the pH is usually performed by acid/base addition in combination with controlled CO_2 sparging or

aeration of the medium. Cells can be very sensitive to pH variation; variations as small as 0.1 pH can impact on productivity and cell growth and metabolism[54,55] and a variation of 0.4 pH has shown a 10-fold decrease in antibody productivity (from 500 mg/mL to 50 mg/mL)[30]. The addition of acid or base requires the medium to be well mixed in order to avoid local concentration of acid/base. Oxygen levels are regulated by O₂ sparging or aeration of the medium[56]. Sparging can also lead to cell death. It has been demonstrated that when bubbles burst they damage the surrounding cells[57]. Bubble size and sparging rate have to be optimized to limit this effect. A surfactant, such as pluronic F-68 can be added to limit the impact of bubble burst[44].

Bioreactors are usually made in glass and/or steel. However, since the last 15 years, industries and research labs have increasingly adopted the use of disposable bioreactors[58]. They are usually used for the propagation of cells, development of larger non-disposable bioreactor, the preparation of inoculum or production at the smaller scale[39]. Their volumes vary from mL to 1000 L. The first disposable bioreactor still largely used up to now is the wave bioreactor. The rocking motion it exploits enhances mass transport at the air-liquid interface and allows effective mixing[59]. The other common bioreactor is a disposable version of the stirred bioreactor. Disposable bioreactors are particularly attractive due to their low cost, flexibility and simplicity of operation. These advantages provide important cost savings as well as reduced validation and process lifetime[43,58].

1.4.3.4 Towards the unique format of suspension cell culture using floating cells or microcarriers

It has already been introduced that cells, most particularly animal cells, can depend on the presence of a solid substrate to proliferate. These cells are usually cultured on the vessel walls. However, this strategy is impractical for scale-up and to achieve high density cell cultures, and therefore, exhibits insufficient productivity compared to suspension cell culture. As a consequence, two predominant strategies have been introduced to allow cells to be cultivated in suspension[44]. One of these strategies is to adapt cell lines to be cultured in suspension. Such adaptation requires time (several subcultures) and practical experience[39]. However, some cell lines simply cannot be adapted to suspension culture or will not be productive enough when they are attached to a solid substrate[60]. The other strategy is to rely on microcarriers, usually in the shape of microbeads (Figure 7).

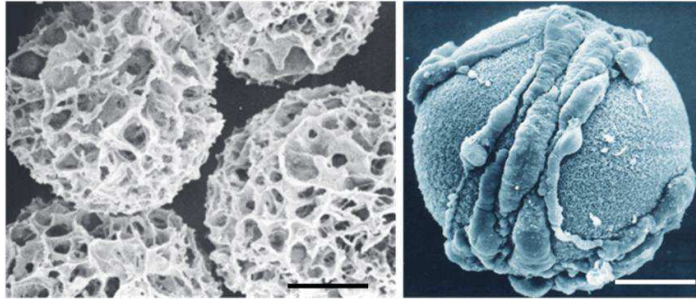


Figure 7. Scanning electron microscopic images[61]: Left: macroporous microcarriers (Cytopore) Right: cells growing on a solid-filled microcarrier (Cytodex). Scale bar is 50 μm .

Microcarriers have a density similar to the medium and therefore can easily be set in suspension with standard bioreactor agitation. The fact that microcarriers settle relatively quickly ($\sim 13\text{cm/min}$) is both an advantage and a drawback[44]. On the one hand, settlement eases media exchange during cell culture and facilitates cell retention in bioreactors. On the other hand, agitation has to be increased compared to suspension culture to avoid gradients in cell density. Using microcarrier also increases the cost of cultures. Table 2 summarizes the different commercial microcarriers available on the market. Microcarriers can be divided into solid-filled (sometimes referred to as microporous) and macroporous. With microporous carriers cells are cultured on their outer periphery while with macroporous carriers cells are allowed to grow inside them. Macroporous carriers can reach higher cell densities and are a means to protect cells from shear stress during culture[60]. However, they are more subjected to limited mass transport in their inner part when cell density is high[43,62]. Microcarriers exist in different materials such as dextran, plastic, gelatin, glass, collagen, silicone, and cellulose, and with different surface modification (charge, fibronectin, collagen)[44,63]. The selection of the appropriate carrier depends on the cell line and the purpose of the culture[64]. The most common microcarriers are the Cytodex for the microporous case and Cytopore and Cultisphere for macroporous case.

Table 2. Non-exhaustive list of commercial microcarriers and their characteristics.

Type	Name	Material	Surface modification	Diameter (µm)	Density (g/cm ³)	Ref.
Solid-filled	Cytodex 1	dextran	charged (N-diethylaminoethyl coated)	147–248	1.03	[44,60,63]
	Cytodex 3	dextran	collagen coated	141–211	1.04	[60,63]
	Hillex II	polystyrene	charged	160-200	1.12	[44,63]
	ProNectin	polystyrene	recombinant protein coated	125-212	1.03	
	Fact III	polystyrene	charged, collagen coated	125-212	1.03	
	Biosilon	polystyrene		160–300	1.05	[60]
	2D MicroHex	polystyrene		125x25 (hexagonal)	1.05	[44]
	Glass-coated	polystyrene	silica	125-212	1.03	[44]
Macroporous	Cellagen	collagen		100-400	NA	[63]
	Cytopore	cellulose		220-280	1.03	[44,63]
	Cytoline	polyethylene, silica		120-220	1.32	[44,63]
	CultiSpher	collagen		130-380	1.04	[44,63]

1.4.3.5 The need for enhanced scaled-down cultures

Despite the fact that higher productivity seems related to higher volume, much attention is being paid to small-scale culture systems particularly in pharmaceutical industry. To understand this point, one needs to understand the general process for bioproduction. The process is divided into 4 phases[51] (Figure 8):

- Cell line development: Cells are genetically transformed to create productive clones. Then they go through several consecutive selections, starting with a 100-1000 clones until only 1-2 remain. Clone selection is performed with screening studies based on the clone stability (for expression), cell growth specific productivity and volumetric productivity. After each selection, the volume of culture is increased from that of a 96-well plate (hundreds of µL) to that of a shake flask (a few mL) or a lab-scale bioreactor (hundreds of mL to a few L).

- Media and process optimization: different medium compositions are evaluated to support cell growth with low waste production, while at the same time achieving high titer of high quality. The same evaluation is performed with medium feeding and process parameters which impact on the process outcomes (see Figure 6). Medium and process optimizations are known to be labor-intensive and time-consuming. High-throughput cell culture scaled-down systems and statistical design of experimental approaches are commonly combined to shorten such optimizations.
- Pilot-scale culture: Scalability tests and production at the manufacturing scale are carried out for preliminary tests (e.g. toxicological test, pre-clinical tests).
- Commercialization: This step involves process characterization, scale-up, technology transfer, and validation of the manufacturing process. A deep understanding of the process parameters on the product quality is undertaken (process characterization). Tools, equipment, materials and information are transferred to a manufacturing facility (technology transfer) to conduct scale-up production. Production is validated when it passes regulation approvals.

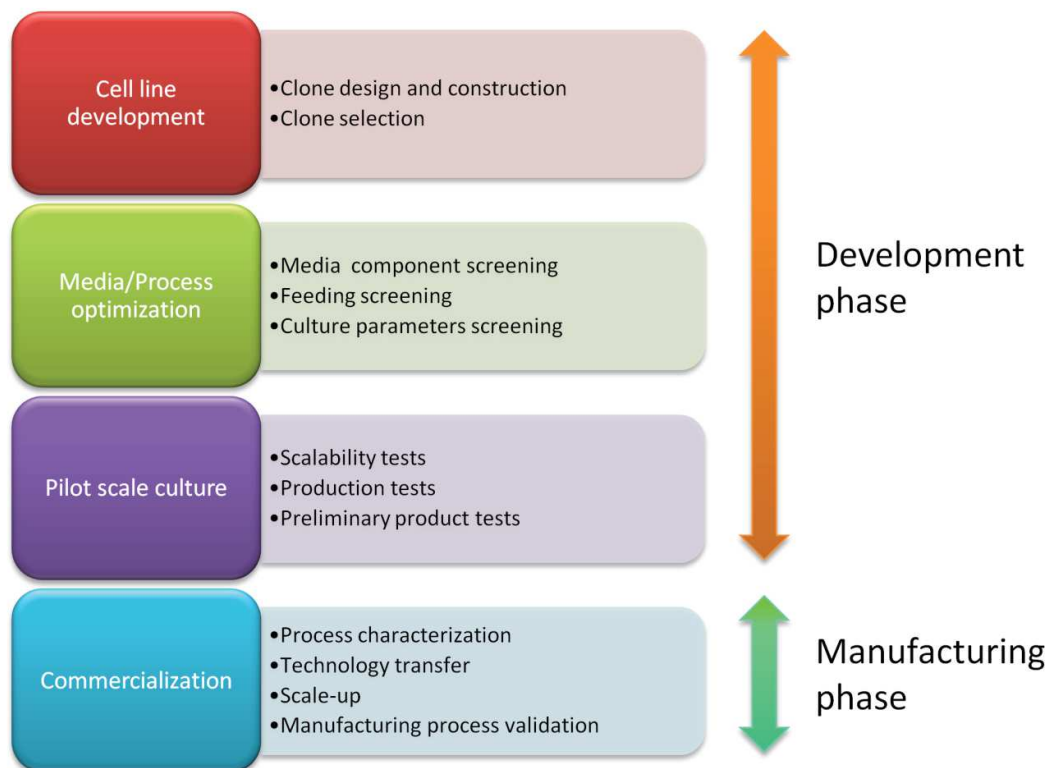


Figure 8. The 4 phases of a bioproduction process. A bioprocess is characterized by 3 successive development phases before reaching the ultimate manufacturing phase where a product is commercialized. These 3 development phases are: cell line development during which a clone is established and selected, the media/process optimization during which the best media and culture parameters (feeding, pH, T°, O₂ ...) are identified and the pilot scale culture where tests of scalability and of production are conducted.

The whole process is very long and associated with high costs. For instance, in the case of pharmaceutical product, it takes almost 10 years before reaching the market and the investment of about €0.6 billion[65]. Therefore, industries are struggling to optimize the development phase which ends where commercialization begins. Many studies agree that such optimization lies in the improvement of scaled-down bioreactors, which play a key role in the development phase[51,65,66,67,68,69]. More precisely, cell line development and media/process optimization would benefit from new miniaturized high throughput bioreactors to early collect bioprocess data, identify more rapidly the best production clone, medium formulation and culture conditions while consuming less materials (biological and reagents) in order to get the best productivity and quality at large-scale[51]. In order to successfully address the aforementioned points, it is of the utmost importance that miniaturized culture systems demonstrate a high degree of controllability over process parameters to mimic the large-scale bioreactor environment[66]. The complex impact of the culture conditions on the productivity, product quality and cell metabolic profiles justify this criterion. The current test tubes, microtiter plates and shake flasks, commonly used in process development, miss this important feature[67]. Scaled-down models are also involved in characterization and validation studies during commercialization since the availability of large-scale reactors is limited and their operation for such studies expensive[51]. Microfluidic cell culture systems appear as promising scaled-down bioreactors and some have already reached the market[65,67,68]. Academic research demonstrates a similar interest in these devices as they can allow studies beyond standard culture ware[70] (see section 1.4.2.4 on Manual laboratory cell culture limits). Microfluidics applied to cell culture is hereafter introduced.

1.4.4 Microfluidic systems for cell culture

1.4.4.1 Microfluidics

Microfluidics is the science and technology of systems that process or manipulate fluids at the sub-millimeter length scale[71]. At this scale, some physical phenomena which were negligible at the macroscale enter in competition with those commonly know at the microscale. To evaluate this competition according to the scale, dimensionless parameters expressing the ratio of these phenomena have been introduced[72]. The most famous is the Reynolds number. It characterizes the relative importance of inertial forces over viscous forces. In microfluidics, fluid velocity field obeys the Navier-Stokes equation:

$$\rho \left(\frac{\partial \mathbf{u}}{\partial t} + \mathbf{u} \cdot \nabla \mathbf{u} \right) = -\nabla p + \mu \nabla^2 \mathbf{u} + \mathbf{f} \quad (\text{Eq. 3})$$

where ρ is the fluid density, \mathbf{u} the fluid velocity field vector, p the pressure, t the time, μ the fluid dynamic viscosity and f body force densities.

The non-linear term $\rho \mathbf{u} \cdot \nabla \mathbf{u}$ is related to the inertial forces and the term $\mu \nabla^2 \mathbf{u}$ to the viscous force. Hence, the Reynolds number can be derived as:

$$Re = \frac{\rho \mathbf{u} \cdot \nabla \mathbf{u}}{\mu \nabla^2 \mathbf{u}} \sim \frac{\rho U_0^2 / d_H}{\mu U_0 / d_H^2} = \frac{\rho U_0 d_H}{\mu} \quad (\text{Eq. 4})$$

where U_0 is the mean fluid velocity and d_H the hydraulic diameter (or characteristic length). At high Re (≥ 2000) fluids are turbulent, they mix stochastically. Fluids at lower Re are conversely laminar; they usually exhibit a predictable parabolic profile. Microfluidic systems are almost always in the laminar regime since they are characterized by a low Re (Figure 9).

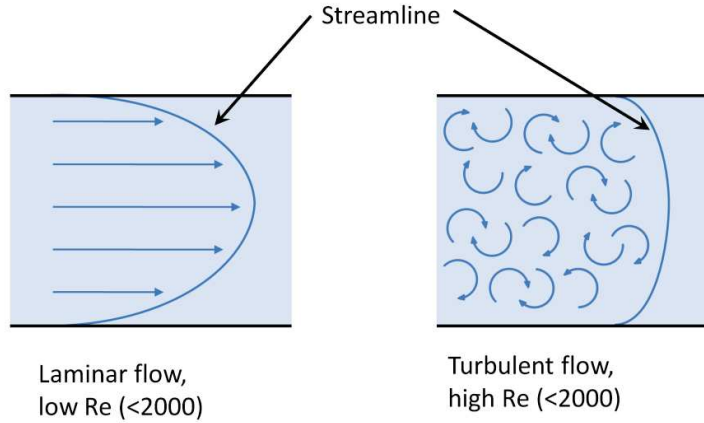


Figure 9. Laminar vs turbulent flow. At low Reynold's number (<2000), fluids usually exhibit a predictable parabolic profile while at high Reynold's number (>2000), they are turbulent and mix stochastically

Two other important dimensionless numbers in microfluidics are the Péclet number and the capillary number. The Péclet number describes how molecular transport occurs.

Molecular transport can be described by the following equation:

$$\frac{\partial C}{\partial t} = D \nabla^2 C + \mathbf{u} \nabla C \quad (\text{Eq. 5})$$

where C is the concentration of the considered specie and D the diffusion coefficient of that specie.

The Péclet number is defined as the ratio of the convective term to the diffusive term:

$$Pe = \frac{\mathbf{u} \nabla C}{D \nabla^2 C} \sim \frac{U_0 C / d_H}{DC / d_H^2} = \frac{U_0 d_H}{D} \quad (\text{Eq. 6})$$

For $Pe \ll 1$, diffusive transport dominates while for $Pe \gg 1$ convective transport prevails. The evaluation of the Péclet number helps in the design of multiple systems aiming at sensing, sorting or filtering[72].

The capillary number is of less importance in this thesis but still has a significant importance in droplet microfluidics (dealing with the generation, manipulation, and applications of droplets in microfluidic devices)[73]. It compares interfacial stresses with viscous stresses and is defined as follows:

$$Ca = \frac{\mu U_0}{\gamma} \quad (\text{Eq. 7})$$

where γ is the interfacial tension between two immiscible phases (e.g. liquid-liquid, solid-liquid, air-liquid...). The design of droplet microfluidic devices heavily relies on this number.

Many other dimensionless numbers exist in microfluidics and have been reviewed by Squires and Quake[72].

As a summary, microfluidics systems are characterized by laminar flows, where fluid and particle behavior can be predictable[70].

1.4.4.2 Materials

Several classes of materials are used to fabricate microfluidic systems. They include, silicon, glass, plastics (thermosets, elastomers, thermoplastics), hydrogel and paper.

Originally, silicon and glass were used, as these materials were familiar to those in the microelectronic industry[71] from which microfabrication techniques have been borrowed. They are resistant to organic solvents, metal depositing is easy (to form electrodes for instance), and they have high thermo-conductivity and stable electroosmotic mobility[74]. However, these materials are expensive and require costly equipment, making them hardly accessible, to fabricate microfluidics devices in most labs. Besides, silicon is not compatible with conventional microscopic methods since it is opaque to visible light and ultraviolet. Between silicon and glass, glass is preferred to perform biological experiments, but it is not a long-term solution[70]. Microfluidics systems made of plastics have become more popular, especially for biological applications[75] because plastics are cheaper materials and their fabrication more accessible. They also have good optical properties and fairly good solvent resistance[74].

Three categories of plastics are used to fabricate microfluidic systems: elastomers, thermoplastics and thermosets.

Polydimethylsiloxane (PDMS) has been the elastomer that permitted the expansion of microfluidics[70]. PDMS is - questionably[70,76] - biocompatible, easy to set-up for fabricating

systems and its elastic properties allow the integration of valves and pumps directly on the microfluidic circuitry. Due to these features, PDMS is still a material of choice, especially in biology[74,75]. PDMS presents, however, certain amount of drawbacks. Improperly cured, it can leach toxic oligomers[76]. It is a porous material which is an advantage to supply gases during cell culture but a major disadvantage to control medium evaporation. PDMS also absorbs hydrophobic molecules and water. Both gas permeability and absorption capability can lead to a detrimental shift in osmolarity and other biomolecule concentration in the cell environment[77]. Berthier et al.[78] raise other concerns about PDMS as an appropriate material for cell-based studies, such as deformation and non-stable surface functionalization over time. Although many of the PDMS limitations have been overcome, these solutions require additional equipment, time and experience to be properly developed[76]. Finally, PDMS microfluidic systems are not suited to mass production and therefore commercialization.

Thermoplastics have gained a lot of interest in the microfluidic community since the deployment of more accessible fabrication techniques[70]. Moreover, these materials naturally overcome the shortcomings presented by PDMS. The most common thermoplastic materials are polymethylmethacrylate (PMMA), polycarbonate (PC) polystyrene (PS) and cyclic olefin (co-)polymer (COC, COP). A recent review discusses the use of thermoplastic materials over PDMS[78]. The authors highlight that PS should be preferred for cell-based experiments due to the wide knowledge from biologists in using such a material. From their analysis also arises that olefin polymers are showing great promises and could replace PS for biological applications.

Thermosets are stable even at high temperatures, resistant to most solvents and optically transparent. Some example of thermoset microfluidic systems exist in the literature. However, their application in microfluidics is limited[74].

Hydrogels are only used for cell culture and most of the time for 3D cell culture[74]. In many cases, cells are encapsulated in hydrogels rather than adhered on top of it. The encapsulation of cells in hydrogels allow re-creating a 3D *in vivo*-like environment, with hydrogels mimicking the so called extra-cellular matrix (ECM); or cell scaffold. Through the porous matrix of hydrogels, cells can be supplied with nutrients, oxygen or other molecules provided, that the hydrogel is thin enough (<500 μm)[75]. Hydrogels are either injected in devices made of other materials or molded to form complete microfluidic systems.

Recently, there has been an increasing interest in developing paper-based microfluidic devices[70]. Very simple and inexpensive chips can be fabricated by using paper. Such devices are expected to provide solutions to fabricate portable, disposable and low-cost diagnostic systems to be deployed in emerging countries[74]. Paper microfluidics is also showing promises

for 3D cell culture[79]. Many challenges remain to improve and broaden the use of paper-based microfluidics such as sensitivity of detection, evaporation from open channels, demonstration of the fabrication of more common microfluidic functions (valves, pumps, droplets) and density integration (i.e. fabrication of channels smaller than 200 μm)[74].

1.4.4.3 Fabrication of microfluidic chips: structuring

Microfluidic chip fabrication can be divided into two steps. The first one is the structuring of the materials constituting the device. The second is the bonding as microfluidic chips are usually made of several layers of homogeneous or heterogeneous materials to incorporate diverse functions or simply to close the structures previously formed.

The fabrication sections will focus on the methods used to fabricate plastic microfluidic systems, as they have previously been identified as the main material used to fabricate microreactors. Structuring can be performed by using diverse techniques depending on the materials, the resolution one wants to achieve, the costs and the time needed to structure. It can be distinguished soft lithography, micromachining, laser ablation and micro molding methods such as hot embossing and micro injection molding can be distinguished (Figure 10). The first method, soft lithography, is adapted to the fabrication of PDMS devices while the other methods are usually employed for thermoplastics.

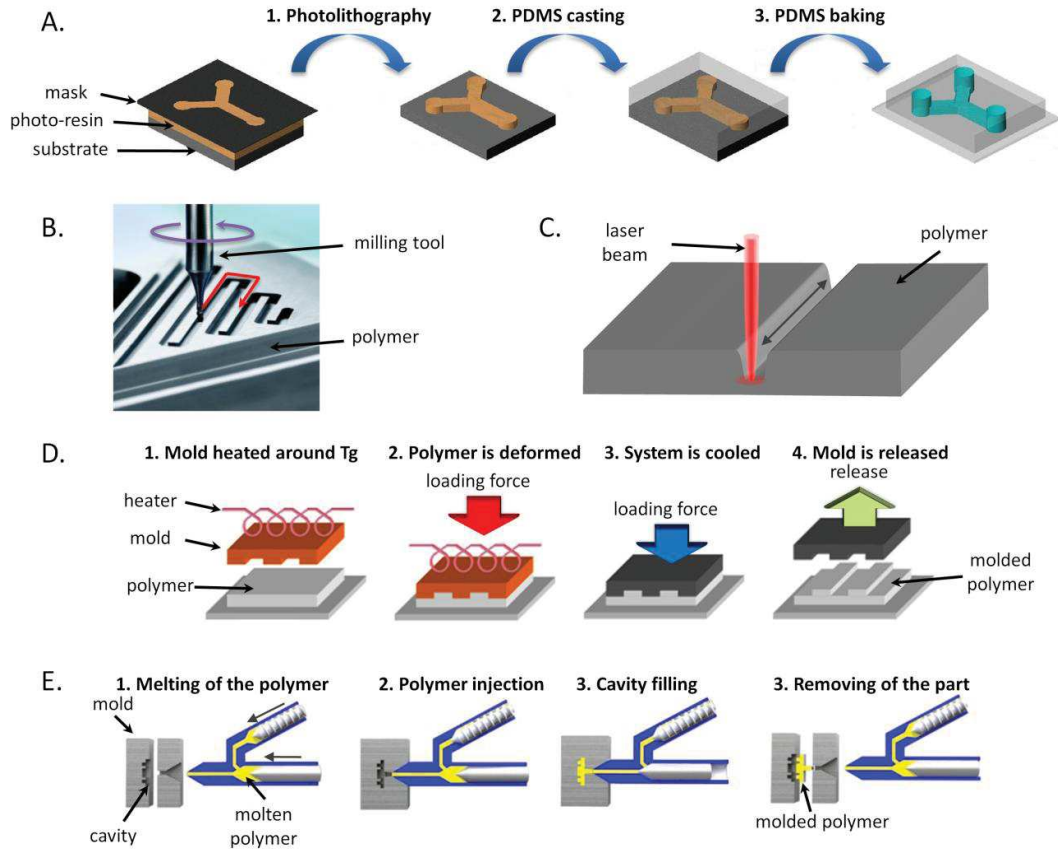


Figure 10. Schematic representation of the principle of the different methods used to structure plastic microfluidic chips. A) Soft lithography. B) Micromilling; C) Laser ablation. D) Hot embossing. E) Micro injection molding.

Soft lithography uses a structured mold onto which the elastomer is poured. The mold is fabricated by photolithography or micromachining and contains a negative replicate of the final structures to be formed. After pouring, thermal curing follows to crosslink the elastomer which is then peeled off from the mold. Highly resolved structures can be created due to the high resolution (sub micron) when photolithography is used to create the mold[80].

Micromachining is an abrasive method. A micromilling tool mounted on a computer assisted machine is guided by a computer software along the desired path to create the structures. Holes are made using microdrilling tools. This technique suffers from wall surface roughness and poor tolerances[81].

Laser ablation utilizes the energy of a pulsed laser beam to remove some materials of a solid surface by breaking the polymeric bond. The depth and width of the channels are defined by the laser intensity and the repetitive beam exposures along the same path[80].

The hot embossing technique gradually presses a structured mold into a polymeric substrate. At the same time, the mold is heated slightly above the glass transition temperature of the polymer (T_g) to soften the polymer so that it fills the mold. The mold microstructures are therefore

replicated with details into the polymer. The mold and the substrate are cooled before withdrawing the plastic[82].

Micro injection molding is an adaptation of the macroscopic injection molding. A mold cavity containing microstructures is closed and heated above the T_g of the polymer to be shaped. The polymer is heated in a separate unit and forced to flow in the mold cavity. The set-up is then cooled below the substrate T_g to demold the polymeric part[82].

Molding techniques are more suitable for mass production since they can rapidly produce polymeric components. The costs associated with mold fabrication make these methods hardly accessible to research labs or other low-volume production units. Micromachining, laser ablation or soft lithography are more adapted for smaller production or when the device design is not fixed[83].

1.4.4.4 Fabrication of microfluidic chips: bonding

Bonding methods can be classified in two classes: direct bonding and indirect bonding[84]. They differ by the presence (indirect) or not (direct) of an intermediate materials to seal the chip layers. The mechanism of bonding involves in general the interaction of charges (electrostatic, chemical (covalent bonding, acid/base interactions or Van der Waals forces) or the inter-diffusion of the substrates at the bonding interface[85,86].

The choice of the bonding methods depends on the material and the bond strength one wants to achieve. For instance, microfluidic systems that will be operated with fluids under high pressures will need to have a bond strength that can withstand these high pressures. The preservation of the surface integrity can additionally drive the choice of the bonding method in the case where the substrates have been functionalized (chemically or biochemically) and may be altered by the bonding process[83].

Indirect bonding is reduced to adhesive bonding. For adhesive bonding, a UV- or thermal-curable glue is deposited in between the material surfaces to be bonded. The glue can be deposited using different methods such as contact printing, screen printing or capillary-mediated gluing. During contact printing a thin glue layer is transferred onto the surface. Screen printing transfer glue dots on the surface by pushing the glue across a fine mesh. During capillary-mediated gluing, glue is introduced and fills a small volume right above the surface by capillarity. The main challenge with adhesive bonding is to avoid clogging of the structures by undesirable infiltration of glue. Sacrificial channels can be used to contain the excess of glue that might be deposited, preventing structure clogging. Additionally, the glue must wet the surfaces to achieve a proper bonding. However, the common glues used exhibit poor wetting on some plastics such as COC or PS.

Direct bonding includes thermal bonding, solvent-assisted bonding, local welding or the use of surface treatments[84]. Thermal bonding is the most common methods for bonding microfluidic thermoplastics components due to its simplicity and the high bond strength achievable[84]. It uses pressure and heat to mate substrates. The polymer is heated to around its Tg and the parts pressed together to create an intimate contact force by the inter-diffusion of the polymer chains to form a strong bond. The challenge with this technique is to control both the pressure and the temperature to avoid structure collapse while ensuring sufficient bond strength.

Solvent-assisted bonding is performed by exposing the thermoplastic surfaces to a solvent in its vapor or liquid phase. Vapor phase usually permits a better control of the solvent. The solvent induces the solvation of the surface polymer chains. They become mobile and can diffuse readily across the solvated layer forming a bond exceptionally strong, stronger than adhesive and thermal bonding. Care must be taken to avoid structure deformation by selecting the right solvent(s) and by controlling the exposition time to the solvent. Pressure and/or temperature can be used after solvent exposition to enhance the bond strength, as well as deep UV irradiation.

Localized welding uses ultrasonic waves, microwaves or infrared (IR) light to induce heat and soften the thermoplastic interface to bond. The utilization of microwaves requires the insertion of a thin metallic layer to absorb the wave's energy while the utilization of IR light imposes one of the substrate to be opaque to IR light in order to induce the energy absorption at the interface. Localized welding has the advantage to create local or uniform bonding. However, this technique is not very practical, due to the complexity introduced by the need of a special design to direct the energy at the weld points, or the constraints associated with the requirement to deposit a metal layer, or the constraints to utilize polymers with different absorption characteristics.

Surface treatment is carried out by exposing the polymer surfaces to UV, UV/ozone or plasma. Such treatments increase the surface energy and by breaking chemical bonds can form reactive radicals. This enables the inter-diffusion of polymer chains and the possibility to form electrostatic interactions or even to create covalent bonds. High bond strength can be obtained. Surface treatments induce a modification of the surface which can be an advantage or a drawback. As a drawback, surface modification producing charges can undesirably interact with analytes. On the other hand, it can be used to obtain more hydrophilic surfaces or further enable other molecular grafting. Surface treatment can be combined with thermal bonding. The pressure and the temperature needed are lower, though.

1.4.4.5 Advantages and application of microfluidic cell culture systems

Microfluidic systems adapted to cell culture propose a number of advantages which overcome the limitations of standard cell culture format and propose new tools for cell biology. Table 3 summarizes the advantages provided when a microfluidic format is used. It has already been underlined that due to the scaling effect microfluidic systems are characterized by laminar flows where diffusive mass transport can prevail. These key characteristics grant the possibility to precisely control temporally and spatially the cell microenvironment[87]. Homogeneous physical and biochemical levels around the cells can be guaranteed, or cells can be exposed to stable gradients[88,89]. Microfluidic tools such as gradient generator or gas exchanger are combined with cell culture chambers to expose cells to different stimuli (Figure 11.A). The variations to which cells are exposed can be quickly changed. Variations within seconds to a few minutes have been reported compared to tens of minutes for conventional macrosystems[90]. The control of the microenvironment has had a major implication in the study of cell behavior and cell interactions[91].

Another advantage due to the scale of microfluidic systems is the high level of integration and automation they can provide. The incorporation of software-controlled pumps and valves allow addressing the high number of culture chambers that can be embedded on a single microfluidic device[92]. Bioreactors have been developed to perform drug screening studies[93,94]. The potential demonstrated by high-throughput screening methods have largely improved over the recent years by increasing their automation level and miniaturizing assay volumes. However, they face major challenges such as liquid evaporation leading to poorly defined culture conditions[95]. This problem can be avoided with enclosed microfluidic systems. As mentioned in section 1.4.3.5, microfluidic systems are expected to improve bioproduction by providing screening tools for media formulation, clone selection and automated systems capable of controlling culture conditions to mimic scale-up bioreactors.

Additionally, microfluidic culture systems have proven higher physiological relevance compared to standard cell culture. Numerous microbioreactors include perfusion strategies which mimic the body vascular system ensuring that cells constantly receive an adequate amount of nutrients and are cleared of their wastes. Microfluidic systems also have the ability to perform 3D cell culture and co-culture. It is well known that cells demonstrate a more *in vivo*-like behavior when cultured in 3D while losing phenotypic behavior when cultured in 2D[96]. Similarly, co-culture experiments increase the consistency of cell culture studies as presented also in a review[97]. Increasing the physiological relevance is an important criterion for drug testing and the study of cell behavior and interactions[95,98]. In the first case, efforts are currently undertaken to replace animals models commonly used for drug validation. Despite the ethical and economical

concerns associated with animal models, questions are being raised since they inadequately represent human responses due to species-specific differences[95].

Table 3. Basic requirements for cell culture, and improvements when microfluidic methods are used[76].

Requirements	Conventional cell culture	Microfluidic cell culture
Control of temperature and gasses	Large fluid volumes prevent fast changes	Small volume allow dynamic control
Addition of nutrients and removal of metabolites	Infrequent, manual exchange of large volumes	Precisely measured, continuous or transient exchange of media
Stimulation with drugs/proteins and simultaneous imaging	Mostly not feasible	Feasible
Parallelization of cellular assay	Not feasible	High capability for parallelization
Automation of cell culture tasks	Bulky, expensive fluid-handling robots must be used	High capability for automation in compact and inexpensive format
Single-cell manipulation and analysis	Manually involved, inaccurate, low throughput	Accurate and high-throughput

Models mimicking biological organ functions are appearing under the appellation of “organ-on-chip”[99]. Examples of liver[100], artery[101], heart[102], lung (Figure 11.B)[103] and kidney[104] mimicking systems have been already reported. Some of them have been coupled to create “body-on-chip” systems. Organ and body-on-chip have been used to perform toxicological studies[105,106]. The development of organ-on-chips is likely to provide models to study pathophysiological diseases[107,108].

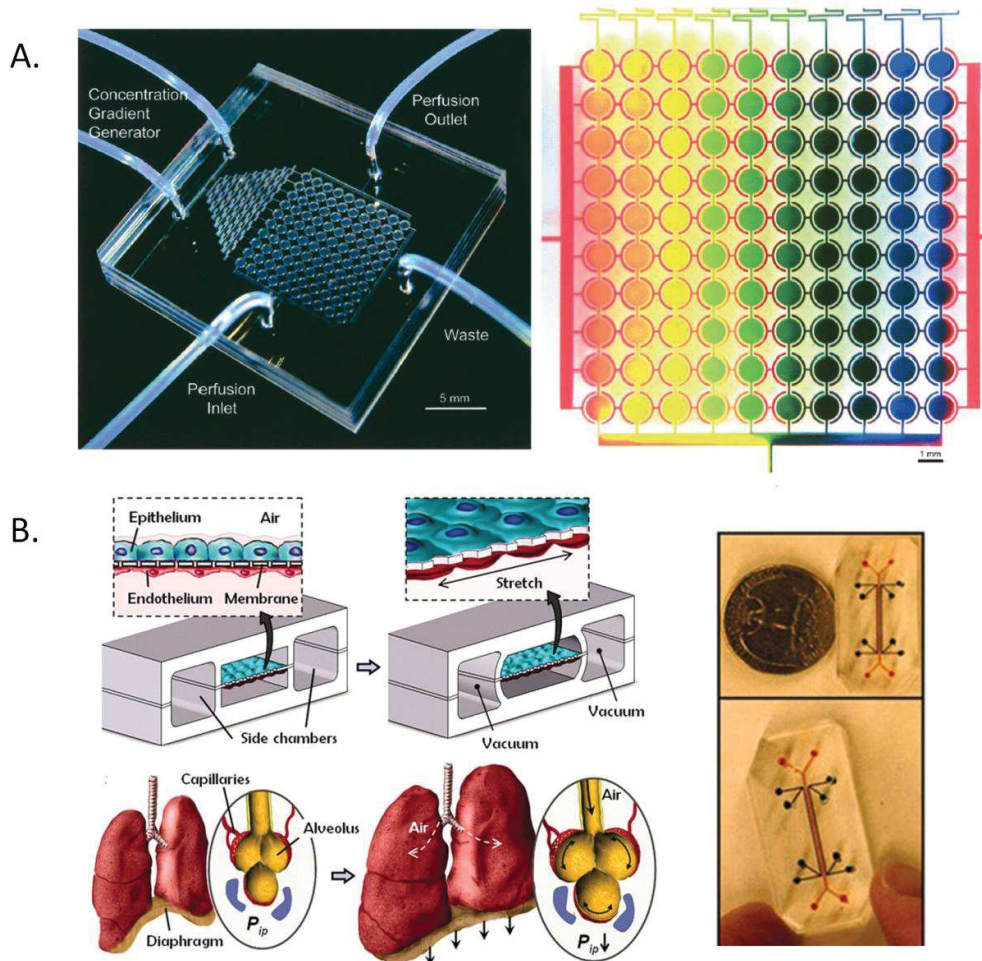


Figure 11. Microfluidic cell culture system allow high screening and more physiologically relevant experiments.
A) Example of a high-throughput microfluidic systems controlling the environment each culture chamber[109]. A gradient generator upstream creates streams of different concentrations; each of them feeding a row of culture chambers.
B) Example of a lung-on-chip[110]. A porous membrane, on which lung epithelial cells and lung endothelial cells are cultured on either side, can be stretched to mimic lung breathing by applying a vacuum in channels aside.

Eventually, the key advantages offered by microbioreactors can lead to important time and cost savings due to the utilization of cheap disposable materials and the consumption of reduced amounts of biological materials and reagents. For instance, Cheong *et al.* estimated their prototype microfluidic device uses ~150-fold lower amount of costly drug libraries and chemical media enabling a gain per data around \$1-2[111]. The savings for a standard large-scale libraries consisting of hundreds of thousands of compounds becomes significant.

1.4.4.6 Cell culture format in microbioreactors

The format for cell culture in microfluidic systems started in 2D with cells cultured on the channel floor. To mimic the native cell environment cells are now cultured in 3D, mainly by filling microbioreactors channels with cells embedded in a hydrogel. 3D cell cultures of mammalian or bacteria can be performed by their encapsulation in hydrogel microdroplets (Figure 12.A) greatly increasing biological characterizations throughput[112]. Micro-cultures of cells in suspension have been performed for mammalian cells, bacteria and yeasts. Mammalian suspension cell culture in microfluidics is principally related to spheroid cell culture, spheroids being used as model for drug toxicity[113]. Examples of bacteria and yeast microfluidic cell cultures were related to the development of miniaturized chemostats (Figure 12.B)[114,115].

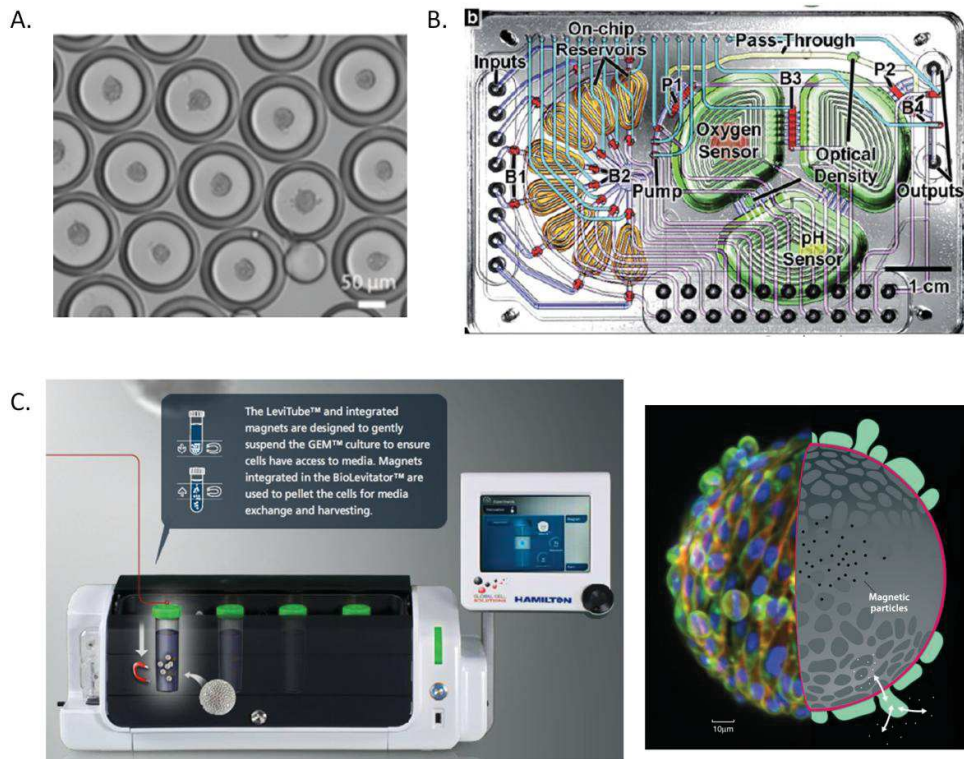


Figure 12. Cell culture format in microfluidic and miniaturized systems. A) Mammalian cell culture in microdroplets[116]. B) A microfluidic chemostat for bacteria suspension cell culture[115]. C) Left: The BioLevigator™. Right: the GEM™ microcarriers.

Despite the wide variety of microfluidic cell culture formats, no major work has attempted to explore microcarrier-based cell culture even though microcarriers are routinely used in the industrial scaled-up cultures. The smallest culture systems performing such a culture is a commercial system (Figure 12.C), the BioLevigator™, utilizing 75-150 μm microbeads, GEM™ (Global Eukaryotic Microcarriers). The beads are made of an alginate core containing magnetic

nanoparticles and exist with different coatings on their outer surface: laminin, fibronectin, Collagen I, Collagen IV, matrigel, poly-d-lysine and gelatin. A magnet surrounding a 50 mL vial is moved in cycles upward and downward to move the beads with cells providing homogenization of the culture environment. However, cells are cultured in static conditions and the volume remains large compared to microfluidic volumes.

1.4.4.7 Microfluidic cell culture automation

In microfluidic chips the automation of the culture steps (seeding, proliferation, subculture) is usually reduced to the automation of the seeding and proliferation phase. The reason is that most of the experiments aim at studying the cell behavior/interactions or re-create *in vivo*-like environments. However, some biological analysis (proteomics, genomics) may require the extraction of cells from the culture systems or alternatively to replat them in other systems.

An overview of microfluidic systems used for the production of cells and their characteristics is given in Table 4.

Table 4. Example of microfluidic bioreactors used for the production of cells and their characteristics.

Type of culture	Material	Volume (μL)	Dimensions	Cell type	Measurement and control	Ref.
batch	PS	250	Φ^a : 3 mm H ^b : 35 mm	bacteria	DO ^e -pH-T ^o -OD ^g	[117]
Batch, fed-batch, continuous	PDMS	100	Φ : 8 mm H: 2 mm	yeast, bacteria	DO-pH-T ^o -OD	[118]
semi-continuous	PDMS/PMMA	1000	W ^c : 17.7 mm L ^d : 23.6 mm H: 2 mm	bacteria	DO-pH-T ^o -OD	[115]
semi-continuous	Gold (electrodes)	0.15	W:0.8 mm L: 0.8 mm H:0.2 mm	mammalian	Incubator (5% CO ₂ , 37°C)	[119]
semi-continuous	PDMS	0.02	Φ : 0.8 mm H: 40 μm	mammalian	Incubator (5% CO ₂ , 37°C)	[120]

^a Φ : culture area diameter, ^bH: height of the culture area, ^cW: width of the culture area, ^dL: length of the culture area, ^eDO: Dissolved Oxygen (in medium), ^fT^o: Temperature, ^gOD: Optical Density (evaluating the cell concentration)

In the case of anchorage-independent cells such as yeast or bacteria, harvesting has been easily implemented since it can simply be achieved by fluid handling[114,115]. In the case of anchorage-dependent microfluidic cell culture more development is required to achieve cell harvest.

Microbioreactors mainly rely on enzymatic digestion using a proteolytic enzyme: trypsin. Some reports have demonstrated the possibility to successfully perform several consecutive proliferation-subculture cycles[119,120]. For instance, Zhang *et al.* have performed cell culture cycles in microfluidic chambers incorporating microsieves in a shape of a half-moon (Figure 13.A). During cell loading, the flow traps the cells in the microsieves. After stopping the flow,

cells can proliferate by colonizing the cell culture chamber floor. Once sub-confluence is reached, cells are exposed to trypsin to trigger cell detachment. Then, most of the detached cells are flushed except those close to the microseves which are trapped during cell loading. Eventually, the trapped cells can enter a new cycle of proliferation. Although proteolytic enzymes (trypsin, accutase, collagenase...) have been a gold standard in cell harvest, their use increases the complexity of fluidic design and the amount of reagents consumed and may lead to adverse effects on cells[121,122]. Since most of the proteolytic enzymes are inhibited by culture media, washing steps are required. Therefore, several additional reservoirs, pumping tools and channels have to be added to the microfluidic systems to perform *in situ* cell harvest. Besides, proteolytic enzymes degrade some of the cells membrane proteins[121] and can affect others such as integrins that are involved in regulating cell adhesion, stability and elasticity[123]. Alternative methods in microfluidic format have been investigated. The most intuitive involved high level of shear stress applied to adhered cells in a microchannel by increasing the input flow rate. This method is poorly effective[124] and may affect cell viability[125] and alter the cell phenotype[126]. Some microfluidic systems have incorporated stimuli-responsive polymers to perform cell harvest[127] (Figure 13.B). Stimuli-responsive substrates allow cell detachment upon the application of a physical, chemical or biochemical stimulus. Many of them have demonstrated efficient cell release (> 90%)[127]. However, they have not demonstrated the possibly to perform cell culture cycles yet.

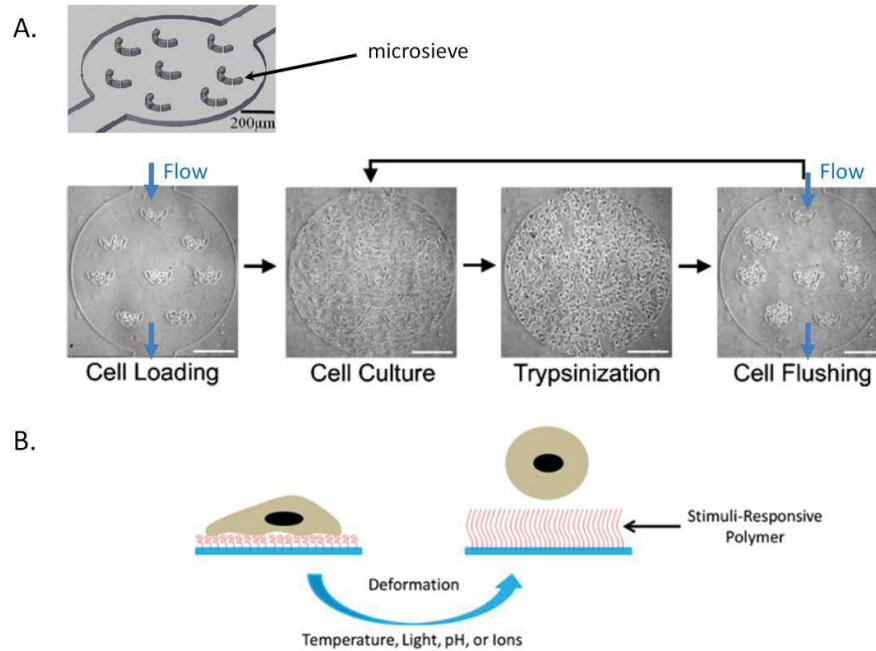


Figure 13. Cell culture automation by integrating cell harvest in microfluidic cell culture systems. A) Example of cell culture cycle in a microfluidic system. Microsieves allow cell trapping and harvest is achieved by dispensing trypsin in the culture chamber ("Trypsinization") [120]. Scale bar is 200 μm B) Working principle of stimuli-responsive polymers [127].

1.5 Conclusion

Since cell culture was invented, it has become a common practice in biological research through the development of standard protocols. It is currently a major tool in the understanding of life science, the study of disease and the discovery of new drugs. Cell culture was quickly transferred to industry and now plays an important role in the production of many food, cosmetic, and pharmaceutical products. However, cell culture still has a number of limitations, such as the consumption of relatively large quantities of material and reagents, the frequent low rates of experiments and the need for qualified operators; all these factors make cell culture an expensive method. More importantly, conventional cell culture does not respond to a growing need to increase the relevance of experiments using more *in vivo*-like models. Similarly, industrial culture under the pressure of demand and the economic context is looking for tools that can speed up and reduce the development costs associated with the production of bioproducts. It is looking for miniaturized systems that can mimic key characteristics of macrobioreactors in order to quickly and by using fewer resources (equipment, trained staff, reagents...) identified the best clones and the best growing conditions for large-scale production. Based on these remarks microfluidic systems represent a promising tool to address these issues and challenges. Technologies derived from microelectronics participated in the development of these microfluidic systems. However, it is the development of fabrication methods for plastics-

based systems that actually allowed the development of microfluidics for life sciences applications. The change of physical behaviors at the small-scale in microfluidic devices allows temporal and spatial control of the cell microenvironment, unattainable with conventional cell culture methods. The level of automation and integration allows the substantial increase of the number of experiments per system. Thus, many small cellular 3D architectures grown under dynamic conditions and in high-throughput have been performed and have demonstrated their ability to quickly re-create more physiological environments. The use of these models is expected to significantly improve the relevance of studies on cell behavior, comprehension of diseases and the development and study of drugs. Regarding industrial culture, miniaturized cultures have already shown their ability to reproduce the characteristics of the culture observed in macrobioreactors. Interestingly, among the myriad of systems developed, none has actually attempted to perform microcarrier-based cell culture in a microfluidic format, despite the fact that this cultivation method is widely used in industry. Similarly, few microfluidic bioreactors have coupled a harvesting function to allow the extraction of adherent cells.

2 Thesis objectives

Based on the literature study, key goals have been defined for the thesis:

- Fabricate a device that fits with the standard microfluidic platform developed in the host laboratory (See Chapter 3)
- Integrate tools and functions to provide the proper conditions for continuous cell culture (see Chapter 3 & 4)
- Investigation of microcarrier-based cell culture in a microfluidic system for cell culture (see Chapter 4)
- Develop a disposable self-sufficient benchtop system (see Chapter 4)
- Investigation of the integration of a harvest function inside the bioreactor (see Chapter 5)

From these requirements, a general approach has been defined with different sub-scenarios. The proposed approach is described in Figure 14.

Cells are initially inoculated inside the fluidic system (fitting a standard format) to be cultivated in a culture area. In this area, a stable and controlled environment is provided by:

- implementing a perfusion function to continuously supply the nutrients needed by the cells and clear, at the same time, the waste they produce
- integrating sensors to monitor the relevant parameters for a proper growth (temperature, pH, oxygen, glucose)
- implementing elements to adjust these parameters for cell growth

Once a certain cell density is reached, cells must be harvested to deliver a part of the cell population to the end-user and sub-cultured to keep a certain population of cells to be able to maintain cell growth.

Three scenarios have been designed for the harvest and sub-culture of anchorage-dependent cells to propose an alternative to cell harvests based on the use of proteolytic reagents. The first scenario consists of extracting a certain number of microcarriers covered with cells while adding the same quantity of fresh microcarriers. Since cells are able to transfer from one bead to another, the proliferation can continue until a certain cell population is reached before initiating another harvest. The second scenario consists of dissolving a certain amount of microcarriers covered with cells while adding the same quantity of fresh microcarriers. The third scenario, the most complex, is based on the utilization of functionalized microcarriers to provide cells separated from the microcarriers to the end user. These microcarriers are covered by a

thermosensitive polymer that swells reversibly according to the temperature. Such a swelling induces cell detachment. Thus, microcarriers covered with cells can be driven in a thermo-controlled area of the bioreactor where cell detachment is thermally triggered. Then, a simple design to perform particles size sorting could separate a part of the detached cell population from a mixture of detached cells and microcarriers to deliver these cells out of the bioreactor. The carriers and the remaining cells are sent back to the proliferation area where cells can adhere again on the microcarriers. Proliferation can continue until a certain cell population threshold is reached before initiating another harvest.

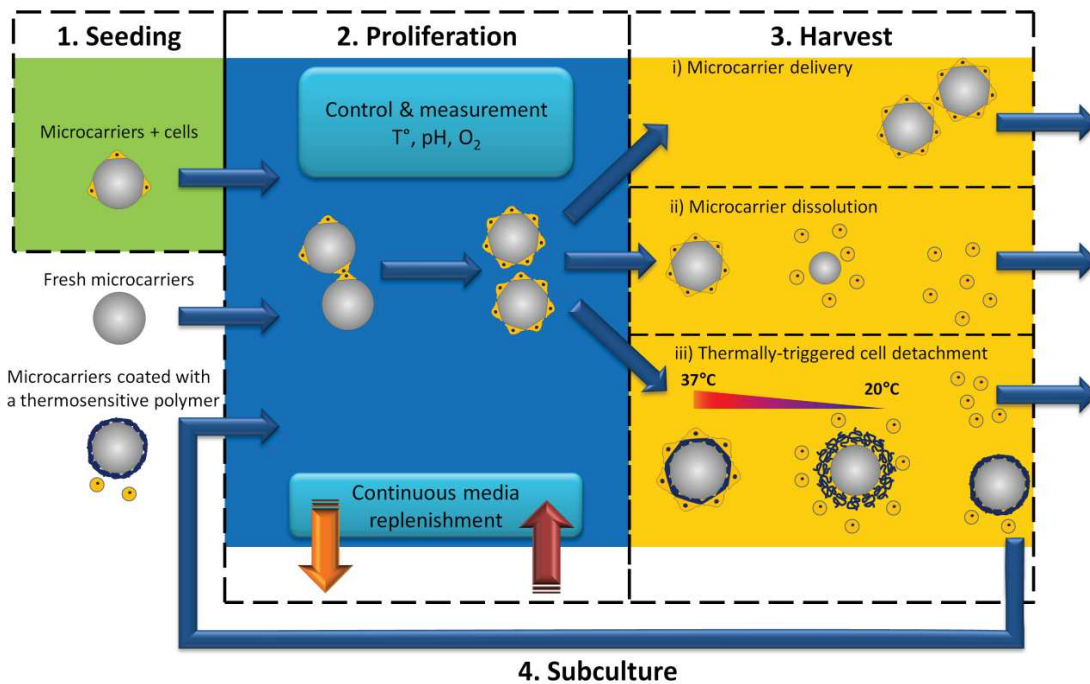


Figure 14. Approach for the development of the microbioreactor. Cells on microcarriers are seeded into the bioreactor. Their proliferation is guaranteed by controlling and measuring the environmental conditions (T° , pH, O_2) and continuously renewing the culture media. Once a critical cell density is reached 3 cell harvest scenarios can be performed: i) simple microcarriers delivery with simultaneous fresh microcarrier addition, ii) microcarrier dissolution with simultaneous fresh microcarrier addition or iii) thermally-induced cell harvest where a part of the detached cells and all the microcarriers are reused for proliferation.

In brief, the cycling of the cell culture relies on microcarriers that support the growth of adhering mammalian cells. In this configuration, the cells can be easily transported through fluids and mastering the hydrodynamics inside the bioreactor can allow a partial collection of the cells adhered or not on microcarriers – depending on the scenario- while keeping the rest of the cells inside the bioreactor. This approach also allows cycling the culture of floating cells such as bacteria, yeast or mammalian floating cells making the device a versatile tool to culture diverse types of cells. This thesis work focuses on the culture of anchorage-dependent mammalian cells.

3 Microbioreactor design and fabrication

This chapter gives an overview of the entire bioreactor. It also describes the bioreactor design and fabrication, and more particularly the design and fabrication of its key component: the cell culture cartridge.

3.1 Microbioreactor overview

The bioreactor is composed of different elements (Figure 15). The main element is the fluidic cartridge which hosts the cell culture. This Cell Culture Cartridge (CCC) includes a perfusion function to continuously supply the cells and clean the waste they produce. On this cartridge is integrated a thermal sensor associated to a reading instrument. The sensor is used to monitor the ambient temperature of the CCC. A heating element is adjoined to the cartridge to provide the necessary heat to the CCC. The feeding perfusion medium is inoculated using a syringe pump. Once the medium has passed through the fluidic circuitry of the culture cartridge, it is collected in a waste recipient. Tubing is used to connect the syringe pump, the fluidic cartridge and the waste recipient. A homemade holder comprising a clamping system ensures hermetical connections with the culture cartridge. The system can be placed under an upright microscope to observe the cells inside the CCC.

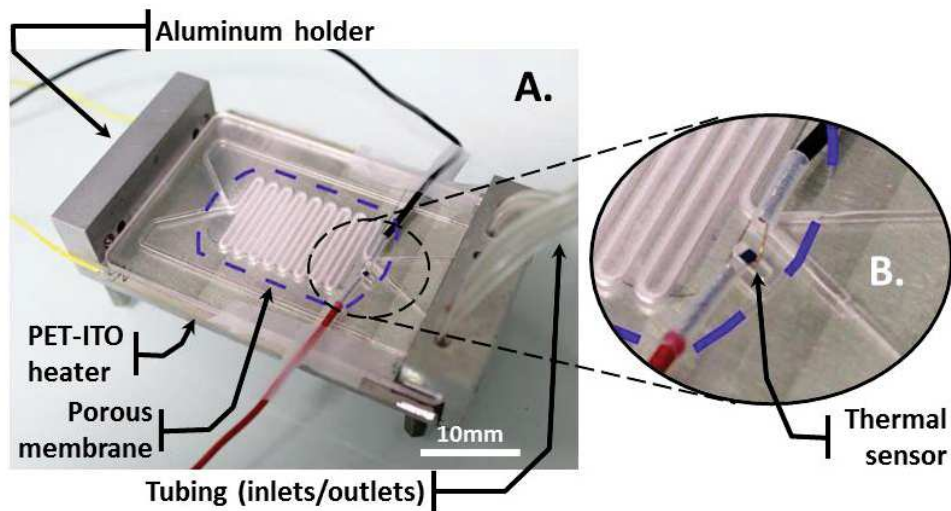


Figure 15. Picture of the bioreactor. A) General view of the microfluidic bioreactor. It is composed of a fluidic culture cartridge which contains a porous membrane defining the culture area, a transparent heater placed beneath the cartridge to warm it up, a thermal sensor placed at the culture height to monitor the culture temperature, and a holder sandwiching the different components and allowing fluidic inter-connections. B) Expanded view of the thermal sensor inserted in the CCC.

3.2 Cartridge design

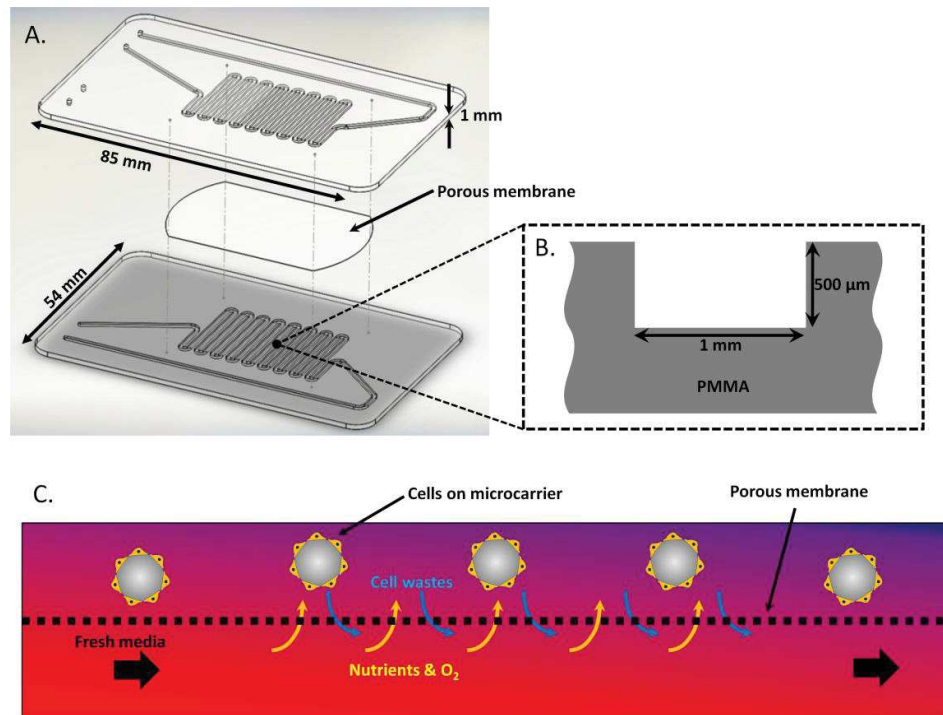


Figure 16. Design and working principle of the CCC. A) Design of the cartridge integrating the porous membrane. The milled PMMA plates sandwich a porous membrane placed in between the two snake-like channels. B) Dimensions of the cross section of the channels. C) Working principle of the culture area. Fresh media is supplied in the lower channel from where nutrients and O₂ diffuse across the porous membrane to reach the cells in the upper channel. Cell wastes, on the other hand, are removed by diffusing across the porous membrane from the upper channel to the lower channel.

The core element of the bioreactor is the CCC. It is composed of two PMMA layers, 1 mm thick each, having a credit card footprint and sandwiching a porous membrane placed in between them (Figure 16.A). In each PMMA layer, a 1-mm-wide and 500-μm-deep channel (Figure 16.B) is milled by a milling machine (Charly4U, Mecanumeric). Each channel features a snake-like shape, 400 mm long, which faces each other. In this area, the porous membrane is inserted to separate the channels. This configuration guarantees that cells in one channel are confined while diffusive transport can occur across the porous membrane to i) provide nutrients and oxygen from the other channel to the cell channel ii) clear cell wastes from the cell channel into the perfusion channel (Figure 16.C). Moreover, cells can be manipulated at will through fluidic transport independent of perfusion. The channel area with the membrane defines the culture area. The geometry of the cell channel in this area provides a culture volume of 200 μL and has a total volume of 260 μL. Details regarding the integration of the porous membrane are given hereafter.

3.3 Perfusion integration

This section details the choice made to consider perfusion based on the integration of a commercial porous membrane. The selection of a porous membrane is evaluated based on several aspects, such as time for molecular transport, ease of integration in the CCC and optical observations. In the meantime, two fabrication methods are tested for the integration of the porous membrane.

3.3.1 Perfusion strategy

Most of the microfluidic systems developed for cell culture are implementing perfusion to continuously provide cells the necessary nutrients and oxygen while clearing their wastes. A more stable and controlled cell environment can be achieved compared to static cultures[128]. Perfusion can additionally be used to deliver other molecules such as drugs or soluble factors. Two sorts of perfusion have been developed in microfluidic systems: perfusion based on convective mass transport and perfusion based on diffusive mass transport[128]. In the first case, the cells are directly exposed to a laminar flow (Figure 17.A&B). Depending on the geometry of the culture chamber or channel, the cells are exposed to shear stress. For a rectangular channel the shear stress can be expressed as[129]:

$$\tau = \frac{6\mu Q}{h^2 w} \quad (\text{Eq. 8})$$

where τ is the shear stress, μ the fluid dynamic viscosity, Q the flow rate, h the culture chamber height and w its width.

Therefore, the higher the flow rate, the higher the shear stress. It has been underlined that depending on their type, cells present different resistance to shear stress. A perfusion based on convective mass transport is not suitable for shear-sensitive cells such as primary hepatocytes[130].

In the second case, perfusion based on diffusive transport isolates the cells from the main stream. Small structures (Figure 17.C,D) (e.g. pillars, microchannels) or porous matrices (e.g. membranes, hydrogels) (Figure 17.E,F) between the cell chamber and the bulk flow are used to shield the cells from direct convective flows[128]. As a consequence uniform mass transfer is achieved. This configuration also has the advantage that it mimics the mass transfer characteristics as observed *in vivo*.

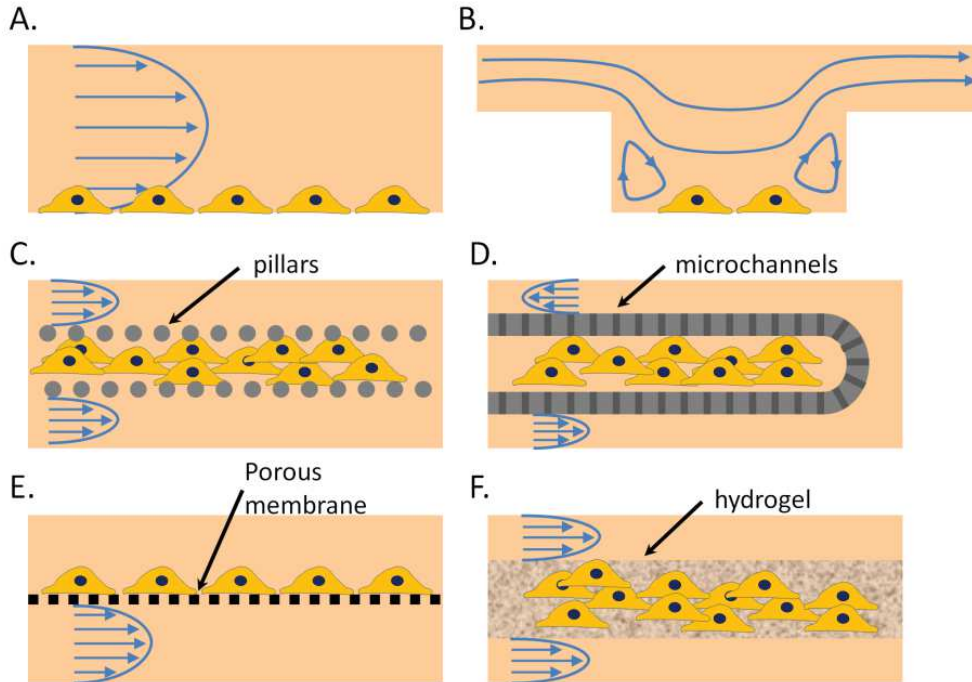


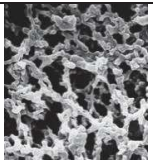
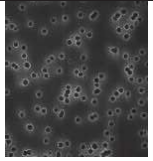
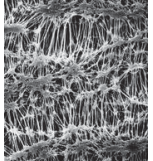
Figure 17. Perfusion strategies in microfluidic systems. A-B) Cells are directly exposed to the main stream of perfusion. C-E) Cells are shielded from the main stream of perfusion by microstructures (C,D) or a porous material (E,F).

The integration of a membrane (Figure 17.E) is the easiest and the most straight-forward way to fabricate a polymeric and disposable perfused bioreactor since a wide variety of membranes is commercially available[131]. For this reason, this method was retained to build the microfluidic bioreactor. Besides, the host laboratory was interested in gaining experience in the development of microfluidic systems incorporating a porous membrane because such systems can realize other functions such as phase extraction or dialysis. Alternatively, membranes or other “isolating” structures can be fabricated either in house as part of the chip fabrication process or within the chip, or by relying on the porous property of the bulk chip material (e.g. hydrogel, PDMS porosity). In many cases these alternative methods are associated with higher costs due to the use of cleanroom facilities or the fact that the fabrication process is more complex and tedious[131]. Some methods may also not be biocompatible or may require extensive washing due to the use of solvents.

3.3.2 Type of membrane

Different commercial porous membranes were tested to be inserted in the bioreactor. Table 5 gives an inventory of the different membranes and their characteristics.

Table 5. Characteristics of the commercial membranes tested for the integration inside the bioreactor.

Name and Ref.	Material	Thickness (μm)	Pore size (μm)	Porosity	Permeability (mL/min/cm ²)	Optical properties	SEM images
MF-Millipore™ HAWP04700	Cellulose ester	150	0.45	79%	60	Opaque, white	
Isopore™ GTPP04700	PC	25	0.2	13.8%	6	Translucent	
Biopore™ BGCM00010	Hydrophilic Polytetrafluor oethylene (PTFE)	40	0.4	60-80%	15	Transparent when wet	

(Data were provided by Merck Millipore, for more information see http://www.millipore.com/membrane/flx4/millipore_filters_hm#tab1=4)

The material was the first choice of selection and was done based on the supplier's (Merck Millipore) recommendations. Membranes used in biochips are usually made of polyester, PC, polyethersulfone, nitrocellulose and polytetrafluoroethylene (PTFE)[131,132]. Therefore, these materials were in good agreement with the literature. The pore size was the second criteria considered in the selection of the membrane. An optimal pore size prevents the cells from crossing the membrane but still should not hinder the diffusion of the nutrients, oxygen and cell wastes. If possible the pore size should also prevent undesirable microorganisms that might contaminate the perfusion to reach the cell culture channel. For this purpose, filters with 0.2 μm pore diameters are commonly used to filter cell culture reagent (e.g. media, buffer...).

One way to roughly compare the membrane performance in terms of mass transport is to assess the time a particle would take to go through it (Table 6). Ideally, the membrane should not slow the diffusion of particles to achieve an effective mass transport. In the case where there are no particles on the other side of the membrane, the time the particles would take to cross is defined as:

$$t_{diff} = \frac{h_m^2}{D_{eff}} = \frac{h_m^2 \tau}{\varepsilon \delta D} \quad (\text{Eq. 9})$$

where h_m is the membrane thickness, D_{eff} is the effective diffusion coefficient in the porous matrix, D the intrinsic diffusion coefficient, ϵ the porosity, τ the tortuosity and δ the constrictivity (see Appendix B).

Table 6. Rough evaluation of the membrane ability for mass transport based on their characteristics (porosity ϵ , tortuosity τ , constrictivity δ and membrane thickness h_m).

	Cellulose ester	PC	PTFE
ϵ	0.8	0.14	0.7
τ	2.5	1	2.5
δ	1	1	1
h_m (μm)	150	25	40
t_{diff}	$\frac{7 \cdot 10^{-8}}{D}$	$\frac{4 \cdot 10^{-9}}{D}$	$\frac{6 \cdot 10^{-9}}{D}$

The cellulose ester membrane is more resistant to the diffusion of particles compared to PC or PTFE by at least one order of magnitude. It means that the time a particle takes to flow through the cellulose ester membrane is at least 10 times longer than that for the PC or the PTFE membrane. The cellulose membrane exhibits lower performance for mass transport. A comparable mass transport is expected between the PC and the PTFE membrane with a slight advantage for the PC membrane. Based on this consideration, they both appear as valuable candidates for the fabrication of the perfusion.

3.3.3 Bonding

The sealing of systems incorporating a porous membrane is a critical step in the fabrication of biochips. Improper bonding will lead to fluid leakage and may compromise the sterility of the system. The integration of a porous membrane is usually simply achieved by clamping or gluing[131]. The methods previously presented in the introduction to bond polymer devices can also be used to integrate polymeric membranes[133].

Two methods to seal the CCC after the insertion of a porous membrane were investigated. One is thermal bonding, commonly used for thermoplastic microfluidic systems. The other uses a glue deposited by screen printing.

Thermal bonding

Thermal bonding is performed by heating up the polymer layers to be bonded to their glass transition temperature. The critical parameters when performing thermal bonding are the pressure, the temperature and the time during which heat and pressure are applied. An excess of one or a combination of these parameters can lead to the deformation of the microfluidic structures but also of the entire cartridge. Deformations can compromise the fluidic

performance or deteriorate the fluidic interconnections. On the other hand, bonding may fail or lead to poor bond strength if pressure and temperature are too low.

For the thermal bonding, the PMMA plates were aligned in a homemade press system (Figure 18.A). The pressure was applied empirically by screwing the upper metal plate down with a given amount of turns. The device under pressure was placed for 1 h in an oven set to 110°C, close to the glass transition temperature of PMMA. Afterwards, it was withdrawn from the oven to be cooled down to room temperature by exposition to the ambient air before releasing the pressure. Figure 18.B shows the results obtained after thermal bonding.

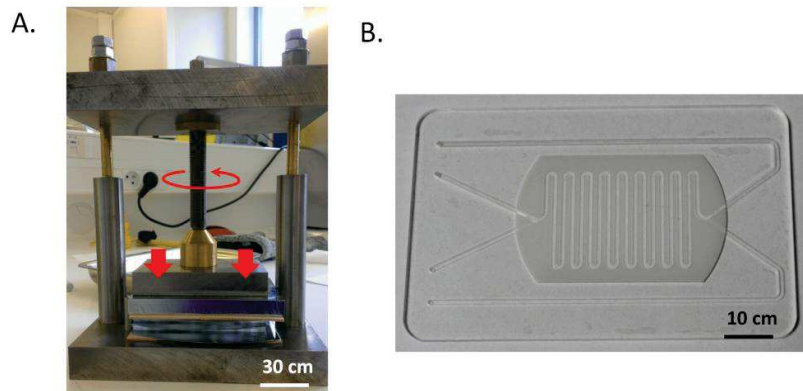


Figure 18. Illustration of the thermal bonding and the result obtained. A) The homemade thermal bonding press. A screwing system pushes the upper thick metal plate against the lower base metal plate. The plastic plates to bond are inserted in between.

B) Microfluidic system integrating a PC membrane after thermal bonding.

Glue-based bonding

The deposition of glue to perform the bonding is carried out by a screen printing method. Figure 19.A shows the working principle of this method. A line of glue is deposited on a screen of fine mesh standing above the substrate to be covered. A squeegee pushes and moves forward this glue line on the screen to force the glue through the mesh openings to wet the underlying substrate. Small volumes of glue are locally deposited along the contact line defined by the squeegee. As the screen peels away from the substrates after the passage of the squeegee, the glue volumes flow laterally due to residual gravitational stress. The glue volumes are usually close enough to merge due to surface tension. Thus, a continuous film of glue is formed behind the squeegee. The thickness of the mesh and the size of the mesh openings determine the thickness of the glue deposited[134] and is given by:

$$t = T^2 \left(\frac{1}{T} - d \right)^2 * 2d \quad (\text{Eq. 10})$$

where t is the printed thickness, T the mesh count (number of thread per cm), d the mesh wire diameter (Figure 19.B). A mesh has a $2d$ thickness and a squared opening with a side length of

$T^{-1} \cdot d$.

A screen with a mesh count of 150 threads per cm and a wire diameter of $34 \mu\text{m}$ was used to print a thickness of about $16 \mu\text{m}$.

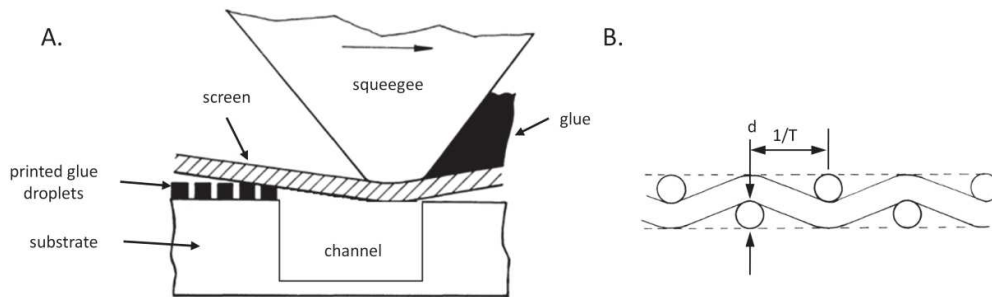


Figure 19. Screen printing technology. A) Screen printing process. A squeegee pushes downward a porous screen and forward a glue deposited on top of this screen. As a consequence, small glue dots are deposited on top of a substrate placed beneath the screen. B) Schematic side view of the screen mesh: d is the mesh wire diameter and $1/T$ is the linear mesh density.

To bond the CCC, 4 different glues regularly used in the host laboratory to perform packaging sealing were available. Prior to carrying out tests to bond the CCC, cytotoxic tests were performed to find out if at least one of them would not degrade the cell viability. One of them, the UV curable epoxy glue OG116-31 from EPO-TEK[®], was found to be biocompatible and was selected to be used in screen printing (see section 3.3.4). To perform the glue-based bonding, the glue is deposited on one PMMA plate face presenting the channel structures using a screen printing machine (Ekra M2H, ASYS). The porous membrane is placed on the “snake-like” channel area. Glue is deposited on the other PMMA plate on the milled face. It must be noted that no glue is deposited on the channel walls due to the configuration of the screen printing process and the small width of the channel structures. Both glue-covered areas are brought together and then pressed together by inserting the plates in a plastic bag in a vacuum pack (Boxer 35, HENKELMAN Vacuum Systems). The bag is exposed to UV light ($100 \text{ mW}/\text{cm}^2$, 365 nm) for 2 min to cross-link the glue, which completes the sealing of the device.

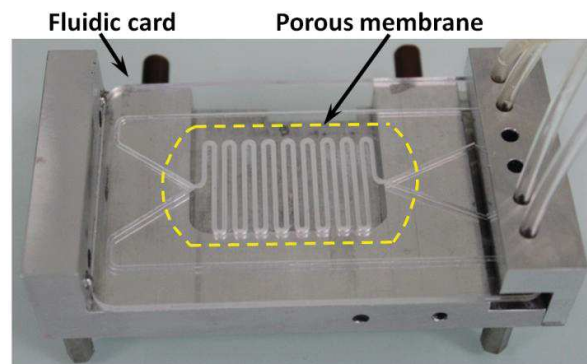


Figure 20. A CCC after glue-based bonding.

Figure 20 illustrates the CCC obtained after fabrication using glue-based bonding. The polycarbonate membrane, which is situated inside the CCC, appears transparent almost everywhere due to the glue wetting. Only the part of the membrane in the snake-like area maintains its white color, which indicates that the glue did not wet this area of the membrane (i.e., by capillarity action for instance). The same kind of observation stands for the PTFE membrane: the areas exposed to the glue turned grey but the area over the snake-like channels kept its color. This indicates that the pore integrity is most likely not compromised for future mass transport. The trans-membrane transport assay further described (see section 4.1.1.1) confirmed this hypothesis.

Thermal bonding versus glue-based bonding

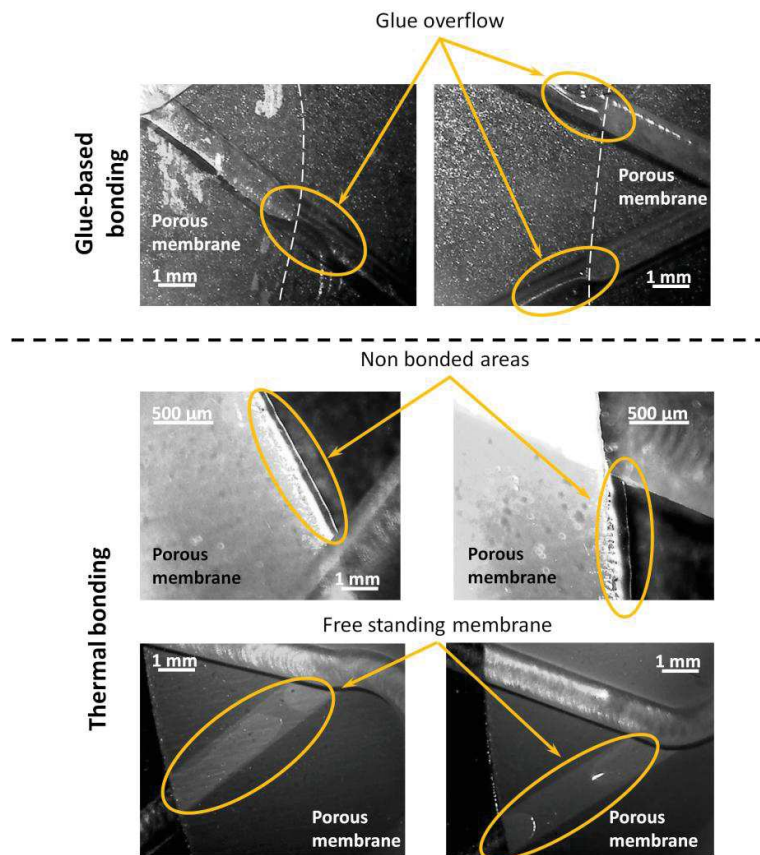


Figure 21. Thermal bonding versus glue-based bonding: microscopic characterization of possible issues. Upper panel: glue-based bonding showing possible overflows of glue inside the channels. Lower panel: thermal bonding showing possible non-bonded areas and free standing membrane areas.

Before running fluidic tests with the fabricated CCC, microscopic observations were performed. Figure 21 gathers the areas that appeared to be relevant to be described for each bonding technique. For the glue-based bonding, some glue could overflow in the channels where the edge of the membrane is located. Particular attention has to be paid as an excess of glue can

clog the channels or block the passage of microcarriers. Controlling the amount of glue deposited avoids blocking the channel but still the glue overflows in the channels. An emulsion can be patterned onto the screen to limit the deposition of glue in the near region of channels. Additionally or alternatively, a sacrificial channel network can be added near these areas to collect the excess of glue[84]. This feature was not implemented in the CCC design since the overflow of glue was small enough not to hinder the proper functioning of the CCC.

For the thermal bonding, a small non-bonded halo was visible all around the membrane periphery. The membrane separates at its edge the PMMA plates which rapidly join together when moving away from the membrane edge. The thermal bonding could not deform enough the membrane or the hard PMMA to achieve a tight sealing locally. As a consequence, a lateral cross flow is possible between the upper and the lower channel. Cross flows must be avoided since they may jeopardize the sterility of the system: if the perfusion medium is contaminated, the contamination can propagate into the channels where cells are growing. Another type of cross flow may occur because the membrane does not stick to the wall of the channel (Figure 22.A). Therefore, when the main stream flows towards the membrane it can be split into one stream flowing above and one stream flowing below the membrane. Modifications in the design can easily overcome these cross flow issues as depicted in Figure 22.B.

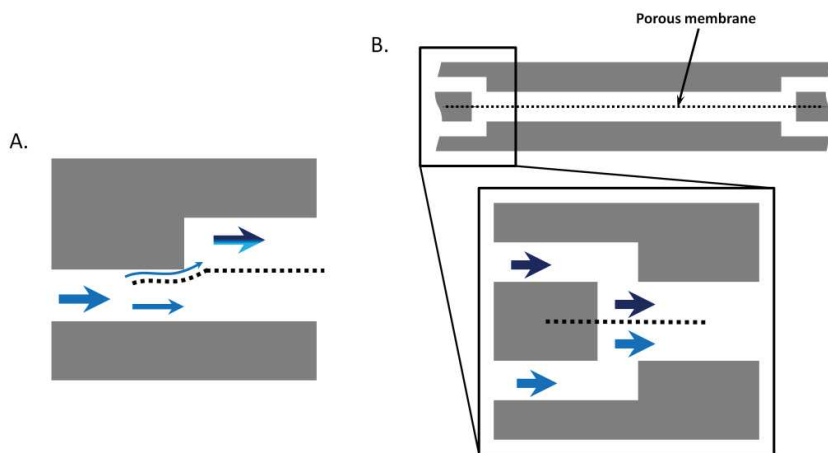


Figure 22. Possible cross-flow after fabrication with thermal bonding (A) and proposition of a design to avoid this issue (B). A) Since the membrane has a free-end which is not attached, the water flow can split. One of the split flow can reach the other channel. B) The improved design sandwiches the porous membrane end in between two layers of PMMA avoiding cross-flow.

Out of the membrane area, the channels shall be milled on the other face of each PMMA plate and join the membrane area by vertical fluidic connections to avoid meeting the edge of the membrane. However, such modifications slightly increase the complexity of the design and the fabrication, and consume more material.

In both methods, the membrane thickness determined if the bonding would be successful or not. The thick membrane in cellulose ester never allowed achieving a successful bonding. Attempts to dig a pocket to compensate the excessive height introduced by the thick membrane did not give satisfying results. The milling machine available failed to create reproducible and uniform pocket heights. Consequently, the use of thick membranes was further avoided.

Interestingly, thermal bonding and screen printing are two industrial processes. The demonstration of their utilization in the fabrication of the CCC promises to impact mass production of microfluidic devices integrating membranes. However, the glue-based bonding technique was preferred since it avoids possible cross-flow and no design improvements were needed. The weaker bonding was sufficient to resist the pressure induced by the low flow rate.

3.3.4 Glue biocompatibility

To perform cell cultures inside a device, the device's constituting elements must be non-toxic. PMMA[135] and Teflon[136] have already been demonstrated to be biocompatible materials when used with cells. However, there were no data available confirming whether the glues present in the host laboratory were biocompatible.

The cytotoxicity of the glues was evaluated in two steps. First, qualitative culture experiments were performed with different glues to identify potential biocompatible candidates. Then, a quantitative assay based on the International Organization for Standardization's ISO-10993-5 was performed on the biocompatible candidates previously identified.

For the qualitative experiments, single drops of UV-cured acrylic 6108-T and epoxies KB4597, KB4594, and OG116-31 were deposited at the center of separated Petri dishes. NIH 3T3 cells were then seeded at $4 \cdot 10^4$ cells/mL in each dish and cultured for 24 h before image acquisition.

The results of this qualitative test are shown in Figure 23.A. Dead cells were characterized by a round shape, whereas healthy cells exhibited an elongated morphological shape. The 6108T acrylic glue and the epoxy KB4597 glue were highly toxic because all cells were found dead. The toxicity of the epoxy KB4594 glue decreased over time. After the second day of culture, cells could accommodate to be cultured with the epoxy KB4594 glue as demonstrated by the reduction of the size of the cell-depleted area. The epoxy OG116-31 displayed a marginal toxicity because the cells appeared to have even proliferated on it. As a consequence, the OG116-31 glue was selected to perform a cytotoxic assay to obtain more quantitative results. However, the KB4594 glue could certainly be used as an alternative to the OG116-31 provided the fabricated system using this glue would be thoroughly flushed or baked before use with cells.

The quantitative assay comprised two types of tests: a contact test in which cells were cultured with the test materials and a conditioning test in which cells were cultured with media

previously incubated with the materials. More precisely, NIH 3T3 cells were inoculated in 6-well plates at a density of $4 \cdot 10^4$ cells/mL in 2 mL of solution. After 24 h, an 8×8 mm² square of the material was added to each well for 24 h for the contact experiment. Silicon dioxide and zinc were used as negative[137] (no death induced) and positive[138] (death induced) control materials, respectively. UV-cured glue OG116-31 was the material that was tested. Triplicate samples were performed for each type of material and for cells not exposed to any material. Additionally, for the conditioning experiment, the medium was changed for each well using 2 mL of the medium exposed to one material over 24 h. Triplicate samples were also performed for the contact experiment and were incubated for 24 h. The materials were then removed, and each well was washed twice with 2 mL of Ca²⁺,Mg²⁺-free Phosphate Buffered Saline (PBS-) solution before adding 1 mL of the culture medium. Cytotoxicity was assessed after 24 h using the WST-1 assay (cell proliferation reagent, Roche), which is similar to the MTT (3-(4,5-dimethylthiazol-2-yl)-2,5-diphenyltetrazolium bromide reagent) assay. WST-1 reagent was added (10% (v/v)) to the culture medium and the plates then were placed in the incubator for 3 h. The absorbance was then recorded at 450 nm (soluble formazan titration) and 690 nm (background subtraction) using a microplate reader (Infinite M1000, Tecan). The absorbance difference (450–690 nm) was directly proportional to the number of viable cells. The percentage cell viability was determined using the following equation:

$$Viability (\%) = 100 \frac{AS - APC}{ANC - APC} \quad (\text{Eq. 11})$$

where AS, APC, and ANC represent the absorbance values of the sample, the positive control (cells with zinc), and the negative control (only cells), respectively.

The results of the quantitative assay are shown in Figure 23.B. In both the conditioning and contact modes, the glue exhibited a toxicity comparable to that of the SiO₂ substrate, which was used as a non-toxic reference material for cells. Consequently, cell proliferation was not expected to be altered by the direct contact of the cells with the OG116-31 glue or by the possible release of the by-products of this glue into the culture media. Therefore, epoxy OG116-31 was chosen to complete the fabrication of the biocompatible device to host mammalian cell culture.

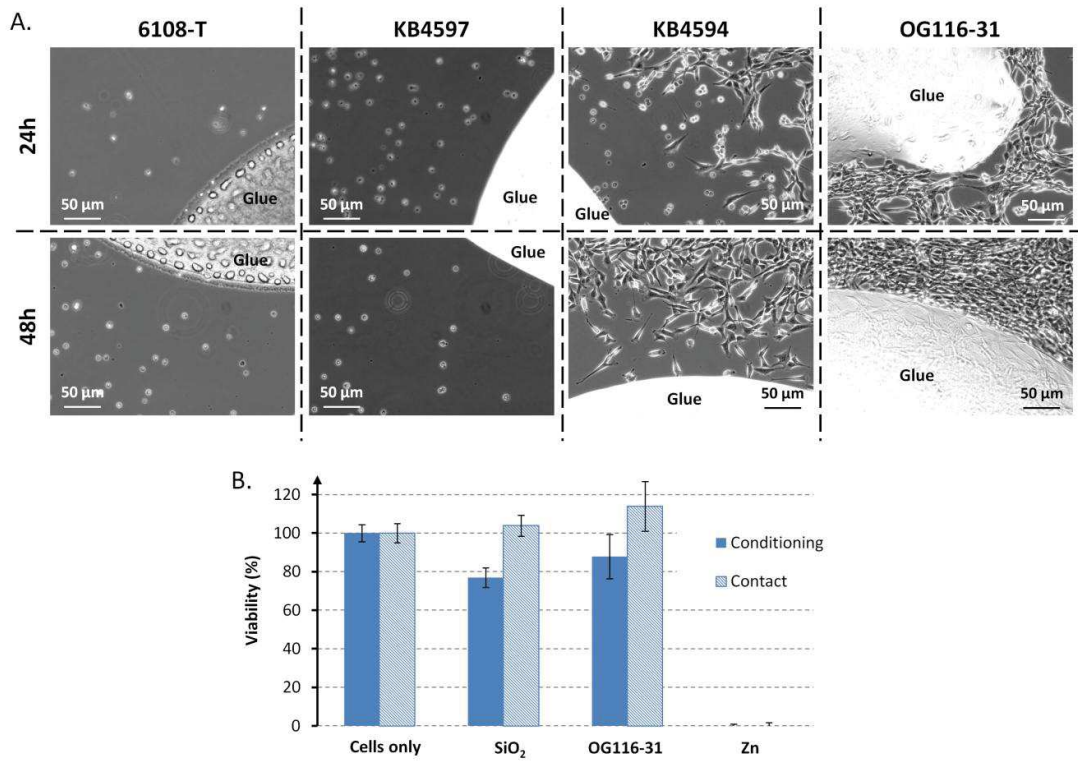


Figure 23. Culture experiments to evaluate the cytotoxicity of the available glues for glue-based bonding. A) Qualitative culture test: cells are simply cultured for 2 days with the glues. OG116-31 appears to be a good biocompatible candidate since cells normally proliferate when exposed to this glue. B) Quantitative culture test: the glue identified with the former test is characterized based on the ISO-10993-5 norm. OG116-31 shows comparable viability than that of SiO₂, a non-toxic reference material.

3.3.5 Leakage tests

To test the successful integration of the different membranes using glue screen printing, leakage tests were performed by perfusing a green and a red stained fluid at 1 mL/min (i.e. 33 mm/s) in the lower and upper channels, respectively. The thick membrane in cellulose ester was integrated by creating a pocket 120 μm deep. The systems incorporating this membrane demonstrated lateral flows of the stained fluids in the membrane area (Figure 24.A). On the other hand, the systems integrating the thinner membranes made in PC or PTFE demonstrated a nice confinement of the liquids over the entire CCC (Figure 24.B). This result sustains their choice to fabricate the perfusion function of the bioreactor.

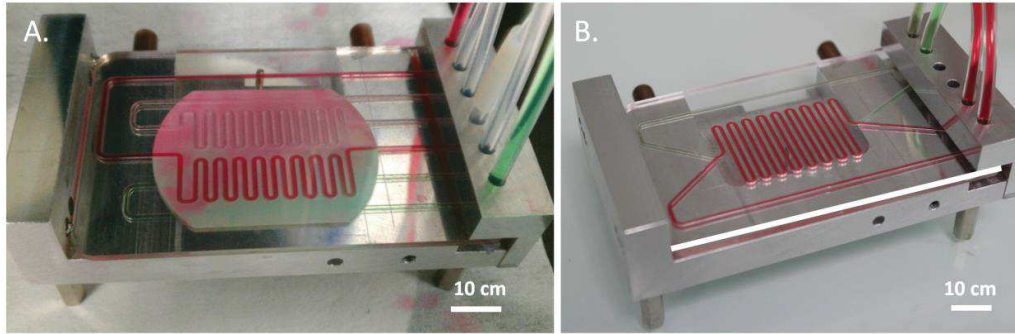


Figure 24. Leakage tests. A) System integrating the thick cellulose ester membrane. The green and red stained fluid could mix and were not well confined. B) System integrating the thinner membrane in PC or PTFE (here PC). No visible mixing, liquids appeared very well confined.

3.3.6 Optical considerations/cell visualization enhancement

To follow the growth state of cell populations inside the bioreactor, the CCC must allow microscopic observations of the cells. Tests to observe the cells inside the CCC were carried out with CCCs integrating the PC and the PTFE membrane, the membranes that allowed a proper bonding. A stereomicroscope (Lumar V12, Zeiss) mounted with a camera (Motic 1000) coupled to an acquisition software (Moticam Plus) was used to observe CCCs filled with media in the lower channel and media with cells on microcarriers in the upper channel. The first attempts to visualize the cells attached to microcarriers inside a CCC integrating the PC membrane were difficult (Figure 25.A) and was possible only in random locations. A lot of time to optimize contrast and brightness was needed to finally observe the cells. The observation of cells out of the PC membrane area were easier and gave better image quality (Figure 25.B). The observation over the PTFE membrane gave fairly good image quality (Figure 25.C). However, the PTFE membrane still introduces a blurred background when comparing with the observations made in the channel areas without the presence of the membrane.

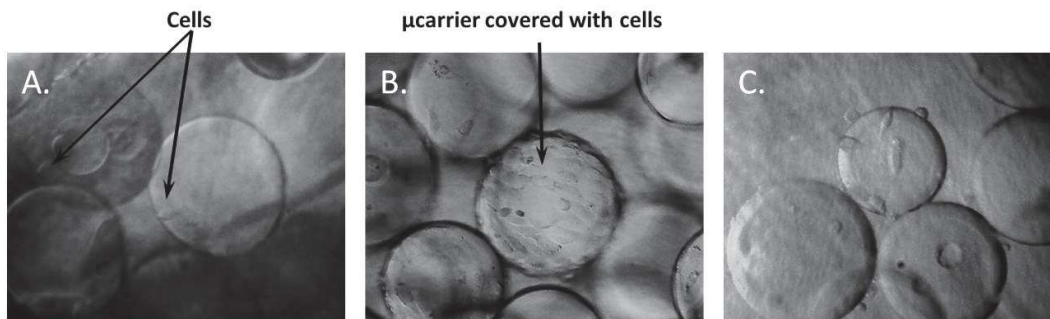


Figure 25. Microscopic observations of cells on microcarriers inside the CCC filled with media. A) Observation over the PC membrane. B) Observation out of the PC membrane area. C) Observation over the PTFE membrane. With the PTFE membrane the cell visualization is enhanced and almost comparable to observations made out of the membrane area.

3.3.7 Conclusions

Three different commercial membranes involved in bio assay applications were considered for incorporation of the perfusion function inside the CCC. Based on the results obtained with the bonding and microscopic observations, and combined with the diffusion time estimations, the hydrophilic PTFE membrane was selected as the best candidate (see Table 7). Its low thickness allowed successful bonding, and its optical properties provided the best cell imaging. However, the visualization through a porous membrane inevitably lowers the resolution of live cell imaging. The PC membrane remains a possible alternative though offering poor optical observation.

Table 7. Qualitative summary of the performance of each membrane tested according to the diverse criteria considered.

Criteria Membrane	Mass transport time through the membrane	Compatibility with bonding methods	Cells observation
Cellulose ester	~	✗	✗
PC	✓	✓	~
PTFE	✓	✓	✓

Two bonding methods were investigated for integration of the porous membranes and bonding the CCC: thermal bonding and glue screen printing. Leakage-free systems could be obtained with both techniques. However, the design of the CCC needs to be adapted to avoid possible cross flow in the case of thermal bonding. Glue screen printing offered a simple and biocompatible way to compensate the excess of height introduced by the membrane. Despite the occasional overflow of some glue in the channels, there was no need to modify the CCC design to provide a good liquid confinement.

The glue-based bonding technique was preferred due to its advantages and because the advantages had low impact later when operating the CCC (see Table 8).

Table 8. Summary of the pros and cons of each bonding method investigated.

	Pros	Cons
Thermal bonding	<ul style="list-style-type: none"> ➤ Biocompatible ➤ Strong bonding 	<ul style="list-style-type: none"> ➤ Possible cross-flow with membrane integration ➤ Longer process (1h)
Glue-based bonding	<ul style="list-style-type: none"> ➤ Biocompatible ➤ Better membrane integration ➤ Faster process (30 min) 	<ul style="list-style-type: none"> ➤ Weak bonding ➤ Possible fluid flow perturbation due to glue overflow in channels

4 Cell proliferation

This chapter details the strategies considered to provide a suitable environment for cell proliferation (section 4.1) and to perform cell harvest (section 4.2).

4.1 Control and monitoring of the cell environment

In this section is addressed the issue of providing a proper environment for cell proliferation considering the main cell needs: nutrients, oxygen, temperature and pH. The following section describes the methodologies and the achievements obtained with respect to these aspects. First, the perfusion was studied by (i) evaluating the ability of the membrane to allow mass transport (ii) simulating the perfusion to optimize it in order to provide a stable biochemical environment to the cells. The monitoring and regulation of the temperature was then developed. Finally, different approaches to regulate the pH were investigated.

4.1.1 Porous-membrane-based perfusion

4.1.1.1 *Trans-membrane transport for nutrient supply*

After fabricating the CCC, the ability of the membrane to enable trans-membrane transport was evaluated. The porous membrane must allow trans-membrane transport to fulfill its function. Cells should be able to receive the necessary nutrients and oxygen and to have their waste cleared (e.g., ammonia, lactate). Diverse verifications were carried out to determine if the performance of the system is not hindered after fabrication. These verifications involve a perfusion experiment, and a numerical and theoretical model of this perfusion. The aim is to correlate the perfusion experimental data with the different models to evaluate if the device behaves as expected. Additionally, comparing the perfusion experiment and the theoretical model with the numerical model will allow this numerical model to be validated to later adapt it for the simulation of the microbio reactor cell culture. In other words, the aim here is also to develop a first numerical model, validate it, and then improve it to simulate the culture occurring in the bioreactor.

Practical experiment: a red solution was prepared by diluting 300 μL of a red food dye (azorubin E122, McCormick) in 50 mL of PBS-. The red solution was co-currently perfused into the lower channel of the device, at the same rate as the color-free PBS- solution dispensed into the upper channel. In this configuration, no convection across the membrane was possible due to the equal pressure in each channel; only diffusion could occur across the membrane. The flow rates tested were 10, 30, 100, 300, and 1,000 $\mu\text{L}/\text{min}$. For each flow rate, the liquids were collected at

the outlets of the device, and 200 μL of the collected solutions were dispensed in a 96-well plate and analyzed using a microplate reader (Infinite M1000, Tecan) to measure their absorbance level. The chosen red food dye has a molecular volume (or particle radius), and therefore, a diffusive property comparable to that of the cell culture media constituents considering the Stokes-Einstein relation:

$$D = \frac{k_B T}{6\pi\mu a} \quad (\text{Eq. 12})$$

where k_B is the Boltzman constant, T the temperature of the medium surrounding the particles, μ the dynamic viscosity of the medium surrounding the particles and a the particle radii.

Azorubin has a molar mass of 502 g/mol and a density of about 1.6 g/cm³ meaning a molecular volume of about 520 \AA^3 (i.e. a radius of 0.5 nm) using (Eq. 13):

$$V = M / (10 \cdot \rho \cdot Na) \quad (\text{Eq. 13})$$

where V is the molecular volume (in \AA^3), ρ the density of that molecule (in g/cm³), M its molar mass (in g/mol) and Na the Avogadro number. As an example, for comparison, glucose has a molar mass of 180 g/mol and a density of 1.54 g/cm³ meaning a molecule volume of 194 \AA^3 (i.e. a radius of 0.4 nm). Appendix C gives a rough comparison between azorubin and the many components of cell culture media. Azorubin has a molecular size comparable to many of the medium components (sugars, salts, amino acids[139]).

Numerical model: this model is a simple stationary 2D COMSOL model which is representative of the configuration in the culture area and simulates the previous experiment. Two channels of length L and height H are separated by a porous membrane of length L , height h_m . A flow rate Q is applied to each inlet. A concentration c_0 is initially present in the lower channel and perfused at the lower channel's inlet. The physical equations used in each domain and the different variables are referenced in Appendix D. This model will be later adapted to simulate the perfusion of the cells through a porous membrane (see next section)

Theoretical model: this model describes the relationship between the flow rate perfused and the concentration at each outlet. The concentrations can be defined by the following equations:

$$\frac{C_{bot_out}}{C_{in,azo}} = \frac{1}{\left(1 + \sqrt{\frac{DWL}{2QH}}\right)} \quad (\text{Eq. 14})$$

$$\frac{C_{top_out}}{C_{in,azo}} = \frac{\sqrt{\frac{DWL}{2HQ}}}{\left(1 + \sqrt{\frac{DWL}{2QH}}\right)} \quad (\text{Eq. 15})$$

where C_{bot} is the average concentration at the lower channel outlet and C_{top} the average concentration at the upper channel outlet. This model does not take into account the membrane and is similar to a regular mixing occurring in a common T-channel device. The complete description to derive the formulas above is given in Appendix E.

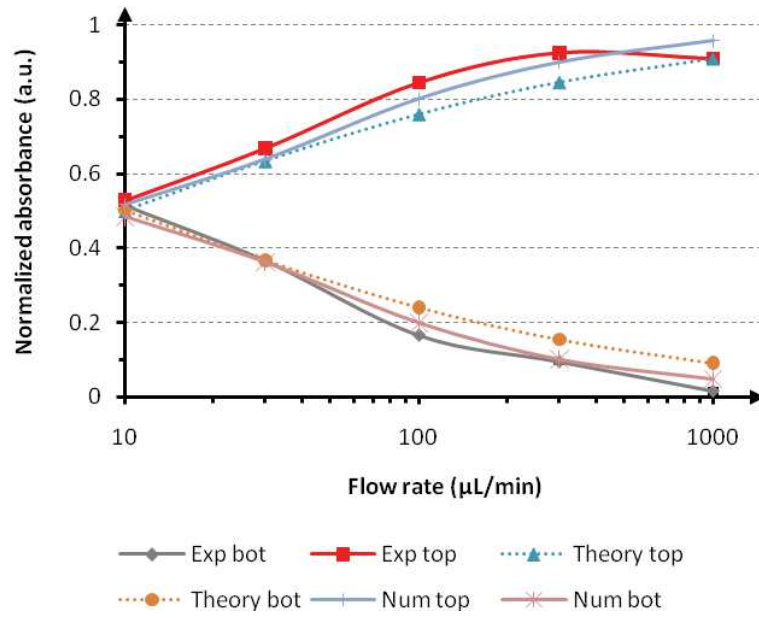


Figure 26. Absorbance levels, measured from the practical experiment and evaluated from the numerical and analytical computation, as a function of the flow rate. As the flow rate decrease, the time allowed to the red die to diffuse from one channel to the other is increased. Therefore, with decreasing flow rates, the absorbance of the collected liquids from the top channel decreases while the absorbance of the collected liquid from the bottom channel increases until merging around 10µL/min.

Exp top: experimental data from the upper channel, Exp bottom: experimental data from the lower channel, Theory top: theoretical data from the upper channel, Theory bot: theoretical data from the lower channel, Num top: numerical data from the upper channel, Num bot: numerical data from the lower channel.

The absorbance levels measured or evaluated are shown in Figure 26. A lower flow rate resulted in closer absorbance values. Indeed, for flow rates less than or equal to 10 µL/min, the absorbance values were equal to half of the maximum absorbance (i.e., the absorbance of the stock red solution), which indicates that a complete exchange of the red dye occurred from one channel to the other through a diffusion process. Therefore, the possibility of trans-membrane transport across the porous membrane with this molecule confirmed that nutrients can diffuse as well across the membrane to feed the cells.

The models and the experimental data fit quite well. However, the theoretical model slightly diverges with increasing flow rates. These results confirm that the models are well representative of the experiment. As a consequence, the impact of the membrane on the diffusion of the media components can be fairly neglected here and the device can be

assimilated as a regular T-channel device. Additionally, it verifies that the membrane area is not altered, by glue wetting clogging the pores for instance, so that mass transport would be impaired. The performance of the device is therefore complete.

4.1.1.2 Simulation of the biochemical environment during perfusion

The next step after validating that transport can occur through the porous membrane is to identify a suitable flow rate for perfusion. Such a flow rate should minimize the amount of medium spent while providing an adequate biochemical environment in terms of nutrients, oxygen and wastes. In order to avoid many long experimental trials, the choice to perform numerical studies was adopted. Finite element simulations were performed (COMSOL, Multiphysics 4.3a) to determine the perfusion flow-rate to maintain the cell culture. The stationary 2D model that was built is representative of the cross-section along the snake-like channels where media renewal occurs. The “Porous media” and “Diluted species” modules from COMSOL were used as the governing physics in this model. Comprehensive details about the model, the governing equations and the parameters values used for these simulations are given in Appendix F. Stationary studies were carried out with a fixed cell density. This density was taken as the maximal cell density obtainable considering the total growth surface provided by the microcarriers and was adapted to the cell type. As a result, the simulations give the state of the biochemical environment in the end of a culture performed in the bioreactor.

Two cell models were considered to perform mammalian cell cultures with the bioreactor and therefore for these simulations: mouse embryonic fibroblasts cells (NIH 3T3) and epithelial prostate cancer cells (PC3). Fibroblasts cells are commonly involved in cytotoxicity studies[140], for the ISO-10-993 norm for instance, and were routinely cultivated in one of the host laboratories. PC3 cells were routinely cultivated by the other host laboratory since this laboratory is mainly focused on the study of prostate cancer. In each case, the metabolic activity of the cells was adapted to the cell line for simulations. Since cell metabolic activity involves enzymes, a Michaelis-Menten kinetics is usually adopted to describe the uptake rate by the cells and has been considered for simulations:

$$\frac{dC}{dt} = -\frac{V_M \cdot \rho_c \cdot C}{K_M + C} \quad (\text{Eq. 16})$$

where C is the substrate concentration, V_M is the saturated consumption rate per cell, K_M is the substrate concentration which yields a consumption rate equal to half of the saturated rate (see graph in Figure 53 of Appendix F), and ρ_c is the cell density.

The simulations focused on the distribution of two vital substrates for cell metabolism activity: glucose and oxygen. Since the accumulation of cell wastes are known to affect cell growth, a study on the lactate distribution was carried out in the case of PC3 cells.

Perfusion flow rates of 1, 5, 10, and 50 $\mu\text{L}/\text{min}$ were screened to analyze glucose and oxygen (and lactate) distribution in the modeled bioreactor. Since the concentration gradient (i.e. variation of the concentration per unit distance) along the height of the bioreactor was small in each case, only the concentration at the middle height of the culture channel and along the channel length were considered.

In the first place, glucose, oxygen and lactate distributions were compared for devices integrating the PTFE membrane (retained as the most suitable membrane) and the PC membrane (less suitable but still a viable option to build perfusion systems). Figure 27 shows this comparison. For each molecule, the concentration distribution was similar disregarding the membrane type used. This is in accordance with the observation made in the previous section that these membranes due to their characteristics (i.e. thickness, porosity, tortuosity, constrictivity) have a negligible impact on mass transport.

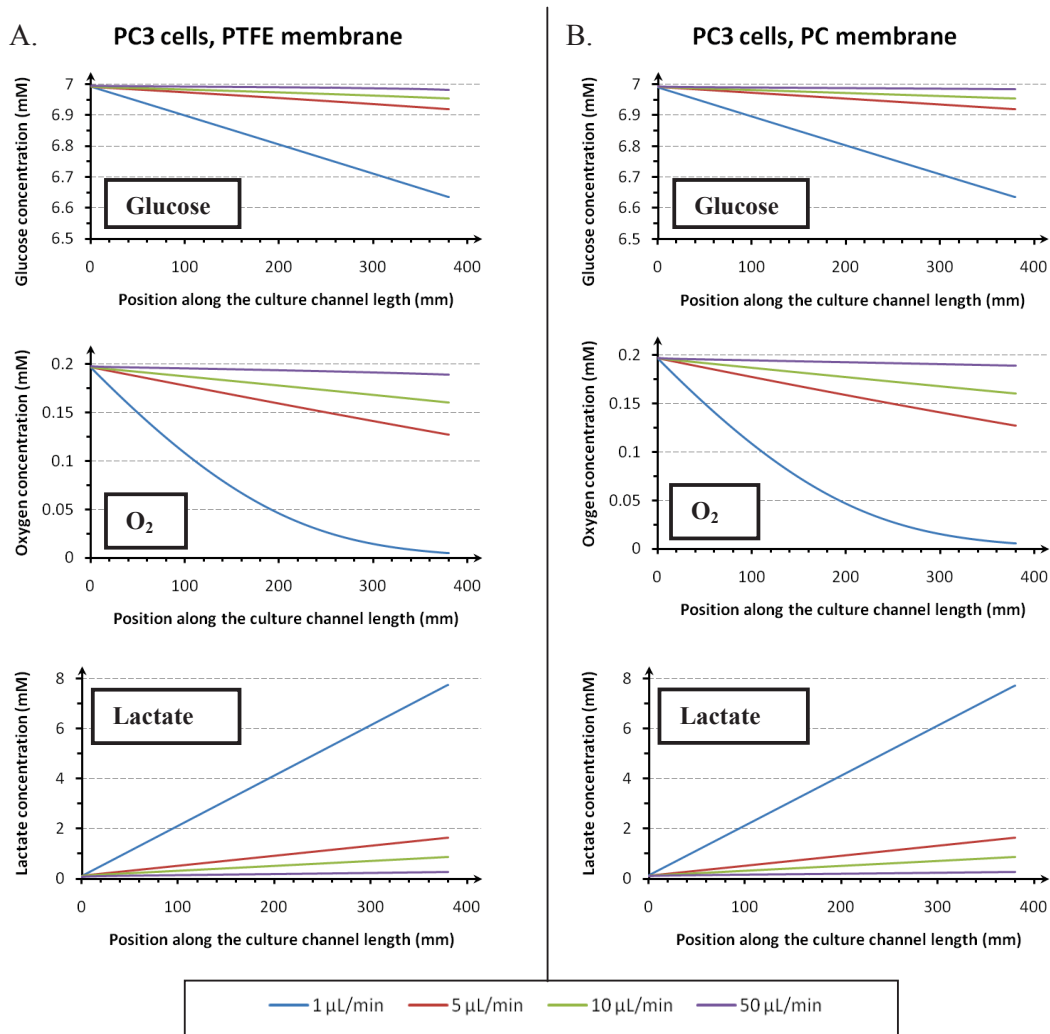


Figure 27. Glucose, oxygen and lactate concentration distribution in the culture channel based on FEM simulations. A) Simulations considering the PTFE membrane. B) Simulations considering the PC membrane.

Moreover, these results also evidence the relation between the perfusion flow rate and the concentration variation for each species. For the consumed species, the levels decreased along the culture channel length. Conversely, the levels of the species produced increased along the channel length. These concentrations vary linearly with the position along the culture channel length except for oxygen when a flow rate of 1 $\mu\text{L}/\text{min}$ is applied. The variation of the gradients according to the flow rates followed the same trend for all the species: the lower the flow rate is, the higher the gradient is. This can be simply explained by the competition between the rate at which new molecules are reintroduced with the perfusion and the rate at which these molecules are consumed by the cells. In the case of cell wastes, it is a competition between the rate at which these are produced by the cells and the rate at which the perfusion will remove them from the culture area.

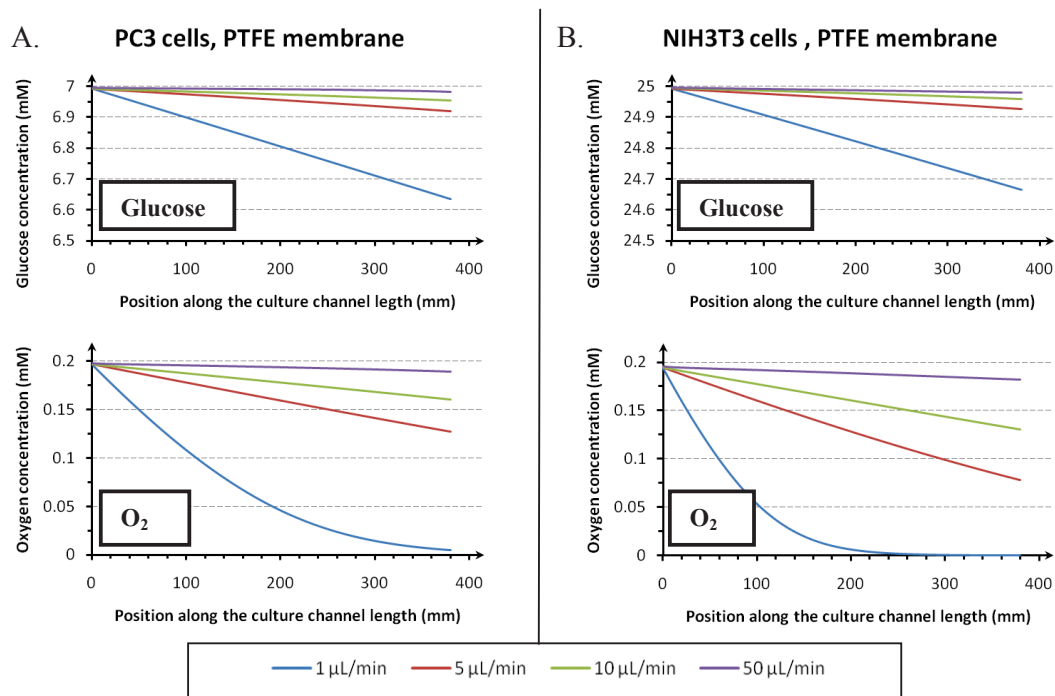


Figure 28. Glucose and oxygen concentration distribution in the culture channel based on FEM simulations. A) Simulations considering the culture of PC3 cells. B) Simulations considering the NIH3T3 cells.

Figure 28 shows the level of glucose and oxygen for the culture of PC3 cells and NIH3T3 cells. Comparable glucose gradients according to the flow rate can be observed between these two cell types. However, oxygen gradients are more pronounced in the case of NIH3T3 cell culture.

The determination of the perfusion flow rate was based on several criteria. The first one is the concentration profile obtained for the species according to the perfusion flow rate. In this case, the higher the flow rate, the merrier. This criterion is balanced by the second one which aims at limiting an excessive consumption of medium. Eventually, the choice was based on a practical constraint from the available equipment to establish the perfusion. Indeed, a syringe pump system was used to perfuse the bioreactor. This syringe pump was rather old and properly functioned with a syringe having a maximum volume of 10 mL. When adding the dead volume of the tubing and the fact that the syringe pump does not empty the syringe, the effective volume for perfusion was about 5 to 7 mL. In order to be able to perform overnight perfusion without human intervention to refill the syringe with media, a flow rate of 5 $\mu\text{L}/\text{min}$ was eventually adopted for the perfusion of the bioreactor. With this flow rate, the simulation shows that the oxygen level may impact the cell culture (variation >50%). If it is the case, the design of the bioreactor could be modified to shorten the length of the culture channel.

It has to be argued that the previous simulations strongly depend on the Michaelis-Menten parameters describing the metabolic activity of the cells. Finding the proper Michaelis-Menten parameters was a tedious task. In many cases the units of the Michaelis-Menten parameters

could not be simply converted into the software units since certain data were not readily available (e.g. cell density). Only a few studies on the specific cell types considered here were available. Therefore, it was not possible to corroborate the values found with other works.

Additionally, the Michaelis-Menten parameters found in the literature have to be considered as apparent values. In reality, the consumption or the production by the cells of the different species cannot simply be described with a simple Michaelis-Menten kinetics since these consumptions or productions are regulated by many enzymatic processes. Therefore, (Eq. 16) should more complex to be completely representative, but in practice such characterization of the cell metabolism activity is hardly achievable and rarely performed.

4.1.2 Thermal management

Temperature was the next parameter to address to provide a proper environment for mammalian cell proliferation. In the first place, the selection and integration of a commercial sensor were realized before investigating the thermal regulation using different heaters.

4.1.2.1 Sensor integration

Three classes of sensors are preferably integrated into microbioreactors: thermistor, resistance temperature detector (RTD) or thermocouple[141]. Thermistors and RTDs function similarly: their resistance varies according to the temperature they are exposed to. Thermocouples exhibit a potential proportional to the temperature due to the so-called Seebeck effect. Thermocouples, thermistors and RTDs are commercially available and exist in small dimensions (around 1 mm³ or less). For a standard cell culture, there is no real advantage to use one or the other.

A RTD sensor was chosen for thermal read-out. A Pt100 RTD sensor with dimensions L:1.2, W:1.6mm, H:1mm was purchased from Farnell (Ref: 1289670) and a 2510 TEC source meter Kethley was used for thermal read-out. Different configurations were tested to integrate the sensor on the former version of the CCC (Figure 29). In each case the sensor was positioned closed to the culture channel or even inside the culture channel to measure the most precisely the temperature to which cells are exposed. Thus, the first sensor was placed vertically in a recess of the culture channel so that medium temperature could be directly measured. The second was placed vertically 200 µm removed from the culture channel and at mid height of the culture channel. The last one, was inserted horizontally 200 µm closed to the culture channel and at the middle height of the culture channel. The bonding glue was used to fix the sensors into their trench.

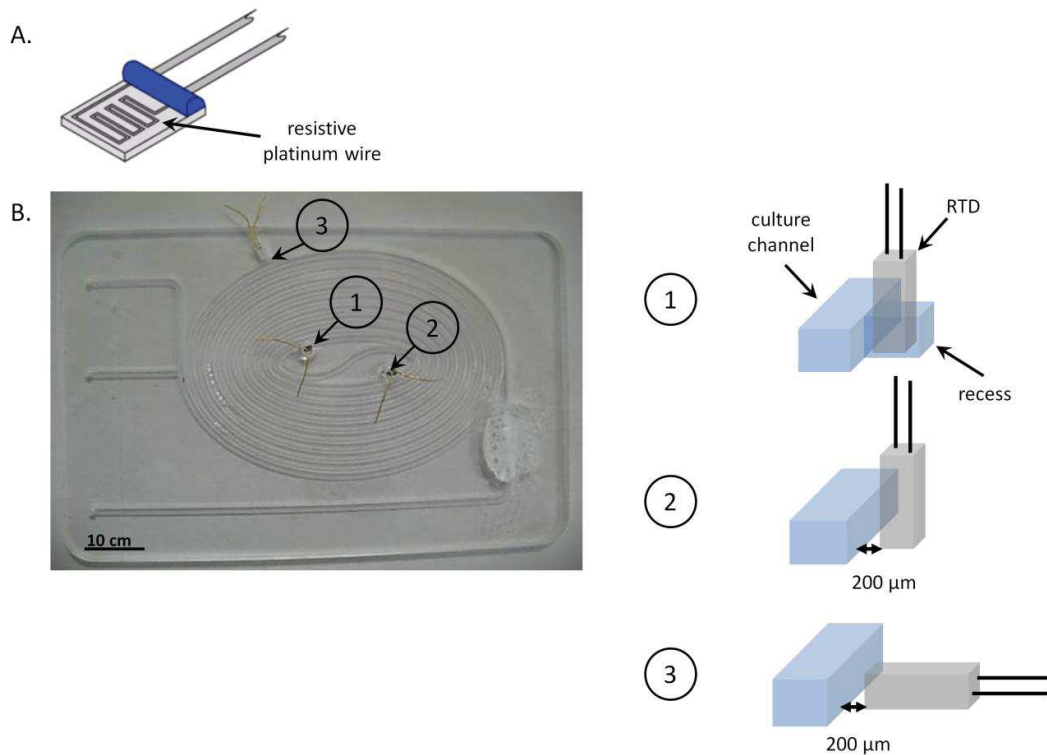


Figure 29. The thermal sensor and the different configurations tested for its integration in the CCC. A) Schematic representation of the resistance temperature detector (RTD). B) The three configurations tested for the integration of the RTD. 1: vertical position in a recess of the culture channel, 2: vertical position 200 μm far away from the culture channel and 3: horizontal position 200 μm far away from the culture channel. In blue, the fluidic channel and in grey, the RTD.

Although the first configuration appeared as the most suitable to measure the temperature of the cell environment, it was not practical as air bubbles could easily get trapped at the level of the recess when filling the culture channel. No major differences were observed with the two other configurations from a practical point of view and for measurement tests.

4.1.2.2 Scaling down the heater

The critical goal of thermal management in cell culture systems is to provide a uniform heat across the culture area. Taking this point into account, thermal regulation of microbioreactors has been addressed by different techniques. For instance, incubators have been used to control the temperature of cell culture systems[128,141]. However, incubators are relatively large compared to the culture system. They can host several systems at once but will not allow independent control of the temperature in each system. Another approach is to flow thermostated water from a hot water bath through the base of the culture system. Such a strategy increases the space occupied by the entire culture setup since the hot water bath is usually large. More integrated solutions such as hot plates/sheets or electrical microheaters can be used to control the temperature of a culture system. With microheaters, the temperature of

several microcultures can be independently regulated but more development is needed to ensure an even heat distribution is provided. This is mainly due to the high surface-to-volume ratio usually present in microbioreactors which may lead to large heat dissipation and the apparition of strong thermal gradients. For the parallel operations of several microheaters insulation must be implemented to prevent thermal cross talk.

Three setups were investigated to control the culture temperature of the CCC: the flow of thermostated water through the base holder of the CCC (Figure 30.A), the insertion of a Peltier element in a cavity in the base holder right beneath the culture area (Figure 30.B) and the insertion of a thin transparent plastic sheet coated with a metal layer in between the base holder and the CCC (see Figure 15). These setups were analyzed using an infrared (IR) thermal camera (Flir A20). This tool allowed a rapid characterization of the thermal distribution homogeneity granted by each approach.

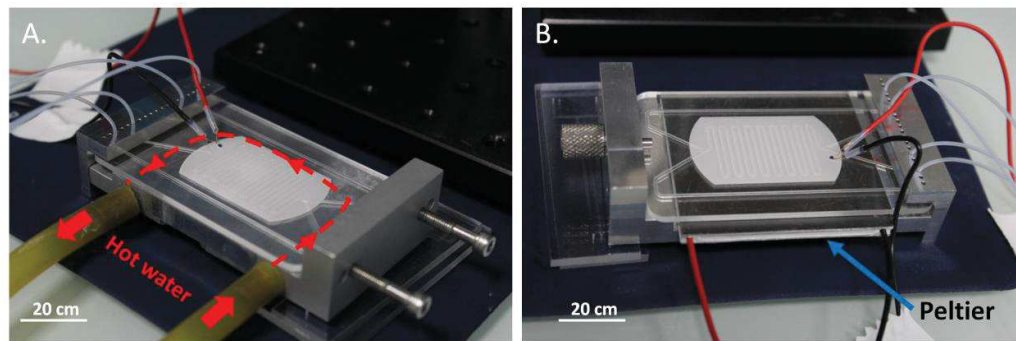


Figure 30. Thermal regulation setups. A) Thermostated water flowing in the base holder heats the entire system. B) A Peltier element heats the CCC.

Initially, the regulation of the temperature was achieved by thermostated water flowing into the aluminum CCC holder. This was the first option easily available in the host laboratory. A U-shaped copper pipe was inserted into the base holder. The use of aluminum (holder) and copper (pipe) demonstrated, as expected, an efficient thermal transfer of the heat from the warm water to the CCC. As already reported, this solution was not very practical due to the large footprint associated to the use of a hot water bath (Figure 31) despite the good homogenous thermal distribution it provided (Figure 32.A).

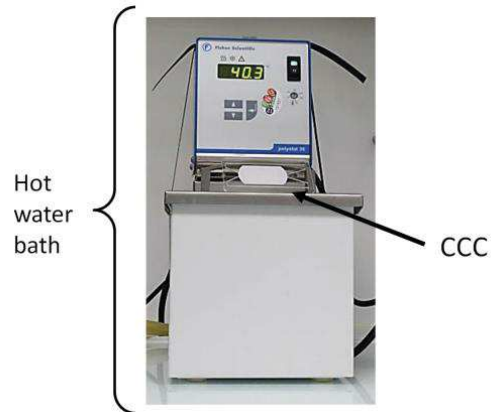


Figure 31. Size comparison between the CCC and the hot water bath used.

In that way, the other scaled-down heating systems represent a better approach. The Peltier was purchased from Farnell (Ref: 1639739). When a voltage difference is applied across the Peltier element, one of its plates becomes hotter while the other one becomes colder. The TEC source meter served as a power supply for the Peltier. The thermal homogeneity that was produced by the Peltier element was comparable to the regulation provided by the thermostated water (Figure 32.B). The thin transparent sheet coated with a metal layer consists of a 200- μm -thick polyethylene terephthalate (PET) sheet coated with 400 nm of indium tin oxide (ITO). A silver-filled epoxy glue (EPO-TEK[®], H20E, Epoxy Technology, Bussy-Saint-Georges, France) is deposited sideways along the length of the sheet onto the ITO layer to create the electrodes. Once an electrical current flows through the resistive ITO layer thermal energy is generated by Joule effect. The thermal distribution is analog to the previous setups (Figure 32.C). The interesting feature with this PET-ITO heater is that it is completely transparent and does not alter cell observation. Several systems in the literature have used this approach for this purpose[142,143,144,145,146]. In the current configuration, this feature is not really exploited as it was easier to have a better contact with the CCC by inserting the heater in between the holder and the CCC. However, one could consider positioning this layer on top of the CCC, provided there is good contact with the CCC. Having a PET-ITO heater on each side of the CCC could also cancel the actual vertical temperature gradient without compromising the optical observation. For instance, the bioreactor is characterized by a thermal difference of 3.4°C between the top face and the bottom one (see Appendix G).

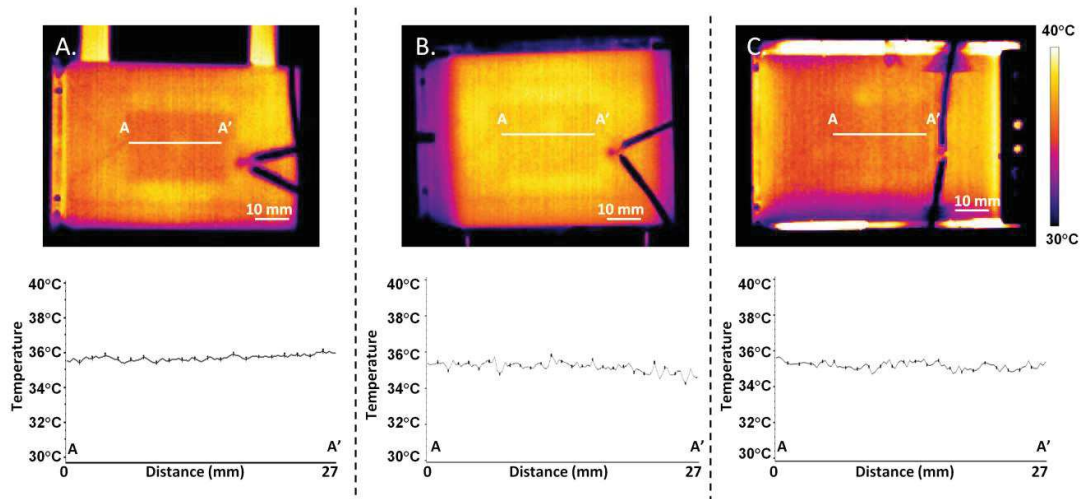


Figure 32. Thermal characterization by IR imaging. A) Regulation based on thermostated water. B) Regulations based on Peltier element. C) Regulation based on PET-ITO heater. Each type of regulation demonstrates a homogeneous thermal distribution around the desired temperature of 35.4°C

4.1.2.3 Thermal management considerations

In each case heat was applied on the lower part of the CCC. A vertical thermal gradient was induced as a result since the opposite part of the CCC was exposed to ambient air. This gradient has been taken into account to provide a temperature of 37°C at the middle height of the culture channel. In

Appendix G the temperature along the CCC height is evaluated. Assuming that measuring a temperature of 37°C with the IR camera or the thermal sensor is sufficient to provide the right temperature for cell culture is incorrect. Indeed, the IR camera only reads the temperature on top of the CCC while it has been observed (with thermal imaging) that the temperature where the thermal sensor is inserted is locally lower (Figure 32) than the rest of the CCC (~1.5°C). Considering that the target temperature to read by the IR camera or the thermal sensor should be of 37°C is likely to provide a higher temperature in the culture channel. As highlighted in the introduction, over-heating the culture of a few degrees may jeopardize the culture as cells can hardly survive over 40°C[23]. As a consequence of this observation, the target temperature to reach during the tests performed to characterize the different heating setups was of 35.4°C with thermal imaging. During the culture tests, the monitoring of the temperature, which only relied on the thermal sensor readout, had a target temperature of 34°C.

To conclude on this part, scaled-down solutions to regulate the bioreactor temperature were found to have comparable performance as the use of a cumbersome regulation based on thermostated water. Among these scaled-down solutions, the PET-ITO heater appeared as the most integrated solution due to its low thickness and simple implementation. It also has the

great advantage to be transparent, allowing microscopic observations. Based on these criteria, this type of heater was further used to control the microfluidic bioreactor temperature.

4.1.3 pH regulation

Regular cell culture media achieve a stable pH of 7.2-7.4 when they are immersed in 5% CO₂ atmosphere controlled by the incubator in which cell culture is performed. The regulation of the pH occurs through acid-base reactions based on bicarbonate equilibriums (see (Eq. 1) and (Eq. 2) in section 1.4.2.3). However, in a normal atmosphere (0.04% CO₂) the pH of these media drifts towards higher values since the CO₂ escapes from the liquid phase in accordance with the bicarbonate equilibriums. Different approaches have been validated in the literature when working out of an incubator. Some works have added a HEPES buffer to the culture media in order to maintain the pH[93,147]. HEPES is a zwitterionic buffer meaning that it presents an equilibrium between two neutral forms: one presenting no distinct charge and one presenting simultaneously opposite ionic states (positive and negative charges) negative and a positive charge. Exposition to ambient light should be minimized when working with HEPES since it has been demonstrated that toxic reactive oxygen species can be generated[148]. Alternatively, perfusion culture systems operated outside CO₂-regulated incubators have relied on commercial CO₂-independent media[149]. These media regulate the pH through a combination of free basic amino acids, phosphate buffers and higher levels of galactose and sodium pyruvate[150]. As a result, the medium does not require supplementation with sodium bicarbonate and can be used under atmospheric level of CO₂. Finally, microfluidic cell culture systems have implemented CO₂ exchangers to replenish the media with CO₂ before perfusing the cells[151,152].

All the cultures of mammalian cells performed within the bioreactor were realized using standard culture media. However, such media are not suitable for long term cell culture outside a CO₂ incubator. Therefore, the use of HEPES supplemented medium or CO₂-independent medium was investigated based on the literature. Specific DMEM medium containing 25 mM of HEPES (DMEM-HEPES) for NIH3T3 cell culture was purchased from Life Technologies (Ref: 21063-029). A CO₂-independent media (L-15) was also bought from Life Technologies: Leibovitz's L-15 Medium, GlutaMAX™ Supplement (Ref: 31415-029). This medium was the closest in composition to the DMEM medium with red phenol (DMEM-Phenol Red) used for the routine culture of NIH3T3 (Ref: 41966-029).

Initially, pH measurements at different time points were performed to evaluate the stability of these media under atmospheric conditions. A pH-meter (InLab® Micro Pro, Mettler Toledo) was used to measure the pH of 1 mL of medium contained in a 2 mL vial (Eppendorf) for each condition. Results are shown in Table 9. Unfortunately, the pH electrode was not calibrated at

37°C for measurements at this temperature. Considering that pH electrodes are temperature-sensitive (Nernst equation) there is most likely an overestimation of approximately 0.4 pH in the temperatures acquired at 37°C.

Table 9. pH measurements of different type of culture media after exposure under atmosphere at different time point.

Media	pH			
	stock solution	Incubator (5% CO ₂ , 37°C)	20 min, open air, room temperature	1h30, open air, room temperature
DMEM-Phenol Red	7.87	7.78	8.18	8.51
DMEM-HEPES	7.01	7.11	7.63	7.90
L-15 (CO ₂ -indep.)	7.46	-	7.53	7.54

The DMEM-Phenol Red medium has the highest drift (0.7 pH) over time and is the furthest from the recommended pH range for cell culture (7.2-7.4). The DMEM-HEPES present a lower drift but still is out of the recommended range. The literature studies that relied on the addition of HEPES to regulate the pH used higher concentrations, up to 60 mM[93], compared to the 10 mM in the DMEM-HEPES medium here. Concentrations higher than 40 mM may exhibit toxicity[150]. Therefore, increasing the HEPES concentration is a double-edged sword. Moreover, HEPES only slows the pH drift but cannot prevent the CO₂ (from hydrogenocarbonate ions) to escape. For these reasons HEPES was not considered as a viable option to regulate the pH.

As expected, the L-15 medium presents a relatively stable pH value over time (0.1 pH variation). L-15 appeared as an interesting solution to perform long term cell culture under CO₂ atmospheric conditions and was further used to perform comparative proliferation tests with the standard DMEM-Phenol Red medium. NIH3T3 cells were inoculated in 2 mL of either DMEM-Phenol Red medium or L-15 medium in Petri dishes at 4·10⁴ Cells/cm² (i.e. 2·10⁴ Cells/mL). Triplicates were performed for each day of culture and for each medium. The cells cultured in DMEM-Phenol Red were placed in a 5% CO₂ incubator and cells cultured in L-15 were placed in a 0% CO₂ incubator. Cells were harvested (trypsinization) daily and counted with a sceptor (Merck-Millipore).

NIH 3T3 proliferation in CO₂-dependent vs. CO₂-independent media

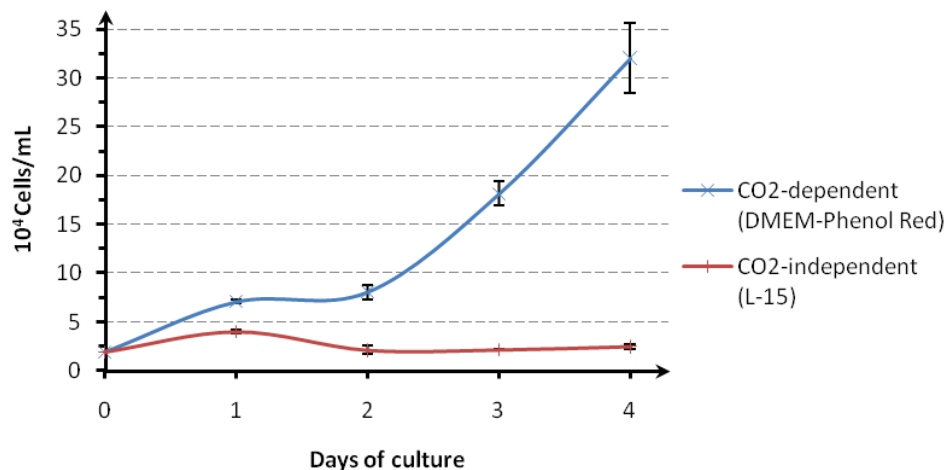


Figure 33. NIH 3T3 proliferation in CO₂-dependent vs. CO₂-independent media (N=3). Cells cultured in the CO₂-independent medium do not proliferate as expected; the cell population remains constant over time instead of growing exponentially as seen in the standard culture medium.

The comparative proliferation test is shown in Figure 33. NIH3T3 population remained constant over 4 days of culture while the cells relatively followed the common pattern of cell proliferation when cultured in DMEM-Phenol Red. The L-15 medium proved to be inadequate for the cell culture of NIH3T3 cells which seemed to be blocked at a certain phase of their division cycle. It is possible that cells need to be adapted to the culture with L-15 medium to achieve a normal growth as suggested by the supplier. Such adaptation could be achieved by culturing the cells in a humidified incubator without CO₂, first, with 50:50 ratio of L-15 and DMEM-Phenol Red. Then, after subculture cells should be cultured in a 75:25 ratio of L-15 and DMEM-Phenol Red. And, finally, the next culture can be performed in 100% L-15 medium.

The different approaches tested were not convincing to promote cell proliferation while maintaining a stable and suitable pH for long term cell culture outside an incubator. Further literature research lead to an interesting patent and commercial product based on this patent. The device is called Petaka™ from Celartia™. It is an engineered system dedicated to culture cells under atmospheric conditions by limiting water evaporation, enabling oxygen mass transport and preventing CO₂ escape. Thus, the medium level remains stable during cell culture, cells can receive oxygen and pH does not drift due to CO₂ escape.

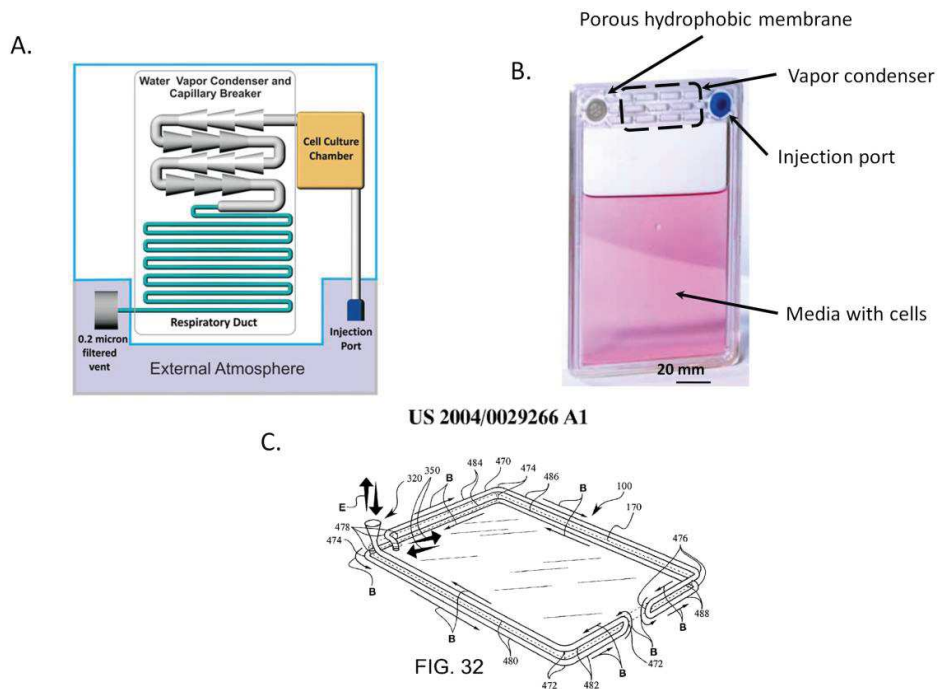


Figure 34. The Petaka™ cell culture device from Celartia™. A) Schematic representation of the device. An injection port allows filling and withdrawing cells and culture media from the culture chamber. Gas exchange between the culture chamber and the outside of the system is performed through a 0.2 micron filtered vent, a long respiratory duct and a water vapor condenser (which serves also as a capillary breaker). B) Picture of the actual device. C) Schematic representation of the respiratory duct.

A specific design permits to obtain these characteristics. Figure 34.A shows a schematic representation of this device and its constituting elements. The air headspace of the culture chamber is connected to a water vapor condenser which presents a meandering path with several consecutive restrictions (Figure 34.B). This condenser is connected to a long meandering respiratory duct (Figure 34.C) terminated by a hydrophobic porous 0.2 μm-sized pore filter.

The Petaka system was tested for cell culture under CO₂ atmospheric conditions. NIH3T3 cells were inoculated at 4·10⁴ Cells/cm² in 20 mL of DMEM-Phenol Red medium and cultured in 0% CO₂ incubator. The same cell density was inoculated in 10 mL of the same medium in a T175 flask and cultured in the same incubator. Figure 35.A&B show the pictures taken daily to follow these cultures. Cells normally proliferated in the Petaka system until reaching confluence on the fifth day of culture. However, the cells cultured in the T175 flask did not survive until day 1 since, as expected, it failed to maintain a proper pH. Indeed, Figure 35.C shows the difference of color between the Petaka device were a pH drift occurred after 3 days under CO₂ atmospheric level and the T175 flask were it did not after 1 day under the same level of CO₂.

The Petaka system is a good example that passive solutions exists to culture cells under CO₂ atmospheric levels. This gives a critical advantage to develop portable and disposable culture devices over systems relying on active CO₂ regulations such as systems integrating a CO₂

exchanger or needing CO₂ incubators. Indeed, active CO₂ regulation often relies on several pieces of equipment and different gas sources which, from a practical point of view, require heavy installations and safety certifications. In the case of incubators, they are expensive tools to sustain cell culture and have a large footprint. All these elements do not act in favor of building miniaturized and affordable cell culture systems. Moreover, the approach considered by the Petaka system seems more suitable compared to engineered media formulation as it does not need to be adapted for each cell type to ensure a proper cell growth.

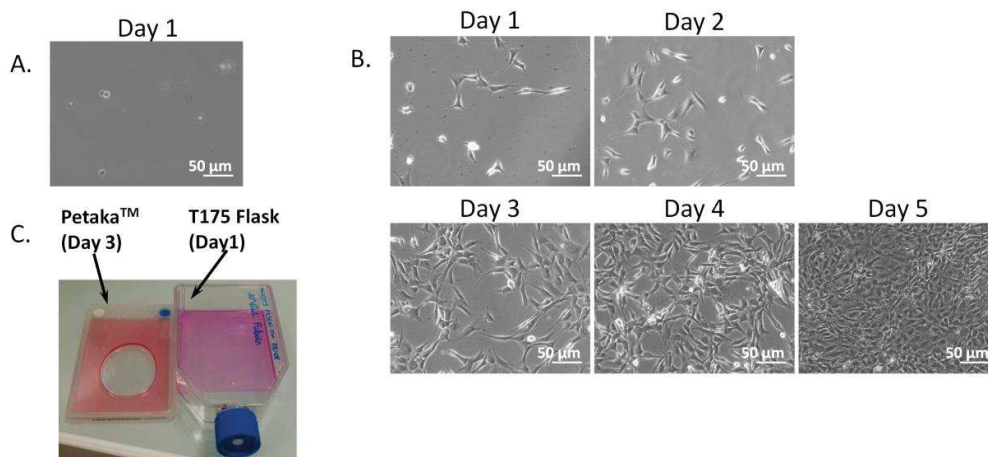


Figure 35. Comparative culture of NIH3T3 cells with the Petaka™ flask and a standard T175 flask. A) Cells cultured in the T175 flask with DMEM-Phenol Red medium in a 0% CO₂ incubator. Cells are seen dead. B) Cells cultured in the Petaka™ flask with DMEM-Phenol Red medium in a 0% CO₂ incubator. Cells proliferate over time. C) Comparison of the phenol red color to evaluate possible pH drifts under atmospheric CO₂ concentration. The Petaka™ system can maintain a red medium color, characteristics of an adequate pH for cell culture, while the vented T175 Flask cannot. The medium turns purple characterizing an increase of the pH out of the recommended culture pH range.

As a conclusion, culture medium supplemented with HEPES is not able to prevent pH drift due to CO₂ escape from the liquid phase after long exposure under ambient atmosphere. Despite the fact that L-15 medium could address this issue, NIH3T3 cells were not able to proliferate although they did not die. Only, the Petaka system could successfully achieve cell culture under ambient CO₂ levels based on specific materials and fluidic design preventing CO₂ escape. Further work would be needed to prove whether this approach can be scaled down to the scale of a microfluidic cell culture system. Doing so would give a critical advantage to develop cheap, portable and disposable microfluidic bioreactors. Additionally, this approach could be a viable solution to better address the issue of maintaining a proper oxygen level for dense cultures in the bioreactor as shown in section 4.1.1.2 by simply relying on the ambient oxygen available and without inducing a pH drift.

4.2 Microcarrier-based cell culture

4.2.1 Microcarrier preparation

Cytodex 3 microcarriers (Ref. C3275, Sigma) with a final mean diameter of 175 μm served as cell (PC3 or NIH 3T3) supports for adhesion. These microcarriers are made of dextran (polysaccharide) and are coated with collagen. They are sold dried with an average diameter of 74 μm and need to be hydrated and sterilized before use. The quantity of cells to inoculate on the microcarrier is dependent on the surface area provided by the beads and therefore by the number of beads. Thus, it is important to know the microcarrier quantity before seeding. Time was spent to optimize the protocol to prepare the microcarriers in order to avoid variations in the microcarrier concentration. Indeed, initially, beads were simply hydrated in PBS- in a standard plastic tube (Eppendorf). However, many carriers stuck to the tube walls. This observation was visible to the naked eye. Recommendations from the GE Healthcare microcarrier cell culture Handbook[61] advised to use siliconized glass ware, add 2-3 drops of Tween-80 per 100 mL of PBS- and let the carriers hydrate for at least 2-3 hours before sterilization. The siliconized glass ware is supposed to avoid carriers sticking and Tween-80 is a surfactant allowing for better carrier wetting and sedimentation. Also, the longer the microcarriers are hydrated the less they stick. As a consequence, microcarriers were hydrated for 24 h in 2 mL low bind plastic tube (LoBind Eppendorf) filled with a solution of 0.2% (v/v) Tween-80 (Sigma) in PBS- up to the 2 mL graduation.

Several strategies can be used afterwards to sterilize the carriers. They can be immersed in 70% (v/v) ethanol in distilled water or autoclaved. Since autoclaving is a more effective solution for sterilization, microcarriers were autoclaved (Systec VE-55, Fisher Scientific) at 120°C for 1 h.

After sterilization, the microcarriers were washed twice with PBS- due to possible Tween-80 toxicity[153]: the tube supernatant is discarded, fresh PBS- is added up to the 2 mL graduation of the tube and carriers are allowed to settle before the next rinse. Microcarriers were then stored in a 4°C fridge. Prior to cell inoculation, microcarriers were rinsed once with warmed culture medium.

4.2.2 Standard microcarrier cell culture

Prior to performing microcarrier cell culture experiments inside the bioreactor, the proliferation of PC3 cells and NIH3T3 on Cytodex 3 microcarriers was investigated in Petri. Cytodex microcarriers are usually used in the range 1-5 mg/mL for cell culture[61]. Microcarrier concentrations of 2 and 5 mg/mL were used for PC3 cells and NIH3T3 cells. Microcarrier cell cultures were performed in 2 mL of their specific media in Petri dishes non-treated for cell culture to force the cells to only adhere on the microcarriers. PC3 cells were cultured in red

phenol F-12K Medium (Kaighn's Modification of Ham's F-12 Medium) with 10% (v/v) fetal bovine serum and 1% (v/v) 100 U·mL⁻¹/100 µg·mL⁻¹ penicillin/streptomycin and NIH3T3 cells were cultured in DMEM-Phenol Red medium supplemented with 10% (v/v) new-born calf serum and 1% (v/v) 100 U·mL⁻¹/100 µg·mL⁻¹ penicillin/streptomycin. Control cultures were performed by simply growing cells in 2 mL of their specific media in Petri dishes treated for cell culture. Cells were inoculated at a concentration of 40 cells/mm² which corresponds to the standard cell concentration for routine cell culture. The surfaces available for cell proliferation for each condition are given in Table 10.

Table 10. Surface area according to the microcarrier concentration or the type of culture ware

	5 mg/mL	2 mg/mL	Petri (Ø 35 mm)
Surface area (mm ²)	2700	1080	962

Culture experiments were conducted over the course of 4 days. The number of culture dishes prepared was defined to obtain triplicates for each day and each condition. Cells were harvested using dextranase combined with trypsin for a better cell harvest efficiency (see section 5.3). The supernatant was removed and replaced by 1.5 mL of dextranase 1% (v/v) in culture media to dissolve the microcarriers. After 20 min of incubation in a 5% CO₂ incubator, cells were washed twice with 2 mL of PBS- and submerged in 1 mL of trypsin for 5 min. 1 mL of medium was added before counting was performed using a sceptor cell counter (Millipore).

The proliferation assay results are gathered in Figure 36. Despite that a concentration of 2 mg/mL of microcarriers and a Petri dish provide the same growth surface area, the proliferation curves were different. In the case of microcarriers, the cells underwent a longer lag phase than in Petri dishes: more than 1 day longer for PC3 and only a few hours for 3T3. After the lag phase, PC3 cells exhibited a maximum proliferation rate of 0.09 cells/h on microcarriers as well as in Petri dishes. However, the maximum proliferation rate of NIH3T3 on microcarriers was more significant 0.21 cells/h compared to 0.1 cells/h in Petri dishes.

At high microcarrier concentration (i.e. 5 mg/mL), the lag phase was shorter compared to the culture in Petri dishes. The same trends as for low concentrated microcarriers were observed regarding the maximum proliferation: PC3 cells exhibited a comparable maximum proliferation rate (0.1 cells/h compared to 0.09 cells/h for Petri dish conditions) while NIH3T3 demonstrated a more significant maximum proliferation rate (1.41 cells/h compared to 0.1 cells/h for Petri dish conditions). The high proliferation rates observed with NIH3T3 may be the result of a stimulation of their proliferation by the collagen coated on the microcarrier.

Besides, the proliferation on microcarriers at high concentration reached a plateau while cells kept growing with the same rate in Petri dishes. This behavior is likely to be the result of the

accumulation of cell wastes and/or the lack of nutrients since the cell concentration was much higher. This observation reaffirms the need to integrate a mechanism by which the culture media can be renewed.

The difference of proliferation observed between the low concentrated and the high concentrated microcarrier cell cultures is most likely due to the microcarriers inter-distances which are larger when microcarriers are in low concentrations. Indeed, cells have the ability to transfer from one bead to another by forming a cell bridge to colonize new available surfaces. Such formation has been characterized by confocal microscopy and is shown in Figure 36.E (see Appendix I for details on the staining protocol). This phenomenon can only occur if the microcarriers are close enough. But, when microcarriers are in low concentration, the probability to form a bridge is reduced. Obviously, the lower is the concentration, the lower is this probability.

Regardless of this aspect, cells cultured on microcarriers behave similarly as when they are cultured on a standard flat surface. Cells settle and when they proliferate colonize more surfaces Figure 36.F. Once the beads are confluent (i.e., completely covered with cells), contact inhibition occurs, and the cells stop proliferating, as observed in regular 2D cell culture[9]. The cell morphology on microcarrier is depicted in Figure 36.G and compared to cell growing on a regular 2D surface.

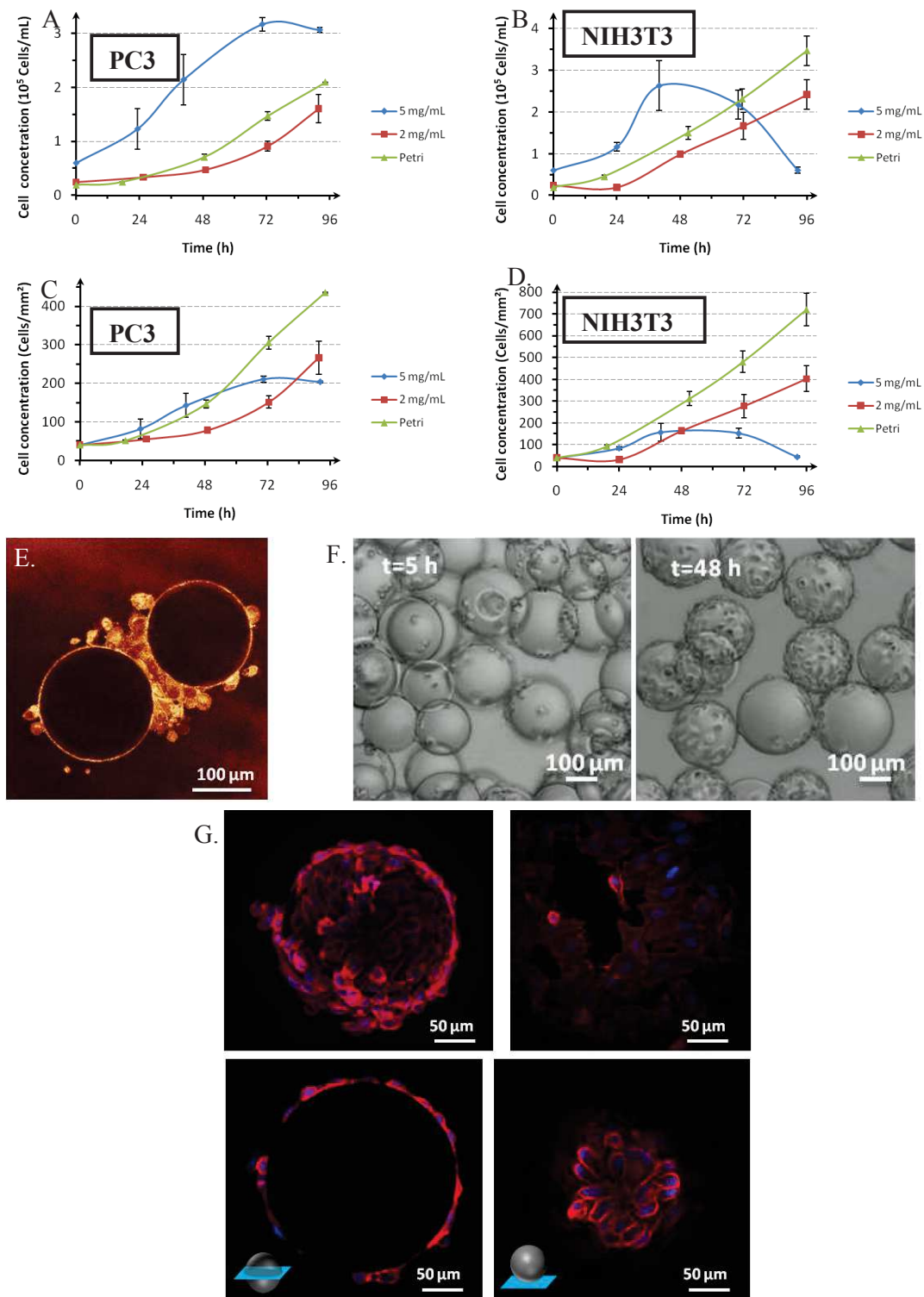


Figure 36. Cell proliferation on Cytodex 3 microcarriers. A,C) PC3 cells. B,D) NIH3T3 cells. A,B) Cell concentration is in cells/mL. C,D) Cell concentration is in cells/mm². E) Cells forming a bridge between two microcarriers. F) Cell proliferation of PC3 cells on microcarriers at 5 mg/mL after 5 h and 48h of culture. G) Immunostaining images of PC3 cells cultured for 4 days on a microcarrier (left images and bottom right image) and on a standard Petri dish surface (top right image). Top left image: a 3D reconstruction of the cells on the microcarrier. Bottom images: cells on the microcarrier at two different planes (see scheme in the bottom left corner): the middle plane (bottom left image) and the bottom plane (bottom right image) of the microcarrier. The nuclei are stained in blue, and phalloidin (actin filaments) is shown in red.

4.2.3 Bioreactor (microcarrier) cell culture

To initiate a culture experiment within the bioreactor, a specific protocol was adopted. The first step concerned the sterilization of the bioreactor. This step appeared to be critical. Initially, culture experiments failed due to contaminations. The source of contamination seemed to come from the cartridge, every time a contamination was detected. Indeed, the number of bacteria increased from the syringe used for inoculation to the cartridge. The sterilization procedure which allowed contamination-free cultures involved:

- thorough cleaning of the CCC holder and the heater with 70% (v/v) ethanol in distilled water under a safety cabinet
- thorough cleaning of the tubing on their outer side with 70% (v/v) ethanol in distilled water under a safety cabinet, followed by 5-10 min of manual flushing of the tubing in their inner side with 1% (v/v) $100 \text{ U}\cdot\text{mL}^{-1}/100 \text{ }\mu\text{g}\cdot\text{mL}^{-1}$ Penicillin/Streptomycin (P/S) in PBS-
- Baking at 100°C for 1h of the CCC to thermally inactivate microorganisms, followed by manually flushing co-currently the CCC channels with 1% (v/v) P/S in PBS- under a safety cabinet

After sterilization, the lower channel of the CCC was filled with the adequate culture medium depending on the cell type. Then, the upper channel was filled with media containing cells. Once the CCC was filled, the syringe for perfusion was connected to the tubing leading to the perfusion channel. The outlet of this channel was connected to the sterile vial serving as waste container. The culture channel was closed at each of its outlets. These operations were made under the safety cabinet. The bioreactor was then placed on its bench. The heater was supplied with power and the thermal sensor connected to the read out instrument. When a stable temperature of 34°C was reached (see section 4.1.2.3), the perfusion was initiated with a flow rate of $5 \text{ }\mu\text{L}/\text{min}$ (see section 4.1.1.2).

Three different types of cells were cultured in the bioreactor: insect *Drosophila* S2 cells (Ref. CRL-1963, ATCC), NIH 3T3 cells and PC3 cells. *Drosophila* cells were used as a simple model and without microcarriers to validate the operation of the bioreactor with fewer variables such as the temperature or possible pH drift. Indeed, the culture of such cells does not require CO_2 regulation when exposed to air; room temperature and the ambient oxygen level are sufficient for their normal growth. Additionally, this cell type can be cultured as adherent cells or in suspension due to their weak adherence. The heater was not used during the culture of *Drosophila* S2. NIH3T3 and PC3 cells were used as more complex models and were cultured on microcarriers. These cells require a constant temperature of 37°C , and when exposed to air, their media requires a partial CO_2 pressure of 5% to maintain pH level. Prior to being inoculated

in the bioreactor, the cells were cultured for 24 h on the microcarriers in a 2 mL Petri dish placed in a CO₂ incubator in their respective medium. PC3 cells were cultured in red phenol F-12K Medium (Kaighn's Modification of Ham's F-12 Medium) with 10% (v/v) fetal bovine serum and 1% (v/v) 100 U·mL⁻¹/100 µg·mL⁻¹ penicillin/streptomycin, NIH3T3 cells were cultured in DMEM-Phenol Red medium supplemented with 10% (v/v) new-born calf serum and 1% (v/v) 100 U·mL⁻¹/100 µg·mL⁻¹ penicillin/streptomycin and Drosophila S2 cells in Schneider's Drosophila Medium (Life Technologies) with 10% (v/v) fetal bovine serum. The concentration of microcarriers used was adjusted to 2 mg/mL with a corresponding cell seeding concentration of 2.4·10⁴ cells/mL (i.e. 40 cells/mm²). At higher concentrations, the microcarriers usually agglomerated to each other and formed a plug at the entrance of the CCC which could not be moved. The surface roughness of the channel due to the milling may provide anchorage points for the beads to adhere.

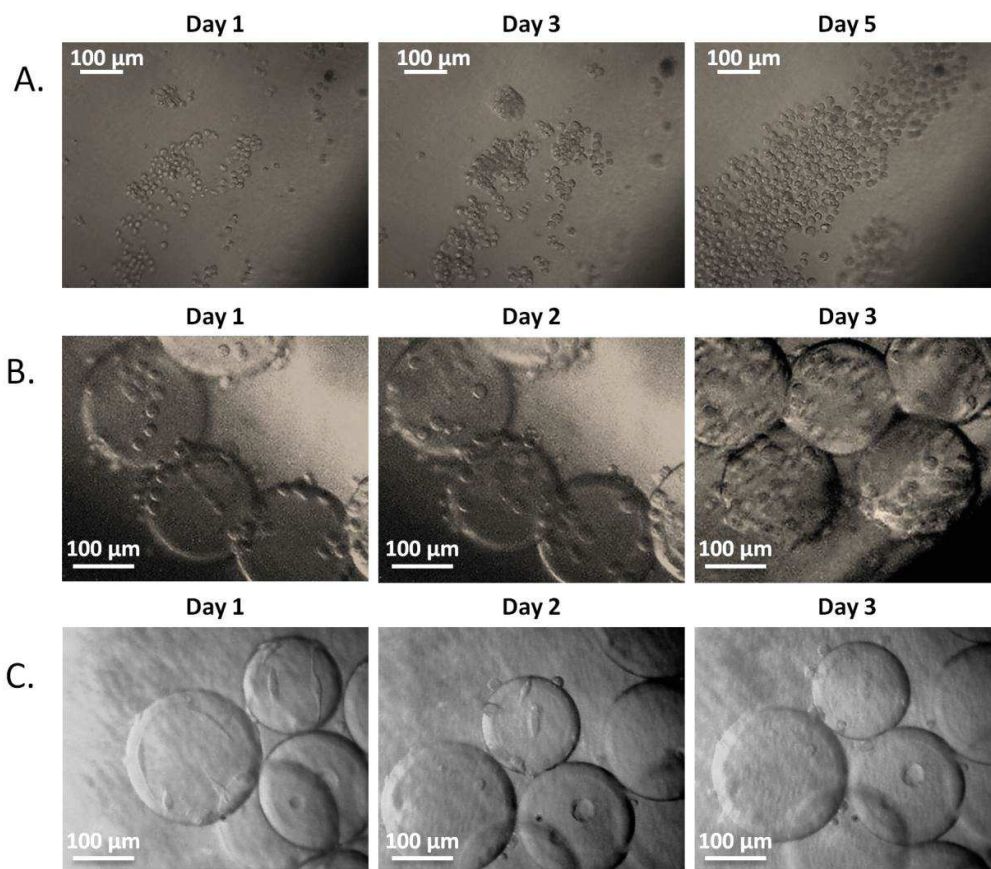


Figure 37. Cell cultures in the microfluidic bioreactor. A) Drosophila S2 cell culture. Cells proliferate over time. B) PC3 cell culture. Cells slightly proliferate over time. C) NIH3T3 cell culture. Cells poorly proliferate.

The cultures of Drosophila S2, PC3 and NIH3T3 cells are illustrated in Figure 37. Drosophila S2 cells proliferated until the fifth day of culture (Figure 37.A) until their culture was intentionally stopped. Such culture validated that i) the bioreactor provides a non-toxic environment for cell

culture, ii) sterile culture can be achieved in the bioreactor for several days (the *Drosophila* S2 medium was not supplemented with antibiotics) , iii) the perfusion function of the bioreactor allows long term cell feeding. The following cultures of NIH3T3 and PC3 cells could last until the third day of culture. PC3 cells demonstrated a slight proliferation until the third day of culture (Figure 37.B) but were found dead on the next day. In the case of NIH3T3, the progressive rounding of the cells (Figure 37.C) seems to indicate that the culture conditions were not quite adequate. A probable hypothesis is that the pH may have drifted. Indeed, it has been noticed that, when the empty syringe for perfusion was replaced by a new syringe filled with fresh medium, the previous medium had purple color indicating an increase of the pH. The tubing (Tygon®, Cole-Parmer) probably presented a sufficient gas permeability to lead to CO₂ escape from the medium.

4.3 Conclusion

The management of several important culture conditions has been addressed in this chapter. Cell feeding has been validated in a first instance through a trans-membrane mass transport study and, later, by enabling the proliferation of a simple cell model, insect *Drosophila* S2 cells, for 5 consecutive days before the culture was intentionally aborted. A first proof-of-concept was demonstrated for the culture of cells which did not take into consideration the issue of the temperature of the culture and the issue of CO₂ escape leading to pH drift.

Regarding the culture of mammalian cells, more particularly NIH3T3 and PC3 cells, the maintenance of optimal culture conditions is more challenging when working outside of an incubator. An integrated heater providing a stable and uniform thermal distribution over the culture area has been successfully developed. This heater has the advantage to allow microscopic observations, due to its transparency. Simulations have shown that under the technical constraints for perfusion, cells would be cultured in a relatively homogeneous nutritional environment at a flow rate of 5 µL/min. However, there may be a need to replenish the culture media with oxygen for dense cultures and cells with higher oxygen requirements. This issue can be addressed in two ways, either by redesigning the CCC by shortening the length of the culture channel, or by developing strategies, at the level of the bioreactor, analog to the Petaka™ device which ensured passive gas exchange with the ambient air without inducing pH drift due to CO₂ escape or dehydration of the culture area. The strategies developed to provide the proper environment for cell proliferation inside the bioreactor are gathered in Table 11.

Table 11. Strategies used to regulate the cell culture environment inside the bioreactor.

	Nutrients	O ₂	Temperature	pH
Strategy	Fresh media perfusion at 5 μ L/min		Sensor: Pt100 RTD Set point: 34°C Heater: PET-ITO	Use as much as possible low gas permeable materials

The actual environmental conditions provided to the mammalian cells could allow 3 days of cell culture on microcarriers inside the bioreactor. The issue seemed to come from the permeability to the atmosphere of the tubing used. The studies on alternative solutions to maintain the pH lead to the conclusion that working on the permeability to gas of the materials constituting the bioreactor remains the most effective solution to avoid pH drift without needing to rely on cumbersome active pH regulation. The use of HEPES supplemented buffer could only slow down the pH drift while the use of CO₂-independent media maintained a stable pH but proved to inhibit cell proliferation.

Eventually, a concentration of 2 mg/mL of microcarriers, as practically possible in the current bioreactor, provides a growth surface area comparable to a standard Petri dish. However, the static cultures performed with microcarriers in the incubator showed that this concentration is less effective for cell proliferation since the cells need the carriers to be close enough to colonize the one where cells are not already present. Therefore, improvements are required to achieve higher concentrated microcarrier cell culture. For instance, reducing the surface roughness of the channel might help to prevent the microcarriers from adhering on the channel walls.

5 Cell harvest

A great effort was put into innovating on cell harvest to overcome the limitations when using proteolytic enzyme and to integrate this function into the bioreactor. After a literature study on cell harvest, one approach was identified: cell harvest using a thermosensitive polymer, Poly-N-isopropylacrylamide. A large investigation on this strategy was led during this thesis and is of main concern in this chapter. However, due to unsatisfactory results, other cell harvest approaches have been considered and are further detailed. They consist either in dissolving the microcarriers or in simply relying on bead-to-bead cell transfer. Figure 38 gives a schematic reminder of the cell harvest and subculture approaches considered in this thesis.

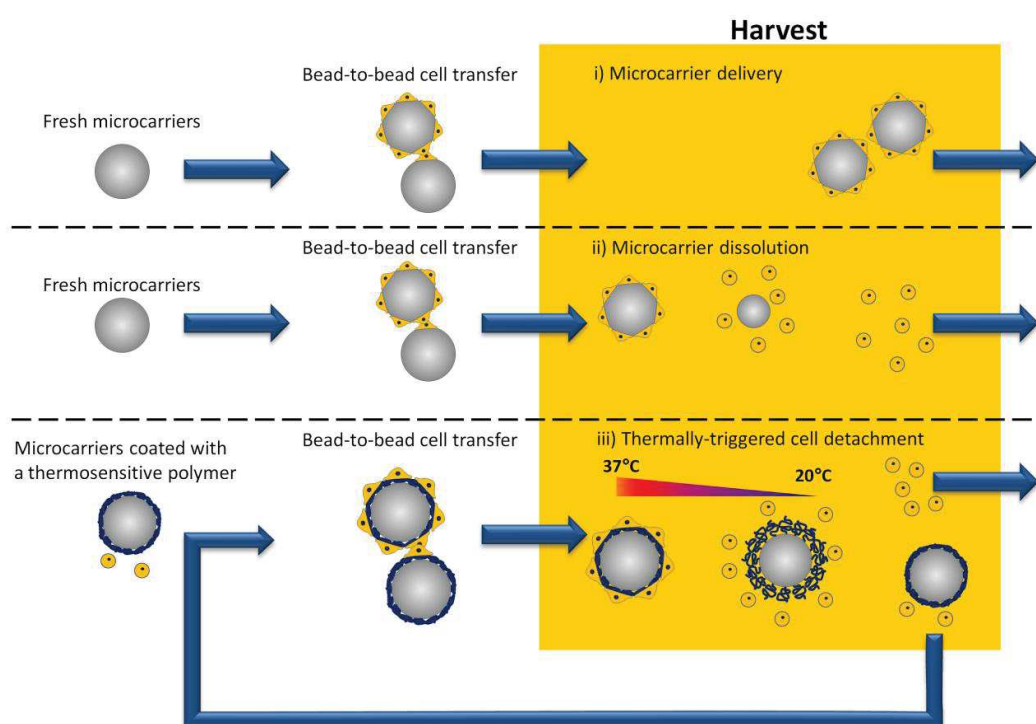


Figure 38. Schematic summarizing the different approaches considered for cell harvest and subculture. i) Simple microcarrier delivery with simultaneous fresh microcarrier addition. ii) Microcarrier dissolution with simultaneous fresh microcarrier addition. iii) Thermally-induced cell harvest where a part of the detached cells and all the microcarriers are reused for proliferation.

5.1 The different strategies for cell harvest

Some applications may require extracting cells from the microbioreactor, for instance, to perform post culture proteomics or genomics analysis of the cultured cells. Another example would be proliferation studies during long-term cultures: to maintain the proliferation rate of the cells by avoiding contact inhibition, culture surfaces must be cleared from cells to offer new available surfaces for proliferation. Therefore, investigations were led to automate the culture within the bioreactor by exploring routes to possibly harvest the cells inside the bioreactor.

Different approaches have been used and developed to harvest cell when performing microcarrier cell culture[61] or in microfluidic format[127]. Table 12 gives a summary of these methods.

Table 12. Summary table of the reported harvest methods used for microcarrier cell culture and those integrated in microfluidics.

Area of harvest application	Harvest method	Description	Cell viability	Detachment rate	Release time	
Microfluidics[127]	Enzymes	Cleavage of cell adhesion proteins or DNA strands	>90%	>90%	5-15 min	
	Shear stress	High flow rate dislodging cells	Poor	>50%	Few sec.	
	Stimuli responsive surfaces	Temperature	Swelling of temperature responsive polymer below 30-32°C	>90%	>90%	20 min
		pH[154]	Swelling of chitosan by increasing the pH to 7.8	NA	>90%	1 h
		EDTA	Dissolution of alginate	90%	NA	10 min
		Light	Photodegradation of light sensitive polymer	>90%	>90%	5-20 min
Electric potential	Application of voltage to SAM substrate inducing protein desorption	>90%	>90%	1-10 min		
Microcarrier cell culture[61]	Enzymes[155]	Digestion of cell adhesion proteins	>90%	>80%	5-15 min	
	Hypotonic treatment	Incubation in hypotonic solution	Poor	>90%		
	Cold treatment	Exposition to 4°C	Poor	>90%	1 h	
	Thermosensitive carriers[156]	Swelling of temperature responsive polymer coated on carrier below 30-32°C	>90%	90%	30 min	

Ease of integration and cell integrity preservation are critical criteria in choosing the right strategy for cell harvest. As a consequence, conditions in which cells are detached must not degrade their viability or irreversibly impair their metabolic activity.

The common strategy for cell harvest is the use of proteolytic enzymes. Among them trypsin is the most employed and has been applied in microcarrier and microfluidic cell culture. Cell harvest is triggered by the digestion of the cell adhesion proteins. However, if cells are exposed over long periods of time, enzymes can degrade other Extra Cellular Matrix (ECM) proteins and other surface protein receptors, and eventually lead to cell death[121,122]. Washing steps are, therefore, of the utmost importance when this method is adopted. Primary cells are also known to be highly sensitive to trypsin[61]. Though this solution has been a standard in cell culture, it is clear that many examples exist where the use of proteolytic treatments is to be avoided. Additionally, trypsin treatment appeared to be poorly effective to detach cells from microcarriers during this thesis (see section 5.3).

Coupled to microfluidics, another type of enzyme-based harvest has been developed. These enzymes are called restriction enzymes and only target a particular sequence of DNA - DNA that cells do not possess on their outer cytoplasmic membrane- making them totally harmless for cells. Their action consists in cutting a DNA strand on a characteristic and specific location they can identify. However, the utilization of such enzymes requires DNA-based substrates along with antibody-DNA conjugates on which cell can be selectively captured as described by Bombera *et al.*[157]. This method has been used for floating cells and no study indicated whether adherent cells could proliferate when captured by antibody binding and would not also attach to the underlying substrate.

Since microfluidics addresses the control of liquid flows, shear stress by high flow rate has been used to dislodge the cell binding to their substrate[158]. However, this approach exhibits a poor viability. In many of the described methods here, moderate shear stress has often been used to improve cell detachment. This is also true at the larger scale, where gentle stirring is commonly employed during cell harvest.

Among stimuli-responsive substrates which have demonstrated capabilities to release cells, we can identify electrosensitive self-assembled monolayers (SAM)[159], photosensitive polymers[160], pH-sensitive polymers[161] and thermosensitive polymers[162,163,164,165]. When a reduction potential is applied to electrosensitive SAM, electrochemical desorption of cells captured by the underlying antibody layer occurs[159]. This method, exploited for floating cells, raises the same questions as for the cell release achieved through enzyme restriction mentioned earlier. Besides, it should be noted that depending on the electrical field, cell damage or cell metabolism alteration can occur[166] and extreme culture medium heating can happen damaging the cells as well[167]. For photosensitive polymers an exposure to UV light induces the photoisomerization of poly(nitrobenzospiropyran-co-methyl methacrylate), which then triggers cell detachment[160]. A UV light treatment may not represent a choice of interest due to the damage that UV can cause to DNA[168].It also requires cumbersome apparatus. Regarding pH-sensitive polymers, they have demonstrated the ability to detach cells within acceptable conditions[161]: pH of the medium was varied from 7.4 to 6.5. Precise control of pH is critical since cell viability will rapidly decrease with the variation of a few pH degrees. Thermosensitive polymers are the most referenced smart biomaterials to perform cell detachment and more particularly Poly(N-isopropylacrylamide) (PNIPAM) has been widely described for that purpose[162,163,164,165]. When the medium temperature drops under a threshold temperature, known as lower critical solution temperature (LCST), the polymer chains experience a transition from a non-solvated state to a solvated one which is at the origin of

cellular detachment. Studies proved the preservation of cell specific functionality, metabolism and viability[169,170]. Microcarriers have been functionalized with thermosensitive polymers[156,164,171].

Instead of enzyme-based harvest, standard microcarrier-based cell cultures have alternatively used cold treatment and hypotonic treatment. However, these methods negatively affect cell viability.

Thermoresponsive polymers appeared to be the best candidate to harvest cell regarding our system, supported by extensive scientific documentation. It fitted with our criteria of cell integrity preservation and ease of integration. Thermal management can be easily addressed for the range of temperature considered to carry out cell detachment (20°C-37°C). Moreover, the protocol seems much simpler than for enzyme treatment or pH-sensitive polymers as no washing step or other liquid handling is required. The fluidics of the system is therefore much simpler. Besides, PNIPAM grafting on microcarriers has already been reported[156,164,171,172]. Last but not least, with the reversibility of the behavior of thermosensitive polymers an innovative procedure for automated cell culture can be achieved. Indeed, cells could adhere on the grafted microcarriers and when close to confluence they can be detached by lowering the temperature of their medium. Then, using a size sorting method, part of the cell population could be delivered out to the user and the other part with the microcarriers kept in the system back to 37°C where cells could re-colonize the empty beads and proliferate again, and so on. Eventually, the only challenge lies on the synthesis of thermosensitive substrates. For that purpose, a collaborative work was established with Lionel Bureau from LIPhy (Laboratoire Interdisciplinaire de Physique), Grenoble, France, to benefit from his expertise.

5.2 Thermally-mediated cell harvest

5.2.1 Poly(N-isopropylacrylamide)

As mentioned previously, Poly(N-isopropylacrylamide) (PNIPAM) is the most prominent thermosensitive polymer for thermally-triggered cell harvest. PNIPAM monomers are composed of an amide moiety bound to an isopropyl group (see Figure 39.A).

While the isopropyl group exhibits hydrophobic interactions, the amide group is able to interact with water molecules by forming hydrogen bonds. Amide moiety interactions with water are temperature dependent. At lower temperature, amide groups form hydrogen bonds with water molecules, and the polymer is dissolved. Upon a temperature rise, these hydrogen bonds break and inter-amide interactions are favored, and the polymer is not solvated anymore. This phenomenon is reversible with the change of temperature and is accompanied by a conformational change of the polymer chains from expanded coils (low temperature) to

compact globules[173]. In the collapsed state the polymer tends to minimize the contact with water molecules and becomes more hydrophobic as shown in Figure 39.B.

The sharp phase transition of PNIPAM is characterized by a Lower Critical Solution Temperature (LCST) which defines the lowest temperature for which the polymer is dissolved. The LCST is around 32°C and can vary depending on the molecular weight (max. 1°C)[174] or external factors such as the solvent pH[175] or with high concentration of solvated salts (a few degrees Celsius)[176]. The synthesis of PNIPAM copolymers can also modulate the LCST towards higher or lower temperature[177,178].

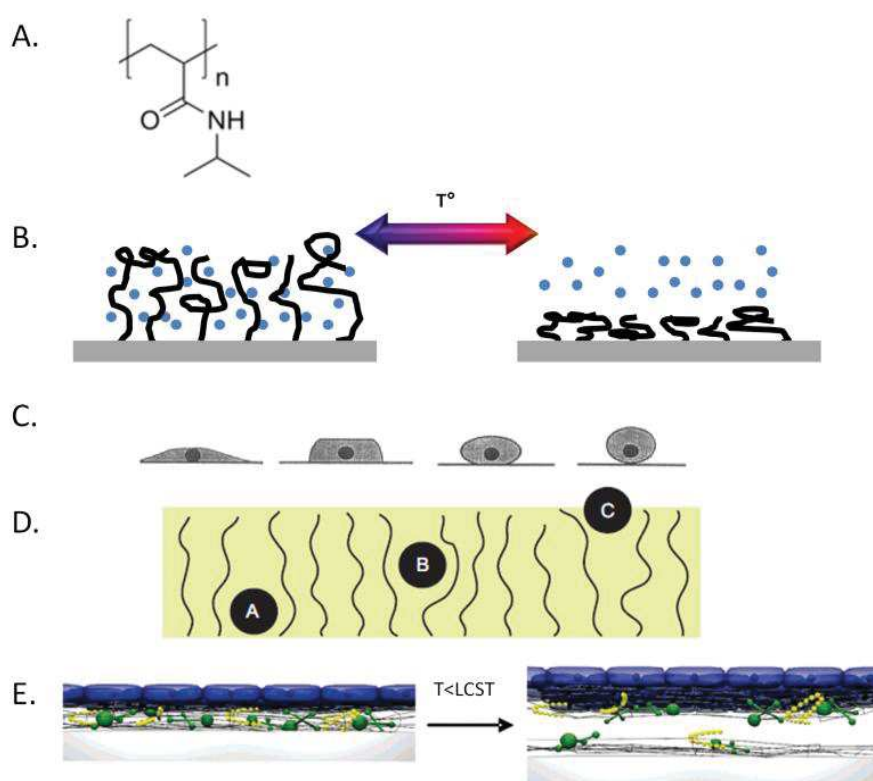


Figure 39. Poly-N-isopropylacrylamide (PNIPAM) characteristics and behavior and the mechanism of cell detachment. A) Skeletal formula of PNIPAM. B) Reversible conformational change from expanded to collapsed water repellent chains upon temperature change. C) Schematic of cell detachment occurring on PNIPAM coated surfaces. Adapted from[179]. D) Schematic view of three protein adsorption modes: (a) primary adsorption at the grafting surface, (b) ternary adsorption within the brush and (c) secondary adsorption at the brush outer edge. Adapted from[180]. E) Schematic of cell detachment: cells detach with most of their ECM, though some proteins remain on the surface. Adapted from[181].

PNIPAM has been used in diverse fields such as optics[182] and rheology[183] but its utilization is mainly addressed in biological application for drug delivery[184] and cell sheet engineering[185]. Commercial products are already on the market for low temperature cell lift-off based on the massive work of Ph. D. Okano T. *et al.*, one of the directors of CellSeed Inc..

However, temperature-mediated cell detachment is still not completely understood and remains mostly qualitative.

A morphological change occurs when cells detach from the surface: cells are initially spread then round up and finally lift off from the surface[179] (Figure 39.C). Cell metabolism and polymer grafting characteristics such as chain length and density have been identified as key parameters in both cell adhesion and detachment on PNIPAM surfaces[179,180,186,187]. In the first instance, PNIPAM substrates must allow cell adhesive protein adsorption; otherwise, cell adhesion will not be possible as observed on dense polymer brush[188]. Moreover, different modes of adsorption exist, referenced as primary adsorption at the grafting surface, secondary adsorption at the polymer chain outer edge and ternary adsorption within the polymer chains[180] (Figure 39.D). The mode of adsorption influences during detachment the way cells will respond to the underlying substrate characteristics. The density of the polymer will greatly impact the efficiency of the detachment, whereas the influence of the chain length will be negligible[187].

When PNIPAM swells with lower temperature it becomes softer and the balance of the forces between the cells and the polymer is lost. Therefore, the cytoskeletal tension forces prevail over a decreased mechanical resistance from the substrate. This loss of equilibrium along with the pressure exerted on the ventral cytoplasmic membrane due to the swelling of the polymer chains leads, most likely, to a combination of ECM protein desorption and ECM-integrin bonds breakage[180]. Those events are sustained by the fact that cells are known to detach with the majority of their ECM[189] and components (i.e. proteins) of that ECM could be found on PNIPAM substrates after cell lift-off[181] as depicted in Figure 39.E.

As outlined, the synthesis of PNIPAM surfaces for efficient cell detachment requires control of the PNIPAM layer thickness and density. Atom-Transfer Radical-Polymerization (ATRP), a class of controlled living polymerization (i.e. type of chain growth polymerization where the ability of a growing polymer chain to terminate has been removed), has gained interest to achieve reproducible grafting of polymer brush with specific thickness and density without the need for expensive laboratory equipment[190]. Based on these arguments, ATRP has been considered for the development of smart surfaces for cell harvest. Instead of moving forward straight to the grafting of the microcarriers with PNIPAM, it was considered more suitable, in the first place, to study and characterize the polymer behavior by using planar surfaces and then, in a second time, move towards microcarriers grafting with PNIPAM. It prompted the establishment of a collaboration with colleagues of the host laboratories developing autonomous cell imaging

systems. The following sections detail the fabrication of PNIPAM-grafted substrates and report the different characterizations performed on these substrates.

5.2.2 Materials and methods

5.2.2.1 Chemicals and substrates

Dulbecco's Modified Eagle Medium (DMEM), DMEM phenol red, Newborn fetal serum, penicillin-streptomycin solution, trypsin-EDTA, Bovine Serum Albumin (BSA), triton X-100, Phosphate Buffered Saline supplemented with Mg^{2+} and CA^{2+} (PBS+) and sucrose were purchased from Life Technologies™.

N-isopropylacrylamide (NIPAM, 97%), copper(I) chloride, N,N,N',N'',N''-Pentamethyldiethylenetriamine (PMDETA, 99%), triethylamine (TEA, ≥99%), 3-aminopropyltriethoxysilane (APTES, 99%), α -bromoisobutyrylbromide (BIBB, 98%), potassium chloride, ethanol (anhydrous, ≥99.5%), dichloromethane (anhydrous, ≥99.8%), n-hexane (anhydrous, 95%), Tween20, NH_4Cl , vinculin (Ref. V9131) and phalloidin tetramethylrhodamine B isothiocyanate (Ref. P1951) were bought from Sigma Aldrich. Anti-mouse FITC (Ref. 115-095-146) was purchased from Jackson ImmunoResearch (France). Fluorescent mounting medium kit (Ref S3023) was obtained from Dako (France). All aqueous solutions were prepared in deionized water obtained using a Synergy® water purification system, Millipore. Microscope glass slides (20 mm x 20 mm) were provided by Dominique Dutscher. Silicon wafers with native oxide were diced into 10 mm x 20 mm pieces.

5.2.2.2 Poly(N-isopropylacrylamide) grafting

The grafting of PNIPAM brushes on microscope glass slides and diced silicon wafers was performed as depicted in Figure 40 with, first, i) a silanization of the glass and SiO_2 surfaces to then ii) covalently attach a surface initiator which eventually promoted iii) PNIPAM grafting by atom transfer radical polymerization (ATRP). For each synthesis, a set of glass chips and SiO_2 substrates were grafted under the same conditions to further perform physical and biological characterization.

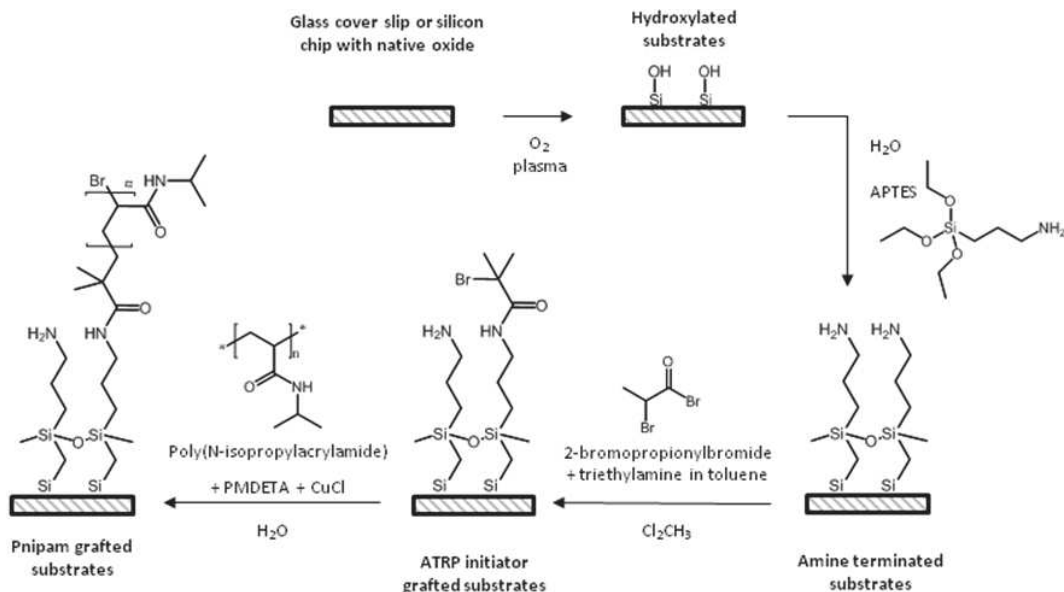


Figure 40. PNIPAM grafting steps.

Silanization: Glass slide and silicon chip surfaces were hydroxylated and cleaned in an O_2 plasma reactor (AST products, Inc.) under a flow of 20 sccm for 5 min and 80 W RF power. Hydroxylated surfaces were immersed for 1 min in a $5 \cdot 10^{-4}$ M aqueous solution of APTES filtered through a $0.22 \mu\text{m}$ filter (Acrodisc® PSF syringe filter, Pall® Life Science). Time of immersion determined the further density of PNIPAM. Slides and chips were rinsed with deionized water and dried.

Polymerization initiator grafting: After silanization substrates were immersed for 30 s in a 25 mL dichloromethane solution containing 1.25 mL of TEA and 250 μL of BIBB (surface initiator). Substrates were rinsed in dichloromethane then ethanol, then deionized water and eventually dried.

PNIPAM grafting: NIPAM was recrystallized 2 times before use in *n*-hexane. A 20 mL aqueous solution with 0.5 g of NIPAM and 150 μL of PMDETA was stirred and bubbled in a round bottom flask under argon for 30 min. It was then transferred to another balloon containing 12 mg of CuCl also under argon atmosphere and stirring. Eventually substrates were immersed for 3 min. The time of immersion determined the chain length of the polymer brushes.

5.2.2.3 Poly(*N*-isopropylacrylamide) physical characterization

5.2.2.3.1 Ellipsometry

To obtain the dry thickness of PNIPAM which is the thickness of the collapsed chain above the LCST, the grafted silicon chips were analyzed by a custom-built rotating compensator ellipsometer[191] with a 632 nm wavelength laser and a 70° angle of incidence. A refractive

index of 1.46 was considered for SiO₂ and 1.47 for PNIPAM[191]. A Si/SiO₂/PNIPAM multilayer was assumed. Measurements were performed in 3 different locations of the chips.

5.2.2.3.2 Contact Angle

In order to characterize the thermoresponsive behavior of the PNIPAM-grafted glass slides, static contact angle measurements were performed using a drop shape analyzer (DSA 100, Krüss, Germany). A temperature control engineered system was used to set the temperature of the substrates. The system was composed from top to bottom of thermal sensor (Pt 100, DM-314, Labfacility, France) glued to a Peltier element (121 W, MCHPE-200-14-11-E, Multicomp, France) which was bound with a thermal conductive tape (BOND-Ply 100, The Bergquist Company, France) to a radiator coupled to a fan (109P5412H2026, Sanyo Denki). The thermal sensor and the Peltier were wired to a thermo-controller (TEC SourceMeter 2510, Keithley) for the control engineering of the temperature (Figure 41). For each glass slide, measurements were carried out from 40°C down to 20°C with a step of 5°C. For each set temperature, 3μL of deionized water droplets were deposited on 9 different points of the glass slides. The average contact angle between the right and the left angle of each droplet was evaluated.

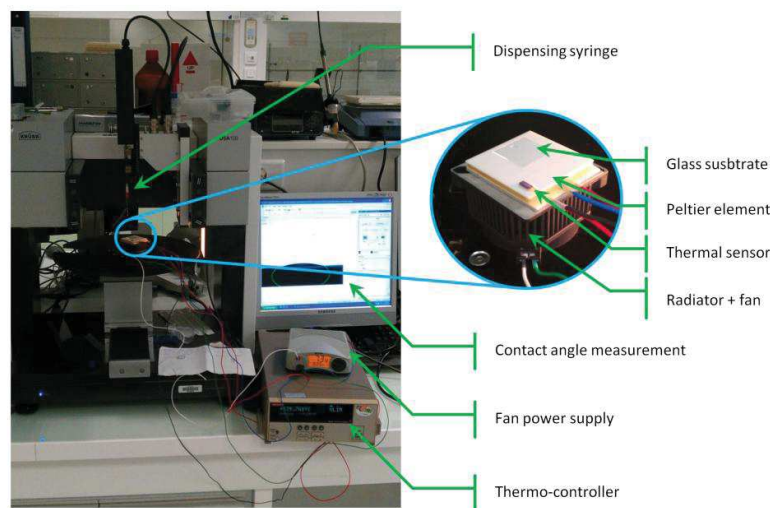


Figure 41. Contact angle measurement setup. The substrate to characterize is placed on a heating system (Peltier element on top of a radiator and a fan) coupled with a thermal sensor, placed on the heating system, to thermo-controller. Therefore, the temperature of the substrate can be precisely set by changing the command temperature on the thermo-controller.

5.2.2.4 Cell culture

Mouse embryonic fibroblast cells (NIH 3T3, ATCC) were grown in a 5% CO₂ incubator (MCO-20AIC, Sanyo) in 75 cm² tissue culture flasks (BD Falcon) with either phenol red DMEM (Dulbecco's Modified Eagle Medium, Ref 41966-019) containing 1 mM sodium pyruvate or non-phenol red DMEM (Ref 21063-029) containing 25 mM Hepes supplemented with 1% (v/v) sodium pyruvate (1 mM final concentration). Media are later respectively referenced as "red"

and “yellow” media based on their color of appearance. Yellow medium, or HEPES supplemented medium, was used to slow pH drift when medium was exposed to ambient atmosphere since the use of CO₂-independent medium was not conclusive (see section 4.1.3). This was to discriminate if pH variations have an impact on cell detachment. Each medium was supplemented with 10% (v/v) New Born Calf Serum (NBCS) and 100 U·mL⁻¹/100 µg·mL⁻¹ of Penicillin/Streptomycin (P/S). Media were changed every second day. Once cells reached a stage of 70% confluence they were sub-cultured by using Trypsin-EDTA (0.025%/0.01%) solution for 4 min at 37°C.

5.2.2.5 Cell detachment monitoring

Thermally-induced cell detachment was characterized using a home-built lensfree system (Figure 42). The lensfree video microscope as demonstrated in [192] consists of a 12-bit CMOS RGB sensor (MT9P031, APTINA) with a pixel pitch of 2.2 µm, measuring 5.7 mm x 4.3 mm and LED (dominating wavelength 525 nm) with a pinhole of 150 µm. In a typical experiment, a Petri dish containing the cells is kept on the sensor as shown in Figure 42.A. Illumination is provided by the Light Emitted Diode (LED) along with the pinhole from a distance of approximately 5 cm. The LED light scattered by the sample and the light passing directly from the source to the sensor interferes to form a holographic pattern, which is recorded by the sensor (Figure 42.B).

Glass slides (with and without PNIPAM) were sanitized by immersion in 70% ethanol overnight. From the harvested cells, a concentration of 10⁴ cells/cm² was seeded into Cytoo™ chambers containing the 20*20 mm substrates and the medium of interest (Figure 42.C). Cells were then cultured for 24h in the 5% CO₂ incubator at 37°C prior to cell detachment experiment.

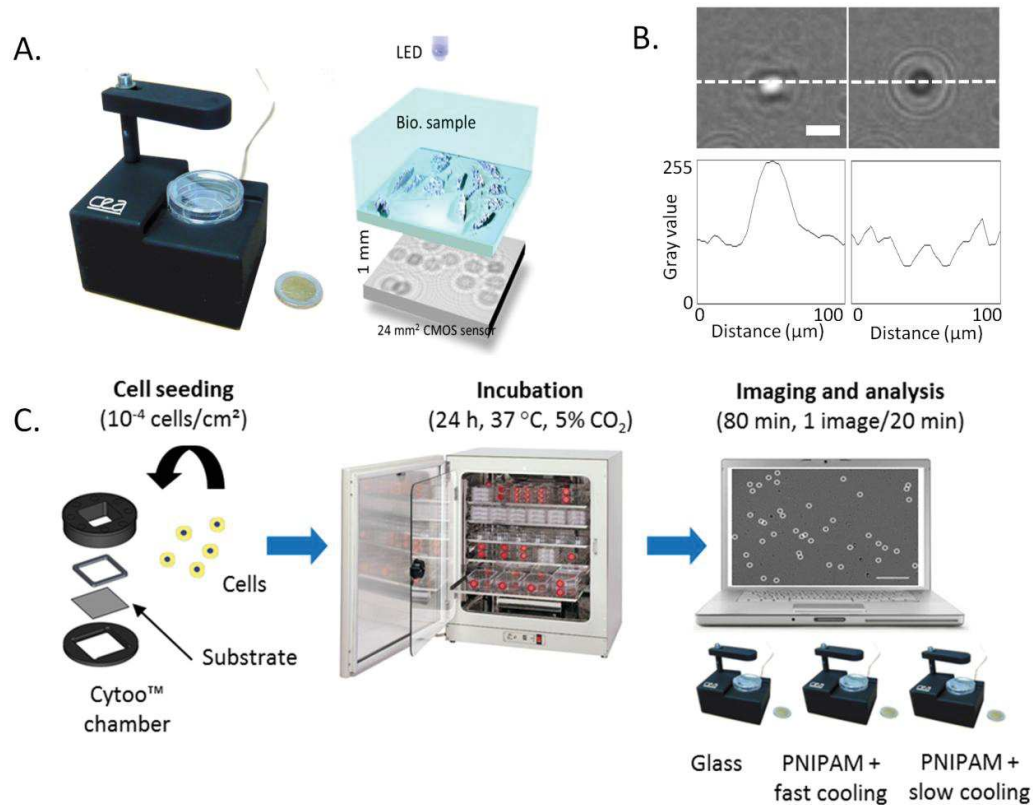


Figure 42. Cell detachment monitoring and set-up. **A)** Schematic of the lensless imaging system. Virtual picture of the system (left); Working principle (right). **B)** Reduction in cell-substrate contact during cell division and the corresponding change in the holographic pattern. Scale bar is 20 μm. Images acquired with 20 min interval. Adapted from [36]. The attached cell appears as a bright ellipse with side ripples whereas, when the cell detaches during division, it appears as a dark disc with concentric ripples **C)** Protocol schematic of a cell detachment experiment and monitoring using lens-free imaging systems.

To perform a run of thermal cell lift-off, 3 lensfree systems were placed in the dark, at room temperature: 1 system had a Cytoo™ chamber with a glass slide and 2 others with a PNIPAM-grafted glass slide. A total of five images were acquired at a rate of one image per 20 minutes to observe cell detachment. Right before the first image, medium was changed with a room temperature medium for one system imaging a PNIPAM-grafted glass slide and later referred as “fast” cooling, while the other system with a PNIPAM-grafted glass slide was let cooled down to room temperature (20-22°C) and later referred as “slow” cooling. Triplicate runs were carried out in order. This set of operations was performed for each type of medium: “red” and “yellow” media. The same operation was carried out with bare glass slides which served as a control experiment. PNIPAM substrates were immersed in 1 mL of trypsin-EDTA for 10 min at 37°C to remove the remaining cells followed by two washes with 1 mL of PBS-. 1 mL of trypsin-EDTA was dispensed afterwards on the substrates for 10 min at room temperature and finally they were

rinsed with 1 mL of PBS-. PNIPAM substrates were stored wet (PBS-) at 4°C between each cell culture experiment.

5.2.2.6 Immunostaining

Cell adhesion was characterized by immunostaining of actin filaments and focal adhesion points. Phalloidin was used to identify actin filaments and focal adhesion points were detected by labeling of vinculin. Cells were plated at 10^4 cells/cm² and incubated for 24 h on bare glass slides and PNIPAM substrates. Immunostaining was carried out either right after cell culture to fix cells before they feel a change in temperature or after changing the media to room temperature media followed by 20 min of incubation at room temperature. For bare glass slides, cells were cultured either in red or yellow medium, while for PNIPAM substrates, cells were only cultured in red media. Then cells were pre-permeabilized for 30 s with 0.5% Triton X-100 in 10% sucrose in cytoskeleton buffer (CB). CB is a deionized water solution with a 6.1 pH adjusted by addition of NaOH and containing 10mM 2-(N-morpholino)ethanesulfonic acid, 138mM KCl, 3mM MgCl and 2mM ethylene glycol tetraacetic acid. Cells were then fixed for 20 min using 4% (v/v) paraformaldehyde (PFA) in a solution composed of 10% sucrose in CB (solution A). Then cells were washed once with solution A and the PFA auto fluorescence was quenched by NH₄Cl (0.1 M) for 10 min. Cells were washed 3 times with PBS+ and non-specific sites were blocked by exposure to 10% goat serum 3% BSA for 1 h. Cultures were incubated with primary antibodies for 1 h (Vinculin diluted 1:800 in 0.1% (v/v) Tween20, 1% (v/v) BSA in PBS+), followed by 3 washes with PBS+. Cultures were then incubated with anti-mouse FITC conjugated secondary antibody diluted 1/500 in 0.1% (v/v) Tween20, 1% (v/v) BSA in PBS+, and actin filaments were stained with phalloidin TetramethylRhodamine B Isothiocyanate (diluted 1:800 in 0.1% (v/v) Tween20, 1% (v/v) BSA in PBS+) for 50 min followed by 3 washes with PBS+. Nuclei were counterstained with Hoechst 1:1000 for 5 min. A last wash was performed for 10 min and glass coverslips were mounted on glass slides with fluorescent mounting medium kit and stored at 4°C before imaging. Cells were imaged using a Nikon Eclipse Ti spinning disk confocal microscope with a 40x/1.3 NA objective.

5.2.2.7 Cell viability

In order to assess the cytotoxicity of the thermally-induced cell detachment, cell fate (i.e. necrosis and apoptosis) was determined by annexin-V and propidium iodide (PI) staining using the fluorescein isothiocyanate (FITC) Alexa Fluor[®] 488 Annexin-V (Dead Cell Apoptosis Kit , Invitrogen). Briefly, in cells undergoing apoptosis, a constituent of their plasma membrane, the phosphatidyl serine, is translocated from the inner to the outer leaflet of that membrane, thus exposing it to the external cellular environment[193]. Annexin V is a protein that has a high

affinity for this constituent. On the other hand, PI is a fluorescent molecule (excitation maximum: 535 nm, emission maximum: 617 nm) that binds to DNA. The membrane of viable cells is not permeable to PI while the one of dead cells is. Thus, cells in an early apoptotic stage can be discriminated from cells in a late apoptotic stage and necrotic cells upon changes of the plasma membrane integrity. Early apoptotic cells present binding sites for annexin V, but the integrity of their plasma membrane still prevents PI to enter and bind to DNA, while for apoptotic and necrotic cells the integrity of the plasma membrane is decreased and PI and annexin V can enter the cell to bind to their specific target[194].

3 types of samples were considered for this assay:

- Cells cultured on bare glass from which cells harvested by trypsin treatment were analyzed, later referred as negative control
- Cells cultured on bare glass undergoing thermal treatment from which only cells collected from the supernatant were analyzed
- Cells cultured on PNIPAM substrates undergoing thermal treatment from which only cells collected from the supernatant were analyzed

Conditions for thermal treatment were analogous to fast cooling, meaning that medium was changed with a room temperature medium just before the cell detachment experiment. This fast cooling assay was applied for the viability tests, so as to place the cells in the most stringent conditions and to evaluate their thermal resistance properties. After this fast cooling treatment, cells remained at room temperature for either 20 min or 80 min. Both media (yellow and red) were screened for each sample type and thermal treatment.

For the staining procedure, harvested cells were washed twice in cold PBS+ and re-suspended in 1× annexin-V binding buffer to obtain an aliquot of 100 µL. 5 µL of annexin-V-FITC and 1 µL of PI were then added and aliquots were incubated for 15 minutes at room temperature in the dark. Afterwards, binding buffer (400 µL) was added and cells were immediately analyzed using a BD LSR II flow cytometer (Becton Dickinson).

Non-stained cells were washed twice in cold PBS- and re-suspended in 1× annexin-V binding buffer to obtain an aliquot of 500 µL. The harvest of these cells was coordinated to analyze them by flow cytometry at the same time as the stained cells.

Triplicates were made for each sample. A viability assay was carried out for each type of medium (“red” medium and “yellow” medium) and 20 min and 80 min after initiating thermal mediated cell detachment, meaning a total of 4 viability assays.

5.2.2.8 Lensfree imaging of cell detachment

Once PNIPAM surfaces were characterized, the glass chips were used to carry out temperature mediated cell detachment experiments. An example to illustrate the counting achieved by the lensfree approach is given in Figure 43.

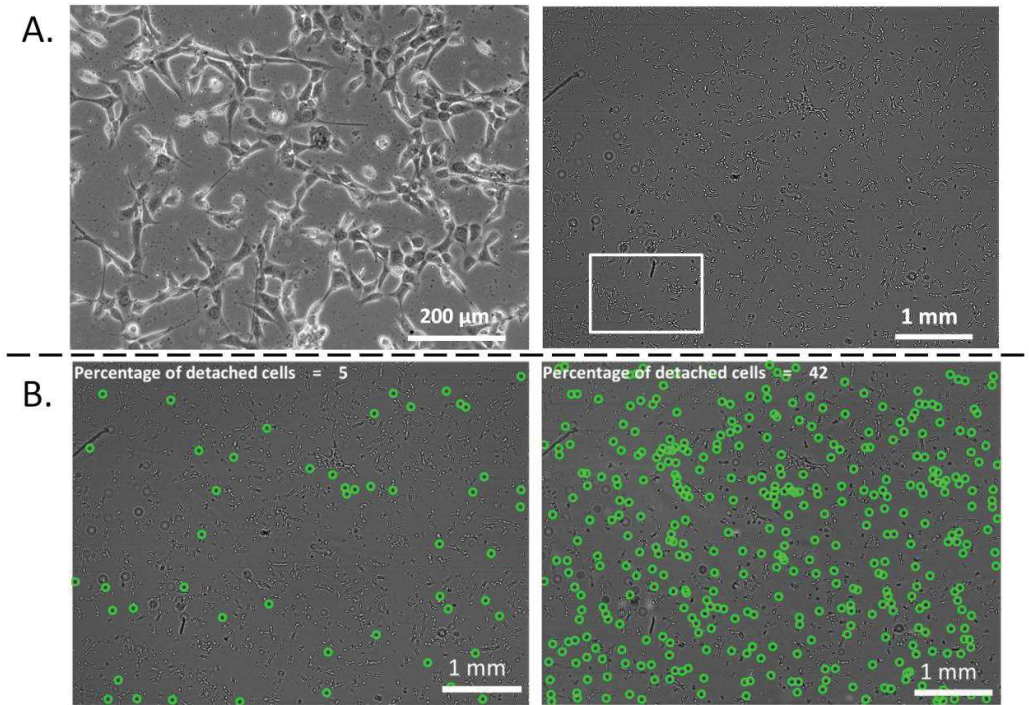


Figure 43. Lensfree imaging of cell detachment A. Comparison between microscopic (x10), left image, and lensless field of view, right image. The white square represents the size of the microscopic field of view. B. Cell detachment quantification based on the data recorded by the lensless system. Cells identified to have a cell-detached-like pattern are counted at t=0 (left) and t=20 min (right) and circled by an algorithm.

Cell detachment was studied in combination of different parameters:

- the rate of the medium temperature variation (“fast” cooling or “slow” cooling)
- the type of medium (“red” medium : red phenol DMEM supplemented with 10% (v/v) NBCS and 1% (v/v) P/S, or “yellow” medium: non-red phenol DMEM supplemented with 1% (v/v) sodium pyruvate, 10% (v/v) NBCS and 1% (v/v) P/S)

For the first point, thermal infrared characterization of the cooling of a Cytoo™ chamber with media from 37°C to room temperature (supplementary SX) showed that within 4 minutes its temperature dropped below the LCST and reached room temperature in less than 20 min (see

Appendix H).

5.2.3 Physical characterization of PNIPAM-coated substrates

The thickness of the polymer layer on PNIPAM-coated surfaces was determined to be 38 nm \pm 5 nm (N=3) by ellipsometry. The thermal behavior of the grafted substrates was investigated through static contact angle measurements on the PNIPAM glass chips and was compared to a bare glass slide before (Figure 44.A) and after several cell culture experiments (Figure 44.B).

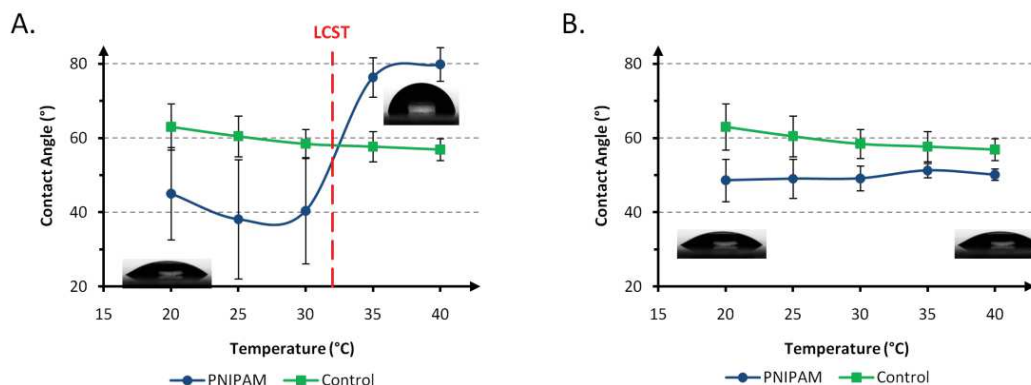


Figure 44. Contact angle as a function of the temperature. A) PNIPAM substrates thermal behavior right after synthesis (N=3). The grafted substrates exhibit the expected “S curve” according to the temperature and a LCST around 32°C. B) PNIPAM substrates after several cell culture experiments (N=3). The substrates do not respond to the temperature anymore.

Before substrates were used for cell culture, the mean contact angle slowly decreased with increased temperature in the case of the glass slide while a characteristic “S curve” was observed for the PNIPAM glass chip with a LCST between 32-33°C (Figure 44.A). The measured value for the LCST was consistent with data reported in the literature and validate that PNIPAM grafting was achieved. After more than 3 consecutive uses of PNIPAM substrates with cells, despite trypsin treatment, PNIPAM seemed to lose its thermoresponsive capability and behaved quite similarly as a bare glass slide (Figure 44.B).

5.2.4 Biological characterization of PNIPAM-coated substrates

5.2.4.1 Lensfree imaging data

The results from the lensfree data analysis are plotted in Figure 45.A for bare glass slides (i.e. control substrates, without PNIPAM) and Figure 45.B for PNIPAM-grafted glass slides. Each condition exhibited strong variability in cell response visible by the large error bars. The most reproducible results were obtained for the control experiments with the “red” medium. The control immersed in the “yellow” medium showed high variability in the initial number of cell detached. This initial detachment may correspond to either dividing cells or dead cells. The graph (Figure 45.B) shows that over time, the “yellow” medium induced a 2-fold higher cell detachment compared to the “red” medium. After 80 min, the percentage of detached cells

reached 30% in the “yellow” medium compared to 15% in the “red” media. By contrast, the type of medium had little influence on cell detachment on PNIPAM chips: for a given cooling speed, curves follow closely the same trends (Figure 45.A). Moreover, in control conditions, a fast cooling speed rate combined with the use of yellow medium induced in the first 20 minutes the highest percentage of cell detachment (nearly 30%), a percentage which plateaus up to 80 minutes in the case of a slow cooling speed rate. Similarly, in the case of PNIPAM, we observed that “slow” cooling conditions induced a linear cell detachment over time from 5% to 25% of detached cells. By contrast to control slides, “fast” cooling conditions induce only a slight increase in the detachment within the first 20 min (20%) followed by either a plateau or a slight reduction of cell detachment.

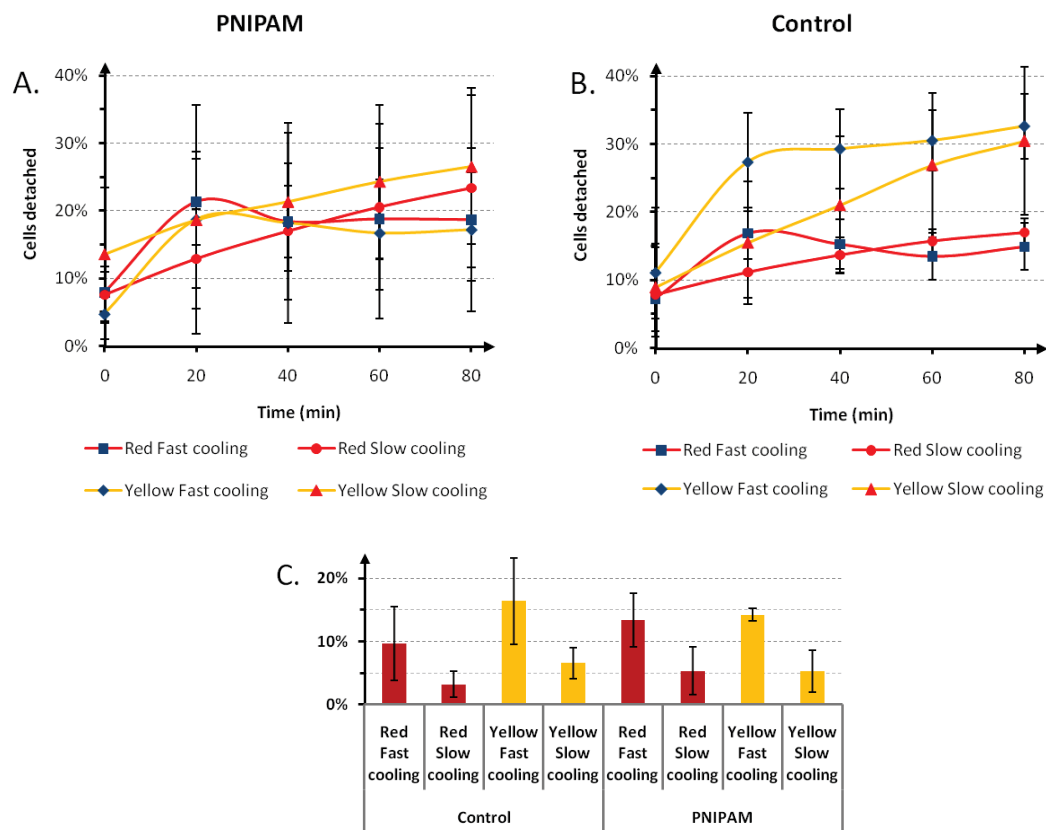


Figure 45. Cell detachment over time for control (bare glass) (A) and for PNIPAM-grafted glass slides (B) from lensfree image analysis. C) Percentage of cell detached between t=0 min and t=20min versus media type and cooling rate (C). N=3.

Since major effects either from media type or temperature variation were mainly observed within the first 20 minutes, data variation between time points of 0 minute and 20 minutes have been represented in the Figure 45.C. The cell detachment at t=0 is therefore subtracted from the cell detachment at t=20 min. Results summarize that in control (uncoated substrates) a high detachment rate was obtained with yellow medium and fast cooling. By contrast, in PNIPAM

conditions (coated substrates) the highest detachment rate was only obtained with fast cooling but was not influenced by the media type.

Among the substrates that were analyzed, the use of one of them could be tracked. It means that the data acquired on cell detachment could be related to the number of time a substrate had been used. Figure 46 shows the detachment rate followed over time for consecutive cell detachment experiments. It clearly shows the loss of efficiency starting from the second time a substrate had been used: from 75 % of efficiency 20 min after initiating thermal cell detachment during the first experiment to 13% in the second. The same poor efficiency in cell detachment is conserved in the next experiment (i.e. third experiment).

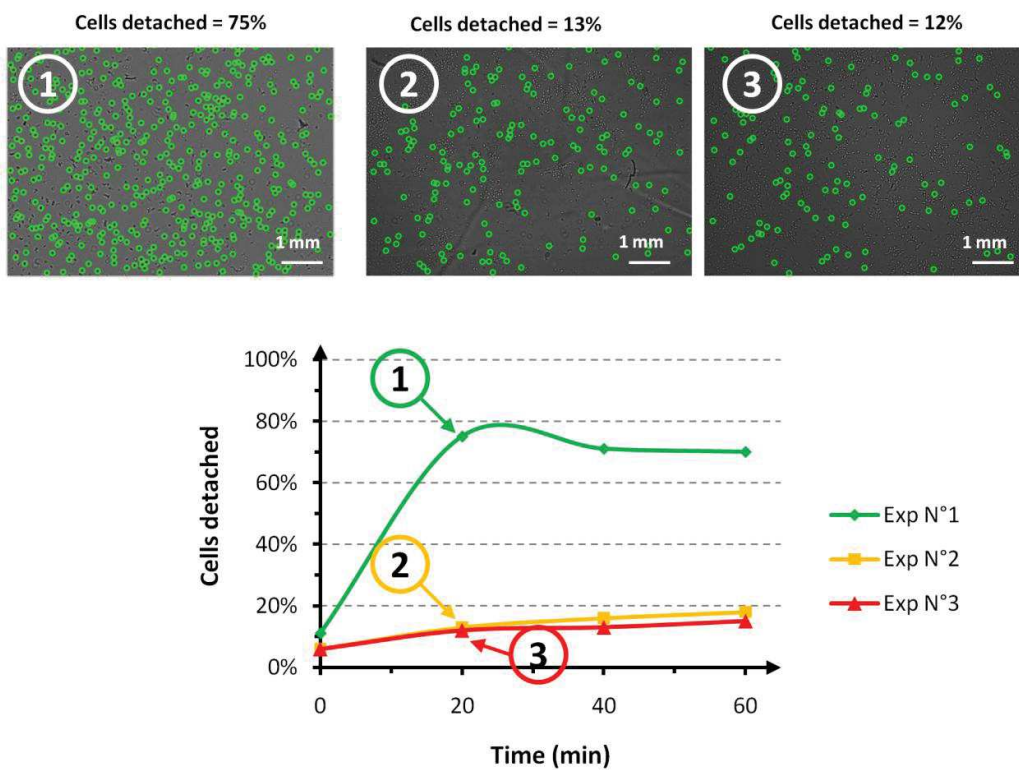


Figure 46. Monitoring of cell detachment rate over time for consecutive assays with the same PNIPAM-grafted substrate. Top images are lensfree acquisitions 20 min after initiating cell detachment: from left to right, the first to the third experiment. There is a significant decrease in the cell detachment efficiency with successive cell culture-cell detachment experiments.

5.2.4.2 Cell adhesion characterization on non-coated and PNIPAM-coated substrates

Cells adhesion involves actin filaments and focal adhesion points that were visualized by immunostaining techniques. The organization and level of expression of vinculin indicates differences in adherence upon different conditions (temperature, type of substrates and media) as depicted in Figure 47.

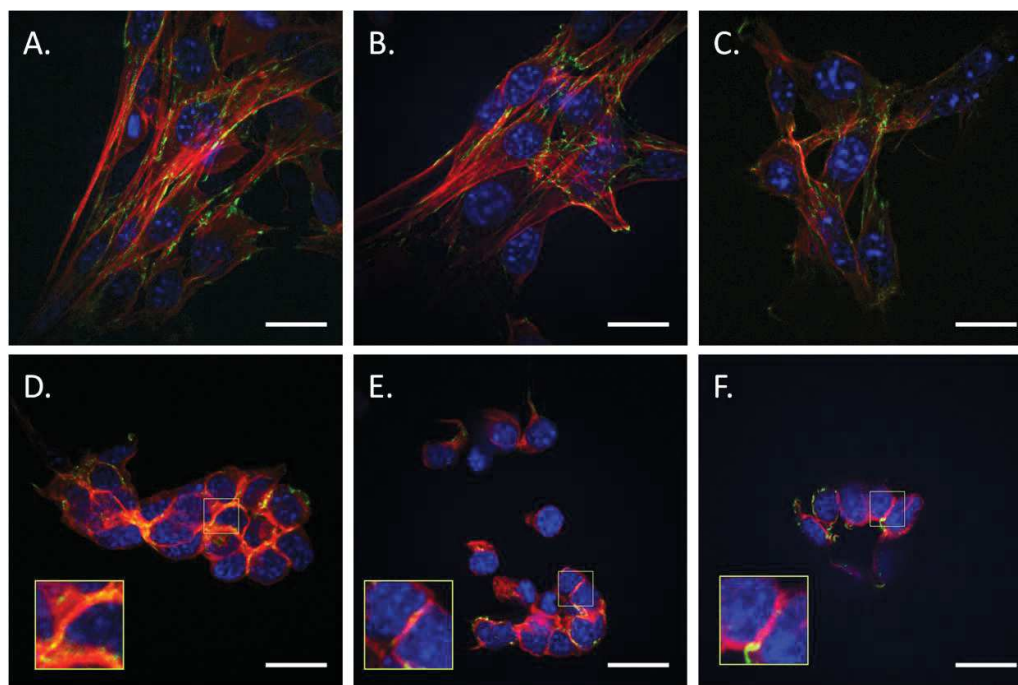


Figure 47. Immunostaining of nuclei (blue), phalloidin (red) and vinculin (green) of NIH 3T3 cells after 24 h of culture. A-C : Cells were stained right after incubation at 37°C; D-F: cells were stained after 20 min incubation at room temperature. A,D cells cultured in red media on PNIPAM. B,E cells cultured in red media on glass. C,F Cells cultured in yellow media on glass. Zoomed inserted images are magnified 2.5 times. Scale bar is 20 μm .

At 37°C cells present an expected elongated morphology when cultured in the red medium on both bare glass and PNIPAM substrates (Figure 47.A & B). Vinculin is present in both samples, at the periphery of the cells at the terminal parts of actin filaments and on the cell surface. By contrast, cells cultured in yellow medium displayed rounder cell morphology and lower expression of vinculin, which indicated a lower cell adhesion (Figure 47.C). Upon change in temperature to 20°C for 20 minutes, cells lost their fibroblastic morphology in all culture media and on all substrate types (Figure 47.D-E). A drastic reorganization of vinculin was observed, as well as co-expression with actin localized at the cell-cell contacts. Cells detaching on PNIPAM substrates presented a higher level of vinculin/actin co-expression while glass substrates, irrespectively of the media used, had lower co-expression consistently with the lower expression of vinculin observed at 37°C.

5.2.4.3 Cell viability upon thermally mediated harvest

In order to evaluate the viability of the cells detached upon thermal variations, a cell viability assay was performed (Table 13). Cells from negative controls had similar high viabilities irrespectively of the culture medium used. However, cell viability decreased upon thermal treatment. Differences were also visible depending on the medium type and the duration of the thermal treatment.

Mainly, cells collected from the yellow medium had a lower viability (about 15%) than from the red medium. Moreover, the longer the cells were exposed to room temperature the lower the viability was, though this difference becomes negligible with time. Detached cells presented high viability after 20 min at room temperature and comparable results were obtained between glass and PNIPAM substrates for cells cultured in red medium. The mediocre viability observed with the yellow medium after 20 min at room temperature from glass may be due to a low number of events (about a hundred events compared to a thousand normally) detected during FACS analysis. Thermal treatment, regardless of the culture conditions, did not favor apoptosis over necrosis according to the cell viability test.

Short cell detachment (i.e. 20 min long) was preferable to obtain a higher percentage of viable cells that endured thermal mediated harvest with no impact from the substrates but from the type of culture medium.

Table 13. Cell viability assay versus medium type and thermal treatment duration. Negative controls are cells cultured on glass and collected after trypsinization. *V: viable, A: apoptotic and N: necrotic.

		Red medium						Yellow medium					
		V*	A*	N*	V	A	N	V	A	N	V	A	N
Negative control	Glass	97.0%	1.9%	1.0%				100.0%	0.0%	0.0%			
		After 20 min at RT			After 80 min at RT			After 20 min at RT			After 80 min at RT		
Thermally treated	Glass	86.2%	6.6%	7.2%	–	–	–	52.0%	28.0%	20.0%	–	–	–
	PNIPAM	88.1% (±2.3%)	5.6% (±0.9%)	6.1% (±3.3)	24.5% (±6.9%)	12.8% (±3.5%)	61.9% (±4.7%)	71.9% (±5.8%)	15.5% (±1.3%)	12.5% (±4.5%)	26.4% (±14.8%)	37.1% (±7.6%)	36.6% (±7.4%)

5.2.5 Discussion

PNIPAM has been developed in 1990 by Okano and his group at the institute of Biomedical Engineering in Tokyo Women’s Medical School. Authors first demonstrated a novel methodology to harvest and expand cells using thermo-responsive polymeric surfaces. Since then it has been used in diverse fields such as optics[195] and rheology[196]. To date, its utilization is mainly addressed in biological application for drug delivery[197] and cell sheet engineering[198].

However, temperature mediated cell detachment is still not completely understood and remains mostly qualitative.

This thesis work focused on the characterization of key features of cell detachment from the synthesized PNIPAM layer and glass. The thermal influence upon fibroblastic cell detachment was studied. The data presented highlight the influence of the culture conditions, such as the type of culture medium and the rate at which it is cooled, on cell detachment yield on both PNIPAM-coated glass and non-coated glass substrates.

To evaluate cell detachment, we relied on a lensfree imaging system. Kesavan et al. were able to correlate a change in the holographic pattern when cells lift off during division[192]. Similarly, cells that are lifting off during detachment experiment can easily be identified by pattern recognition among several thousand of cells. Consistent with the literature[199], a morphological change occurs when cells detach from the surface: cells are initially spread then become rounded and finally lift off from the surface. Even if lensfree video microscopy does not provide detailed morphological information on the imaged cells as compared to a standard microscope, the holographic pattern of cells allows for a rapid and direct screening of cell detachment. This innovative imaging system offers a significant advantage compared to microscopic observations. It grants a wider field of view of 24 mm² as depicted in Figure 43. The imaging area is approximately 10 times larger than that of a microscope at 10 times magnification. Hence, a much higher number of cells can be imaged at once: thousands compare to hundreds with a microscope allowing for significant statistics. Besides, the analysis of standard microscopic images can hardly determine if cells really lift off from the surface. As a consequence, studies have either considered the morphological change of cells[200] or counted the cells from the harvested supernatant[192]. The former do not confirm that cells actually detached and the latter is user-dependent leading to high variability. When detached cells are collected by aspiration of the supernatant, the hydrodynamic shear stress induced, even if low, may contribute to detach other cells that were weakly attached[201]. This shear stress is obviously variable since it is operator-dependent, adding a variability in the evaluation of the number of cells actually detached solely by the effect of the temperature on thermoresponsive surfaces. The lensfree technology overcomes the aforementioned shortcomings since it can detect *in-situ* the change of height of cells due to a change in their holographic pattern without involving the action of an operator. However, there are some limitations when using the lensfree approach to quantify cell detachment. The first is also common to standard microscopic observations since the dividing cells also exhibit a similar pattern to that of cells detached; quantification of cell detachment could be erroneously increased. However, it has to be noted

that dividing cells re-attach to their substrate after cytokinesis. Hence, the erroneous detection is temporary and is usually not observed in the subsequent image frames. Secondly, pattern recognition of detached cells may provide an underestimation if such cells form clusters, especially at high density. Nevertheless, this is not very often observed and can be addressed by the optimization of the density of cell seeded as performed in this study.

As outlined in the introduction of this chapter, the synthesis of PNIPAM surfaces enabling cell adhesion and efficient cell detachment calls for control over PNIPAM layer thickness and density. Atom-transfer radical-polymerization (ATRP), a class of controlled living polymerization, has gained interest to achieve reproducible grafting of polymer brush with specific thickness and density without the need for expensive laboratory equipment[202]. The strategy built here aimed to fabricate planar PNIPAM-grafted surfaces using the ATRP synthesis to evaluate the stability of the biomaterial and more particularly the biological response of mouse fibroblast NIH 3T3 during temperature-mediated detachment. It was first shown with ellipsometry and static contact angle measurements that PNIPAM was successfully grafted on glass slides by ATRP and proved to respond to temperature variations. Ellipsometry measurement confirmed the deposition of a layer with a defined thickness of 38 nm. Furthermore, contact angle measurements validated that this layer was made of PNIPAM since it responded to the temperature with the same characteristics as it has been widely reported for PNIPAM, with a LCST around 30-32°C.

However, successive characterizations of cell detachment based on the lensfree approach indicated that cells detached with a low yield without significant differences between control and PNIPAM surfaces. It could be argued that this low efficiency is dependent on the density of the synthesized PNIPAM substrates as has been already outlined[187]. This data has been missing and could normally be obtained by either:

i) determining the swelling factor of the polymer chains (i.e. ratio between the thickness of the PNIPAM layer in good solvent state and the thickness of the PNIPAM layer in bad solvent state). Malham and Bureau demonstrated the correlation between this parameter and the PNIPAM chain density[203]. They used a surface force apparatus to determine the swelling factor of their polymer.

ii) or characterizing the degree of polymerization of the polymerized PNIPAM chains or their molecular weight. This is usually achieved by co-currently synthesizing free PNIPAM when grafting substrates with PNIPAM[156]. The Polymer chain density can then be obtained with either (Eq. 17) or (Eq. 18)[187,203]

$$\sigma = \frac{h_{dry}}{Na^3} \quad (\text{Eq. 17})$$

where σ is the polymer density (chain per surface unit), h_{dry} the thickness of the polymer in bad solvent state, N the degree of polymerization (number of monomer per polymer chain) and a the monomer size ($\approx 5 \text{ \AA}$)[204].

$$\sigma = \frac{h_{dry}\rho_P N_A}{M_N} \quad (\text{Eq. 18})$$

where ρ_P is the monomer density (0.95 g.cm^{-3} [205]), N_A the Avogadro's number and M_N the molecular weight.

Unfortunately, none of these methods could be applied due to the lack of some equipment and to the difficulty in synthesizing PNIPAM-grafted surfaces because one chemical reagent (BIBB) was identified to be corrupted after many attempt failures.

The poor difference observed between PNIPAM-grafted and bare glass slides regarding cell detachment (Figure 45) rather led to hypothesize that PNIPAM properties had been lost after repetitive culture experiments. Indeed, contact angle measurements performed on recycled trypsin-treated substrates suggests, that PNIPAM chips lost their thermosensitivity (Figure 44), a case not reported so far. Additionally, tracking the detachment of cells on the same PNIPAM substrates using lensfree imaging (Figure 46) highlighted a significant loss of efficiency in cell detachment after the first experiment. When PNIPAM swells with lower temperature it becomes softer and the balance of the forces between the cells and the polymer is lost. Therefore, the cytoskeletal tension forces prevail over a decreased mechanical resistance from the substrate. This loss of equilibrium, along with the pressure exerted on the ventral cytoplasmic membrane due to the swelling of the polymer chains leads, in theory, to a combination of extra-cellular matrix (ECM) proteins desorption and ECM-integrin bonds break[206]. Those events are practically verified by the facts that cells are known to detach with the majority of their ECM[207], but not all, since some components (i.e. proteins) of that ECM could be found on PNIPAM substrates after cell lift-off[208]. Based on this fact, we believe that biofouling of the PNIPAM surfaces from cell ECM proteins might have occurred and hampered its thermosensitivity. The recommendation when using commercial PNIPAM substrates goes in this direction since it advises to “not re-use the product as the residual matrix and media components may absorb to the surface, comprising performance.”[209].

Even if PNIPAM substrates did not work as expected, our experiments showed that cell detachment could occur on standard glass and be modulated according to the culture conditions. More particularly, culturing cells in different media and depending on how fast they were cooled to room temperature relatively changed the quantity of cell detachment. We have observed with the lensfree approach that NIH 3T3 cells detachment is enhanced by both the use

of our yellow medium and fast cooling on bare glass, whereas cells are only sensitive to the cooling rate on PNIPAM surfaces. In addition, immunostaining characterizations evidenced a weaker cell adherence when cells are cultured on glass in yellow medium than in the red one before proceeding to detachment at low temperature (Figure 47). Cells may reduce equally their adherence, but as in yellow medium they were already weakly attached, they were able to detach more easily. The media buffering capacity may be the reason for such a difference since media composition mainly differs by the presence of a HEPES buffer (yellow media) or Phenol Red (red media). Besides, a study from Svajter and Jeras[210] has evidenced that HEPES buffered media had a similar negative impact regarding cell morphology on dendritic cells. However, it is not clear why no difference in cell detachment occurred on PNIPAM substrates from one medium to another.

Eventually, it has been demonstrated that the relevant time scale to consider for thermally-driven cell detachment is around 20 minutes. Above this limit, the viability of the detached cells keeps decreasing while the number of cells detaching reduces. It is most likely that after 20 min, most of the cells detaching are dying cells. The cellular mechanisms involved in cell detachment may occur within the first 20 min.

5.2.6 Conclusion

Efforts were made to identify potential effects of culture conditions on temperature-triggered cell detachment thanks to a novel methodology for cell detachment counting. To do so, quantitative detachment assays were performed by using DMEM Phenol Red buffer or HEPES buffer and by varying the cooling rate of the samples. Little difference appeared between PNIPAM-coated substrates and bare glass substrates (controls) regarding cell detachment performance due to a loss of the thermosensitive properties of PNIPAM substrates, possibly due to biofouling. Despite this fact, cell detachment was enhanced by a rapid temperature ramp down to room temperature on both, bare glass and PNIPAM. This detachment was more significant for cultures carried out in HEPES buffer than on control glass slides. The lowest adhesion of cells, as characterized by their morphology and their down-expression of vimentin protein (focal adhesion point markers) during cell culture in these conditions (i.e. HEPES-buffered media, glass substrate), was correlated with the highest cell detachment. However, the impact of the medium type was not significant with PNIPAM substrates. In addition, both short time for cell detachment and HEPES-buffer-free medium were correlated with greater cell viability. In conclusion, PNIPAM appears to be non reusable to perform thermally-triggered cell detachment. As a consequence, the scenario previously established aiming at re-using PNIPAM-grafted microcarrier for successive cultures inside the bioreactor seems impractical. In the best

case, the use of PNIPAM coated microcarriers could only offer a way to deliver cells separated from the microcarriers a single time.

5.3 Microcarrier dissolution

Since the results obtained with PNIPAM substrates were not meeting initial expectations, another harvest scenario has been investigated. The standard harvest protocol based on trypsin appeared to be poorly effective for the cell detachment from microcarriers. The scenario which has not been reported to any extent consists of dissolving the cytodex microcarrier made of dextran by using an enzyme, dextranase. Cytodex microcarrier dissolution has only been reported by Lindskog *et al.*[211].

NIH 3T3 cells were cultured on microcarriers following the same protocol as in section 4.2.2. Cells were cultured 24h on microcarriers before harvest with trypsin or dextranase. Cell harvest based on trypsin was performed as follows: cells on microcarriers were washed twice in 2 mL of PBS- and then immersed for 10 min in 2 mL of trypsin. Cell harvest based on dextranase was performed by simply replacing half of the culture volume by medium supplemented with 2% (v/v) dextranase (bought from Sigma) to achieve a final concentration of 1% (v/v) dextranase. Microcarrier dissolution was monitored at room temperature under a microscope.

Figure 48.A shows the degree of detachment achieved after using trypsin for cell detachment. A large number of cells remained on the microcarriers even though cells changed their morphology from flat and spread to round. When dextranase was used for cell harvest, the microcarriers dissolved progressively until completely disappearing in about 20 min (Figure 48.B). After microcarrier dissolution, only cells remain in clusters of different sizes or as single cells. Cell clusters are most likely the result of the non-degradation by dextranase of cell junction formed during proliferation on the microcarriers. A proof-of-concept to use dextranase in the bioreactor was carried out by filling with a pipette the upper channel of a CCC with cells on microcarriers (concentration 2 mg/mL) and, afterwards, filling the lower channel with dextranase 2% (v/v) in medium. The microcarrier dissolution was followed by observation with a microscope. The complete microcarrier dissolution took about 5 min longer (Figure 48.C) than in Petri dish since dextranase had to diffuse through the membrane before reaching the microcarrier.

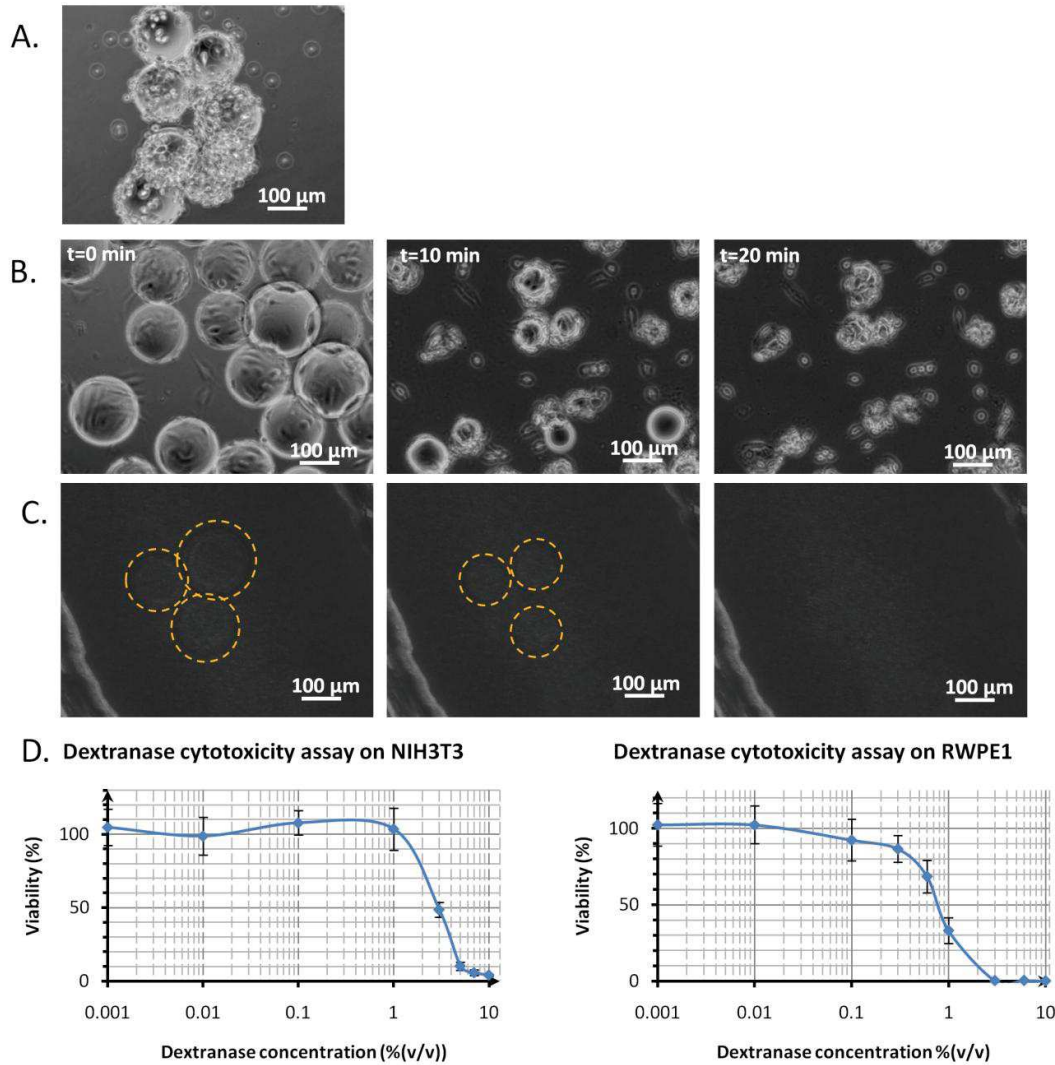


Figure 48. Cell harvest from microcarriers comparing the use of trypsin (A) and dextranase (B-D). A) Cells on microcarriers treated with trypsin for 10 min. B) Microcarrier dissolution using 1% (v/v) dextranase. Images were taken each 10 min. C) Microcarrier dissolution inside the CCC. Dextranase dispensed in the perfusion channel diffuses through the porous membrane and then dissolves the microcarriers in the culture channel. Images taken at 0, 15 and 25 min (from left to right). D) Cell viability versus dextranase concentration (N=6). Left: NIH3T3 viability. Right: RWPE1 viability.

In order to evaluate the impact of dextranase on cells, a cytotoxicity assay was performed with two type of cells: NIH3T3 and RWPE1 (human prostate cells) relatively identical to PC3. Cells were seeded at 10^4 cells/mL in 200 μ L of medium in a 96-well plate and cultured for 24 h. Medium was replaced with 200 μ L of medium containing either a dextranase concentration of 10^{-3} , 10^{-2} , 10^{-1} , 1, 3, 5, 7, or 10% (v/v). Medium without dextranase or with 10 mM H_2O_2 were used for the negative and positive controls, respectively. Six samples were performed for each condition. The cells were incubated for 24 h and then rinsed twice with 200 μ L of PBS-. Afterward, the cells were incubated for 24 h with 100 μ L of culture media. Then, 10 μ L of WST-1 was added to each well. After 3 h, the absorbance was recorded at 450 nm (soluble formazan

titration) and 690 nm (background subtraction) using a microplate reader (Infinite M1000, Tecan). The absorbance difference (450–690 nm) was directly proportional to the number of viable cells. The percentage cell viability was determined using (Eq. 14), where AS, APC, and ANC represent the absorbance values of the sample, the positive control (cells with H₂O₂), and the negative control (only cells), respectively.

Dextranase exhibited a marginal toxicity up to 1% (v/v) (after 24 h of incubation with cells) with NIH3T3 (Figure 48.D). The IC₅₀ (concentration threshold corresponding to 50% viability) was obtained for 3% (v/v) dextranase. RWPE1 cells demonstrated a higher sensitivity to dextranase: the marginal toxicity was up to 0.3 % (v/v) dextranase and an IC₅₀ corresponded to 0.8% (v/v) dextranase (Figure 48.D).

To conclude, dextranase was effective for harvesting cells from microcarriers with, the observation that cells remained in clusters if they had formed junctions during their growth on microcarriers. Moreover, a protocol for cell harvest with dextranase is possible inside the bioreactor. However, the dextranase toxicity has to be evaluated before using this treatment since different cell types demonstrated different sensitivities to dextranase. Also, further studies should be performed to evaluate other effects that dextranase may have on cell metabolism.

5.4 Bead-to-bead cell transfer for subculture

Cell bead transfer is a well-known phenomenon in bioprocess engineering[212] and is one of the methods used to expand cell culture and increase the productivity of a batch. This cell feature creates opportunities to perform long-term cell culture; empty microcarriers can be added inside the bioreactor once a certain number of cells is reached, and part of the microcarriers already covered with cells can be simultaneously extracted from the system. The remaining cells will be able to colonize the empty beads, and proliferation will continue. Repetitions of this process can significantly increase the culture duration and open routes toward continuous cell culture processes.

A proof of concept was not demonstrated during this thesis. However, based on our microcarrier cell culture experiments (see section 4.2.2), it can be stated that the microcarrier concentration will most likely need to be higher than the current microcarrier concentration used in the bioreactor. In this case, bead-to-bead contact will allow the cells colonizing empty microcarriers. An alternative could be to implement in the bioreactor a function that concentrates the microcarriers to facilitate this bead-to-bead transfer.

5.5 Conclusion

From a literature study, microcarrier coating with PNIPAM appeared to be the most relevant alternative to proteolytic treatment to perform cell harvest inside the bioreactor which preserves cell viability and integrity. Besides, trypsin as used in this thesis did not yield an efficient harvest of cells from microcarrier. There remains a need to find a cell harvest alternative. The thermal-mediated strategy would avoid setting complex microfluidic protocols and cell harvest could be simply achieved by cooling the culture environment, which does not represent a technical challenge. However, a limitation which has not been reported in the literature for PNIPAM has been brought to light. Even if studies show that it can reversibly respond to temperature by exhibiting alternatively more hydrophobic and more hydrophilic surfaces with temperature variation around its LCST, re-using PNIPAM surfaces for cell harvest is not possible. The polymer chains rapidly lose their thermal response after successive cell cultures, most likely due to biofouling. PNIPAM remains a viable option to perform simple cell harvest inside the bioreactor but only for a limited number of cell detachments per microcarrier. As an alternative, dextranase demonstrated efficient and complete microcarrier dissolution inside the CCC, within timeframes comparable to a standard cell harvest protocol involving trypsin without affecting cell viability. Additionally, dextranase has the advantage not to be inhibited when diluted in culture media. Specific studies would be necessary for each cell type to determine the proper concentration to use since data in the literature are missing on this aspect. Two different cell types, in this thesis, showed a significant difference of sensitivity to dextranase concentration (about 10-fold). Further work should also address the impact of dextranase on the cell metabolism.

Bead-to-bead transfer may represent another solution to maintain a certain cell population inside the bioreactor provided that microcarriers would be close enough to allow fresh microcarrier colonization by cells on other microcarriers.

Eventually, all the strategies identified to harvest cells from the bioreactor will need to rely on bead-to-bead transfer to maintain a stable cell population inside the bioreactor since continuous proliferation will require new available surfaces for cell growth. The use of methods such as thermally-induced cell detachment from PNIPAM-grafted microcarrier or microcarrier dissolution by dextranase will most likely depend on the need of the end user to obtain cells separated from their growth surface or not.

6 General conclusion

A benchtop microfluidic bioreactor, complying with the standard microfluidic platform and format used in the host laboratory, has been successfully fabricated during this thesis to perform continuous cell culture. Solutions were developed to provide the adequate conditions for cell proliferation (perfusion, thermal regulation...). Integrated cell harvest was also performed with the final goal to achieve long-term cell culture in the bioreactor.

Regarding **cell proliferation**, several integrated tools and functions have been integrated at the level of the bioreactor to regulate the physical and biochemical cell environment:

- porous-membrane-based perfusion has been implemented inside the bioreactor and proved to be fully functional (leakage free, no hinder of the trans-membrane mass transport)
- a numerical model has been developed to characterize the biochemical (nutrients and O₂) cell environment and determine the most suitable perfusion flow rate considering the technical constraints to provide relatively stable levels of nutrients and oxygen over the bioreactor geometry
- the heater has been scaled-down to a thin sheet adjoined to the culture area and coupled to a miniaturized commercial sensor integrated in the bioreactor to provide a uniform and controlled temperature to the culture area
- low gas permeable materials have been used to limit gas exchange with the atmosphere in order to avoid pH drift.

Innovative solutions were considered to integrate and simplify **cell harvest**. The main approach has been chosen to rely on microcarriers, offering growth surfaces, to perform cell harvest by fluidic transport. Three approaches were considered:

- thermally-triggered cell harvest by coating microcarriers with a thermosensitive polymer (PNIPAM)
- microcarrier dissolution by enzymatic treatment
- simple delivery of confluent microcarriers

In the first approach, assumptions that coated microcarriers could be reused to perform consecutive cycles of cell proliferation and cell detachment were not confirmed. A single cell harvest remains a possible option, though. The complete dissolution of the microcarriers at non-toxic levels validated for the second approach makes it a promising method. However, even if the preliminary results remain encouraging, the control of microcarriers through fluidic transport has yet to be demonstrated.

Generally, the presented system proved to guarantee sterile conditions for cell cultures on a regular lab bench. Moreover, these cultures were achieved autonomously without requiring a cumbersome incubator. Such cultures are practically not feasible for most of the microfluidic cell culture systems since they are often made in PDMS, a porous material, suffering from medium evaporation and undesirable gas exchange affecting the culture environment conditions. In the aforementioned conditions, the bioreactor successfully demonstrated the possibility to perform continuous cell cultures of various cell types during several days: insects cells were cultured for 5 days and mammalian cells for 3 days. Regarding the mammalian cell cultures performed, a breakthrough has been achieved compared to the cultures performed in microfluidic systems since microcarriers were used as growth support. Although microcarrier cell culture is routinely performed in the industry, no autonomous microfluidic culture system has addressed this type of culture yet. Such miniaturization is a major step forward for bioprocess applications where the need to develop scaled-down bioreactors that mimic large scale operation has been clearly identified to shorten and reduce the costs associated to bioproduct development.

7 Perspectives and future work

The current system has met with many of the objectives defined. However, some still need to be addressed and, with further improvements, the cultures can surely be extended beyond what has been achieved so far. The next developments should consider:

- The integration of more sensors such as pH or O₂ sensors. Such integration would better qualify the bioreactor and give essential information on the state of the culture. For instance, the integration of a pH probe would quantify the magnitude of the pH drift observed due to the porous tubing. Moreover, acquiring data for culture conditions is a key to understanding and characterizing cell development and behavior. To find application in bioprocess development, more sensors (e.g. glucose, lactate, ammonia, cell density sensors) would need to be integrated since macroscale bioreactors heavily rely on them to monitor and control cell proliferation.
- Solutions to actively and independently regulate the culture conditions to defined levels. Therefore, the system could apply dynamic stimuli to the cells for cell studies or perform different culture runs in different conditions to mimic scale-up operations. These solutions should be coupled with the integration of sensors in closed-loop configurations to provide higher levels of regulation on the culture conditions.
- Increasing the throughput of the culture to benefit from all the advantages that microfluidics may provide. The design should be transformed to propose parallel culture chambers that can operate and control culture conditions independently. This new design will increase the screening capability of the system.
- The integration of micropumps will most likely reduce the actual footprint of the dispensing system.

Further investigations on the proposed cell harvest solutions should be performed. Regarding the thermally-mediated cell harvest, more studies on the impact on cell detachment of the thickness and the density of the thermosensitive polymer have yet to be realized to then graft the microcarriers with the most suitable polymer characteristics. Afterwards, cell detachment characterization inside the bioreactor can be performed. The enzymatic dissolution of microcarriers should be further evaluated to assess impact on the metabolism of several cell types. For each cell harvest strategy, when they will have proved to be operational, the question of the frequency of cell harvest, the quantity of fresh microcarriers that needs to be re-introduced and the amount of sub-confluent microcarriers that need to be harvested will have

to be addressed to maintain an optimal cell proliferation and perform continuous microbioprocessing.

The bioreactor only achieved microcarrier cell culture for mammalian cells. However, other cell culture applications, other than scaled-down cell culture for biopharmaceutical productions, could be tested under dynamic and controlled conditions:

- Multiformats drug testing could be performed. Cells could be either grown on the porous membrane or, as shown in this thesis, on microcarriers to obtain different sorts of 2D cultures, or they could be cultured in hydrogels plugs or beads to form 3D structures. By supplying drugs into the perfusion channel, the response of cells to these stimuli could be analyzed.
- Cell studies could be performed in the proposed system by working with different sort of functionalized microcarriers. The proliferation, differentiation or other metabolic activity could be followed on diverse substrates (glass, polymers, gels...) coated with different ECM proteins, recombinant proteins, peptides or charged molecules.

In any case, the targeted application will need improvements to specifically carry out the desired type of cell culture.

Appendix A

Table A1. Formulation of a Dulbecco's Eagle Minimum Essential Medium (DMEM) (Ref. 41966-029, Invitrogen)

Components	Molecular Weight	Concentration	
	g/mol	mg/L	mM
Amino Acids			
Glycine	75	30	0.4
L-Arginine hydrochloride	211	84	0.398104
L-Cystine 2HCl	313	63	0.201278
L-Glutamine	146	584	4
L-Histidine hydrochloride-H ₂ O	210	42	0.2
L-Isoleucine	131	105	0.801527
L-Leucine	131	105	0.801527
L-Lysine hydrochloride	183	146	0.797814
L-Methionine	149	30	0.201342
L-Phenylalanine	165	66	0.4
L-Serine	105	42	0.4
L-Threonine	119	95	0.798319
L-Tryptophan	204	16	0.078431
L-Tyrosine disodium salt dihydrate	261	104	0.398467
L-Valine	117	94	0.803419
Vitamins			
Choline chloride	140	4	0.028571
D-Calcium pantothenate	477	4	0.008386
Folic Acid	441	4	0.00907
Niacinamide	122	4	0.032787
Pyridoxine hydrochloride	206	4	0.019417
Riboflavin	376	0.4	0.001064
Thiamine hydrochloride	337	4	0.011869
i-Inositol	180	7.2	0.04
Inorganic Salts			
Calcium Chloride (CaCl ₂) (anhyd.)	111	200	1.801802
Ferric Nitrate (Fe(NO ₃) ₃ ·9H ₂ O)	404	0.1	2.48E-04
Magnesium Sulfate (MgSO ₄) (anhyd.)	120	97.67	0.813917
Potassium Chloride (KCl)	75	400	5.333334
Sodium Bicarbonate (NaHCO ₃)	84	3700	44.04762
Sodium Chloride (NaCl)	58	6400	110.3448
Sodium Phosphate monobasic (NaH ₂ PO ₄ ·H ₂ O)	138	125	0.905797
Other Components			
D-Glucose (Dextrose)	180	4500	25
Phenol Red	376.4	15	0.039851
Sodium Pyruvate	110	110	1

Appendix B

The diffusion of particles in porous media is different than in common bulk environment.

The diffusion of a particle is characterized by its diffusion coefficient. In porous media the diffusion coefficient is defined as follow:

$$D_{eff} = \frac{D\varepsilon\delta}{\tau} \quad (\text{Eq. 19})$$

where D_{eff} is the effective diffusion coefficient in the porous matrix, D the intrinsic diffusion coefficient, ε the porosity, τ the tortuosity and δ the constrictivity.

The porosity is a dimensionless number defined as the ratio of the void volume to the total volume of the porous material. Its value is comprised between 0 and 1.

The tortuosity is defined as the ration of the average path length a particle takes to travel through a porous matrix over the thickness of this matrix. The trajectory of particles in porous media often takes a meandering path instead of travelling straight through the porous material (Figure 49). The typical tortuosity of a porous membrane is between 1.5 and 2.5[213].

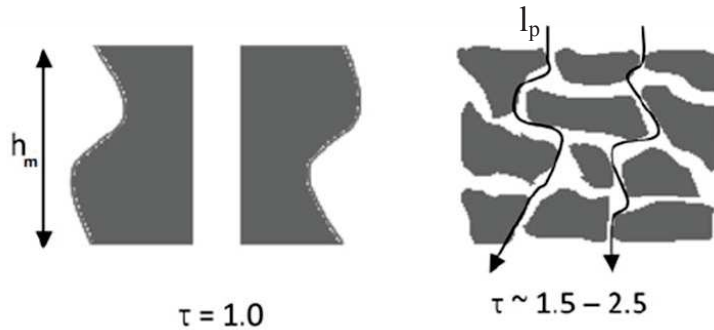


Figure 49. Geometrical representation of the tortuosity

$$\tau = \left(\frac{l_p}{h_m} \right)^2 \quad (\text{Eq. 20})[214]$$

The constrictivity is viewed to depend on the ratio of the diameter of the diffusing particle to the pore diameter. The value of constrictivity ranges between 0 and 1. The constrictivity is defined not for a single pore, but as the parameter of the entire pore space considered. Several empirical formula have been derived for the constrictivity[215,216,217,218] and have similar plot representations. The simplest is:

$$\delta = \left(1 - \frac{\phi_{mol}}{\phi_{pore}} \right)^4 \quad (\text{Eq. 21})[215]$$

where ϕ_{mol} is the diffusing molecule diameter and ϕ_{pore} the average pore diameter.

The determination of the tortuosity and constrictivity is usually complex and these data were not provided by the membrane supplier. For evaluation in Table 6, the worst case scenario has been considered for the tortuosity of the cellulose ester and PTFE membrane, meaning $\tau=2.5$. The PC membrane being a tracked-etched membrane, the pores are straight giving $\tau=1$. Regarding the constrictivity factor, it has been evaluated to 1 in all cases since diffusing molecules are expected to be far smaller than the pore diameter.

Appendix C

Comparison of the particles size of the different media components with the size of azorubine.

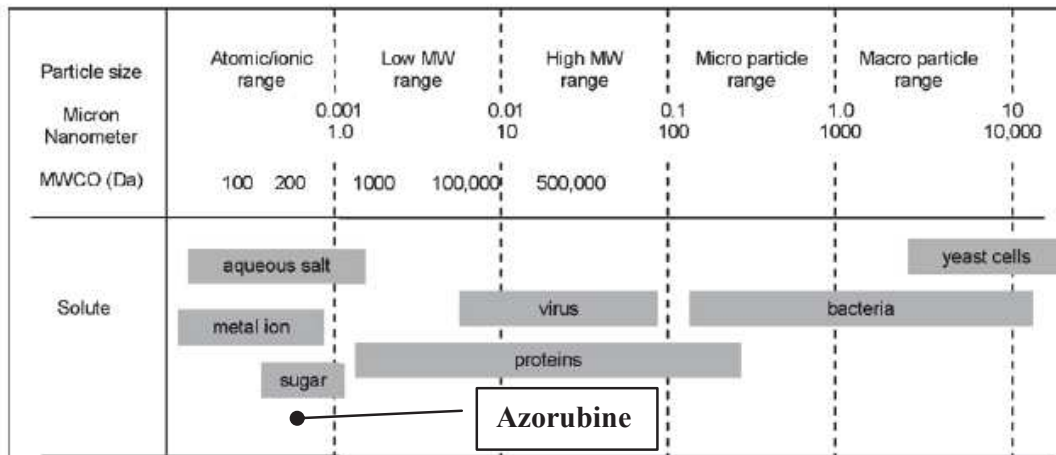


Figure 50. Size of different particles and azorubine. Adapted from[213]

Appendix D

This appendix describes the numerical model used to simulate the operation of the microfluidic system as in section 4.1.1.1. A schematic representation of the model is presented in Figure 51. The governing equations are summarized in Table 14 and the parameters gathered in Table 15.

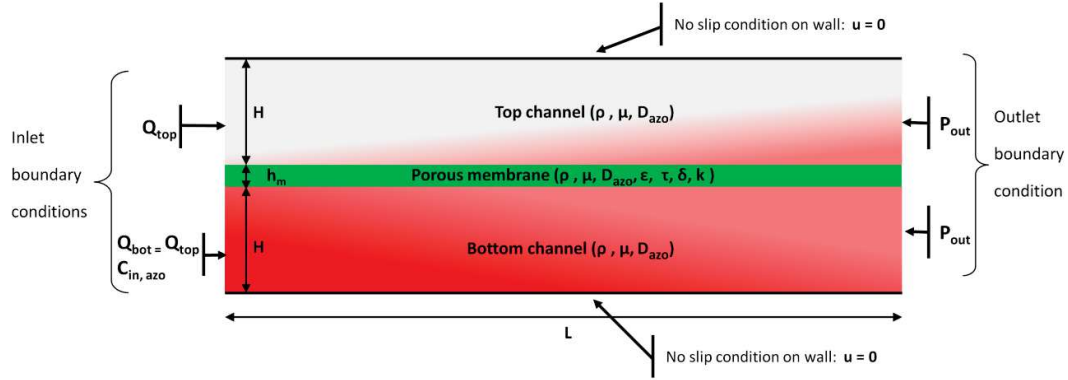


Figure 51. Model for the simulations of section 4.1.1.1.

With:

$$P_{out} = R_{hydr}Q_{bot} + P_{atm} = \frac{8\mu L_{tubing}}{\pi r_{tubing}^4} Q_{bot} + P_{atm} \quad (\text{Eq. 22})$$

P_{atm} is the atmospheric pressure (1 bar), R_{hydr} the hydraulic resistance of the outlet tubing, L_{tubing} (=360 mm) the length of the outlet tubing and r_{tubing} (=0.5 mm) the radius of the outlet tubing.

Table 14. Governing equations for hydrodynamics and mass transport in each domain.

		Domain		
		Bottom channel	Top channel	Porous membrane
Type of the governing equation	Fluid flow	$-\nabla p + \mu \nabla^2 \mathbf{u} = \rho(\mathbf{u} \cdot \nabla) \mathbf{u}$		$-\nabla p + \frac{\mu}{\varepsilon} \nabla^2 \mathbf{u} - \frac{\mu}{k} \mathbf{u} = \rho(\mathbf{u} \cdot \nabla) \mathbf{u}$
	Concentration	$-D \nabla^2 c + \mathbf{u} \cdot \nabla c = 0$		$-\frac{D \varepsilon \delta}{\tau} \nabla^2 c + \mathbf{u} \cdot \nabla c = 0$

For the fluid flow equations, the non-linear term were kept since the Reynolds number can be greater than 1 for flow rates ranging from 10 $\mu\text{l}/\text{min}$ to 1 ml/min (Re ranges from 0.3 to 30).

Table 15. List of parameters used for simulations.

Variable	Value	Description
L	380 mm	Culture channel length
W	1 mm	Channel width
H	500 μm	Channel height
h_m	40 μm	Membrane thickness
ε	70 %	Membrane porosity
k	$3.5 \cdot 10^{-15} \text{ m}^2 \cdot \text{s}$ *	Membrane permeability
τ	2.5	Membrane tortuosity
δ	1	Membrane constrictivity
$C_{in,azo}$	1 mM (arbitrary)	Inflow azorubine concentration
D_{azo}	$5.5 \cdot 10^{-10} \text{ m}^2/\text{s}$ **	Azorubine diffusion coefficient
ρ	$10^3 \text{ kg}/\text{m}^3$	Water density
μ	$10^{-3} \text{ kg}/(\text{m}\cdot\text{s})$	Water viscosity

*The membrane permeabilities were evaluated considering the following formula[219]:

$$k = \frac{\varepsilon d_p^2}{32} \quad (\text{Eq. 23})$$

where d_p is the pore diameter.

**The diffusion coefficient of azorubin is determined using the Stokes-Einstein relation:

$$D = \frac{k_B T}{6\pi\mu a} \quad (\text{Eq. 12})$$

where k_B is the Boltzman's constant, T the temperature, μ the dynamic viscosity of the media in which the diffusion occurs and a the radii of the diffusing molecule.

$$\text{For azorubin E122, } a = \sqrt[3]{\frac{3V}{4\pi}} = \sqrt[3]{\frac{3 \times 520}{4 \times 3.14}} \cdot 10^{-10} = 0.4 \text{ nm}$$

$$\text{and } D = \frac{1.38 \cdot 10^{-23} \times (273.15 + 25)}{6 \times 3.14 \times 10^{-9} \times 0.5 \cdot 10^{-9}} = 5.5 \cdot 10^{-10} \text{ m}^2 \cdot \text{s}^{-1}$$

Appendix E

This appendix gives a detailed description of the analytical model used to derive the laws to compute the azorubine concentration at each outlet of the system as operated in section 4.1.1.1.

For this demonstration, the influence of the membrane has been neglected. The system is therefore considered to behave as a regular T-channel mixer (Figure 52).

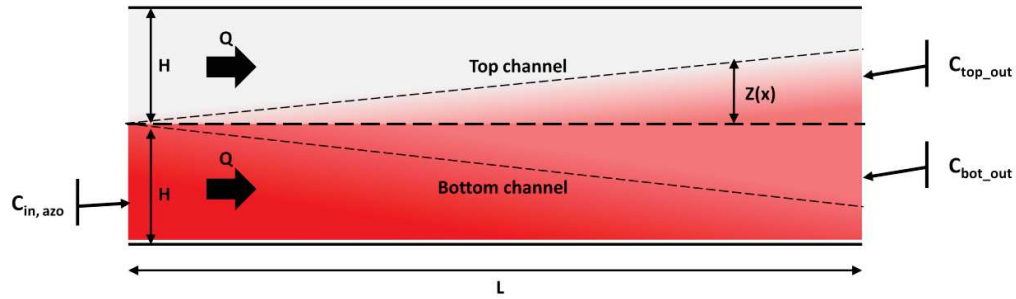


Figure 52. Schematic representation of the system as operated in section 4.1.1.1

The conservation of the quantity of moles gives:

$$n_{top}(x) + n_{bot}(x) = n_{in,azo} \quad (\text{Eq. 24})$$

where $n_{in,azo}$ the quantity of moles entering by the inlet of the bottom channel, $n_{top}(x)$ the quantity of moles in the upper channel at a given distance x from the inlet and $n_{bot}(x)$ the quantity of moles in the bottom channel at a given distance x from the inlet.

The presence of the membrane is neglected here and for the rest of the

Also:

$$n_{top}(x) = C(x)WZ(x)dl \quad (\text{Eq. 25})$$

$$n_{bot}(x) = C(x)WHdl \quad (\text{Eq. 26})$$

$$n_{in,azo} = C_{in,azo}WHdl \quad (\text{Eq. 27})$$

where $Z(x)$ is the “width” of the diffusion area in the upper channel reached by the azorubine particles due to diffusion at a given distance x from the inlet, W the channel width, H the channel height, dl the length of the box in which the concentration at a given x can be considered constant and $C(x)$ the average azorubine concentration at a given x .

Hence, replacing (Eq. 25), (Eq. 26) and (Eq. 27) in (Eq. 24):

$$C(x)(Z(x) + H) = C_{in,azo}H \quad (\text{Eq. 28})$$

But $C(x)$ is also the average concentration at a given x , $C_{bot}(x)$, present in the lower channel where is dispensed the azorubine.

Thus,

$$\frac{C_{bot}(x)}{C_{in,azo}} = \frac{1}{1 + \frac{Z(x)}{H}} \quad (\text{Eq. 29})$$

Now using (Eq. 25):

$$n_{top}(x) = CWZ(x)dl = C_{top}(x)WHdl \quad (\text{Eq. 30})$$

$C_{top}(x)$ being the average concentration in azorubin at a given x in the upper channel.

Therefore,

$$\frac{C_{top}(x)}{C_{in,azo}} = \frac{Z(x)}{H} \frac{1}{1 + \frac{Z(x)}{H}} \quad (\text{Eq. 31})$$

The ratio $Z(x)/H$ can be expressed as a function of the flow rate Q .

By the definition of $Z(x)$ and because diffusion only occurs in 1 dimension:

$$Z(x) = \frac{Z_{diff}(x)}{2} = \frac{1}{2} \sqrt{2Dt_{diff}(x)} = \sqrt{\frac{Dt_{diff}(x)}{2}} \quad (\text{Eq. 32})$$

The time allowed to the particles of azorubin to diffuse at a given x , $t_{diff}(x)$, is equal to the time, $t_{travel}(x)$, they took to travel until this abscissa. This condition gives:

$$t_{diff}(x) = t_{travel}(x) = x \frac{WH}{Q} \quad (\text{Eq. 33})$$

Therefore by replacing (Eq. 33) in (Eq. 32),

$$\frac{Z(x)}{H} = \sqrt{x \frac{DW}{2QH}} \quad (\text{Eq. 34})$$

By replacing (Eq. 34) in (Eq. 29) and (Eq. 31), and by evaluating in $x=L$, the concentration at each outlet can be derived as a function of the flow rate:

$$\frac{C_{bot,out}}{C_{in,azo}} = \frac{1}{1 + \sqrt{\frac{DWL}{2QH}}} \quad (\text{Eq. 14})$$

$$\frac{C_{top,out}}{C_{in,azo}} = \sqrt{\frac{DWL}{2QH}} \frac{1}{1 + \sqrt{\frac{DWL}{2QH}}} \quad (\text{Eq. 15})$$

Appendix F

Model (Figure 53), governing equations (Table 16) and parameters (Table 17) used for the simulation in section 4.1.1.2.

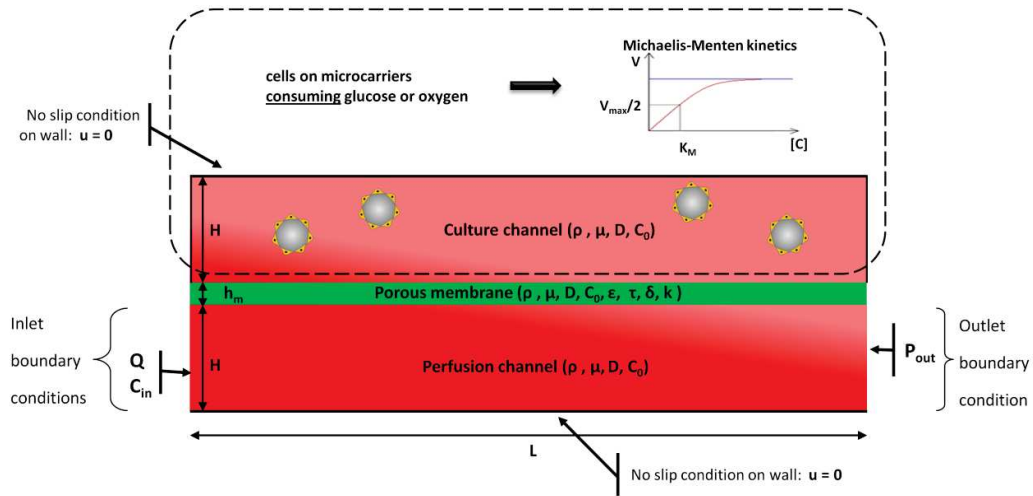


Figure 53. Model for the simulation of section 4.1.1.2

The model used for the simulations in section 4.1.1.2 is depicted in Figure 53. It represents the culture channel (upper channel) and the perfusion channel (lower channel) separated by the porous membrane.

The boundary conditions are:

- a flow rate Q and an inflow of a concentration C_{in} for the inlet of the perfusion channel
- a pressure P_{out} (see (Eq. 22)) for the outlet of the perfusion channel
- no slip condition on the walls

The initial conditions is a concentration C_0 in all the domains

In the culture channel, the consumption due to the presence of cells was based on Michaelis-Menten kinetics (see (Eq. 16)). The lactate production instead was considered as:

$$\frac{dC}{dt} = V_i \rho_c \quad (\text{Eq. 35})$$

Perfusion flow rates of 1, 5, 10, and 50 $\mu\text{L}/\text{min}$ were screened to the study either the glucose, oxygen or lactate concentration distribution within the channels and more particularly in the culture channel.

Table 16. Governing equations for hydrodynamics and mass transport in each domain.

		Domain		
		Perfusion channel	Culture channel	Porous membrane
Type of the governing equation	Fluid flow	$-\nabla p + \mu \nabla^2 \mathbf{u} = 0$		$-\nabla p + \frac{\mu}{\varepsilon} \nabla^2 \mathbf{u} - \frac{\mu}{k} \mathbf{u} = 0$
	Concentration	$-D \nabla^2 c + \mathbf{u} \cdot \nabla c = 0$	$-D \nabla^2 c + \mathbf{u} \cdot \nabla c = -\frac{V_M \rho_c c}{K_M + c}$ (Consumption) Or $-D \nabla^2 c + \mathbf{u} \cdot \nabla c = V_i \rho_c$ (Production)	$-D \frac{\varepsilon \delta}{\tau} \nabla^2 c + \mathbf{u} \cdot \nabla c = 0$

Table 17. List of parameters used for simulations.

Variable	Value	Description	
L	380 mm	Culture channel length	
W	1 mm	Channel width	
H	500 μm	Channel height	
h	PTFE membrane	40 μm	Membrane thickness (see section 3.3.2)
	PC membrane	25 μm	Membrane thickness (see section 3.3.2)
ε	PTFE membrane	70 %	Membrane porosity (see section 3.3.2)
	PC membrane	14 %	Membrane porosity (see section 3.3.2)
τ	PTFE membrane	2.5	Tortuosity (see section Appendix B)
	PC membrane	1	Tortuosity (see section Appendix B)
δ	PTFE membrane	1	Constrictivity (see section Appendix B)
	PC membrane	1	Constrictivity (see section Appendix B)
k	PTFE membrane	$3.5 \cdot 10^{-15} \text{ m}^2$	Membrane permeability (see Appendix D)
	PC membrane	$1.75 \cdot 10^{-16} \text{ m}^2$	Membrane permeability (see Appendix D)
Q	variable	Lower channel flow rate (perfusion)	
C_0	Glucose (PC3)	7 mM	Initial concentration of glucose (from medium formulation, Ref: 21127-022)
	Glucose (NIH3T3)	25 mM	Initial concentration of glucose (from medium formulation, Ref: 41966-029)
	Oxygen	0.2 mM	Initial concentration of oxygen[219]
	Lactate	0 mM	Initial concentration of oxygen
C_{in}	Glucose (PC3)	7 mM	Inflow glucose concentration (from medium formulation, Ref: 21127-022)
	Glucose (NIH3T3)	25 mM	Initial concentration of glucose (from medium formulation, Ref: 41966-029)
	Oxygen	0.2 mM	Inflow oxygen concentration[219]

	Lactate	0 mM	Inflow lactate concentration
D	Glucose	$2.1 \cdot 10^{-9} \text{ m}^2/\text{s}^*$	Glucose diffusion coefficient at 37°C
	Oxygen	$2.8 \cdot 10^{-9} \text{ m}^2/\text{s}^*$	Glucose diffusion coefficient at 37°C
	Lactate	$1.4 \cdot 10^{-9} \text{ m}^2/\text{s}^*$	Glucose diffusion coefficient at 37°C
ρ_c	PC3	$1.1 \cdot 10^6 \text{ cells/mL}^{**}$	Cell density
	NIH3T3	$1.3 \cdot 10^6 \text{ cells/mL}^{**}$	Cell density
V_M	NIH3T3, glucose	$2.2 \cdot 10^{-17} \text{ mol/cell/s}$	Saturated consumption rate per cell[220]
	PC3, glucose	$5.8 \cdot 10^{-17} \text{ mol/cell/s}$	Saturated consumption rate per cell[221]
	NIH3T3, oxygen	$7.0 \cdot 10^{-17} \text{ mol/cell/s}$	Saturated consumption rate per cell[219]
	PC3, oxygen	$4.5 \cdot 10^{-17} \text{ mol/cell/s}$	Saturated consumption rate per cell[219]
K_M	NIH3T3, glucose	0.2 mM	Concentration giving a consumption rate equal to half of the saturated rate[220]
	PC3, glucose	7.2 mM	Concentration giving a consumption rate equal to half of the saturated rate[222]
	NIH3T3, oxygen	0.1 mM	Concentration giving a consumption rate equal to half of the saturated rate[219]
	PC3, oxygen	0.1 mM	Concentration giving a consumption rate equal to half of the saturated rate[219]
V_I		$6.0 \cdot 10^{-16} \text{ mol/cell/s}$	Lactate production rate per PC3 cell[221]
ρ		10^3 kg/m^3^*	Media density at 37°C
μ		$0.7 \cdot 10^{-3} \text{ kg/(m.s)}^*$	Media viscosity at 37°C

*For the medium density the same value than that at 25°C was considered for 37°C since the density varies very slightly according to the temperature. However, the variations according to the temperature are more important for the viscosity. The following relationship was considered to evaluate the viscosity at 37°C[223]:

$$\mu(T) = 2.414 \cdot 10^{-5} \cdot 10^{\frac{247.8}{(T-140)}} \quad (\text{Eq. 36})$$

Regarding the diffusion coefficients, the following formula was considered (derived from the Stokes-Einstein (Eq. 12) formula):

$$D_{T2} = D_{T1} \frac{\mu_{T1} T2}{\mu_{T2} T1} \quad (\text{Eq. 37})$$

**The cell density is taken as the maximum cell density to evaluate the cell environment in the end of a culture run. It is calculated by considering a concentration of 2mg/mL of microcarriers, a growth surface of 2700 cm² per gram of microcarriers[61] and a cell spread area of 510 μm² for PC3 (from PC3 image analysis) and 420 μm² for NIH3T3[187].

Appendix G

The goal of this appendix is to define the thermal gradient along the height of the CCC considering that a thermal source heats a 2 mm thick PMMA layer containing 1 mm of culture media (Figure 54).

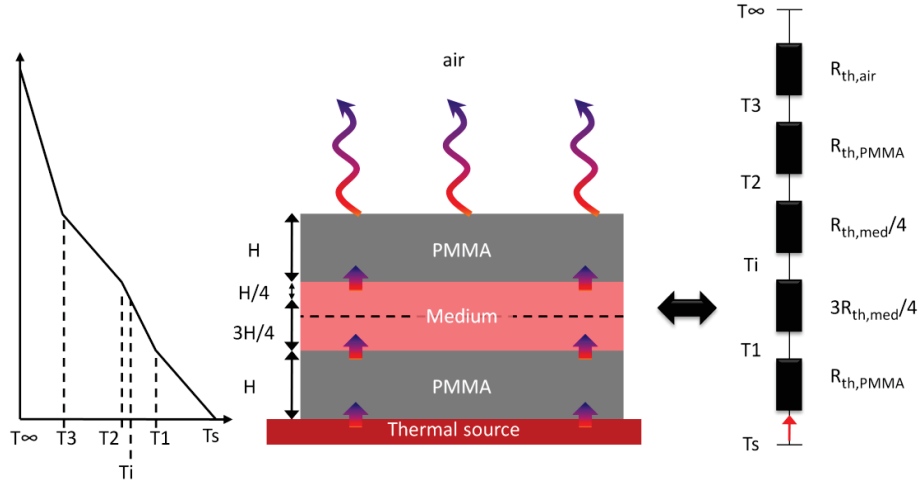


Figure 54. Thermal model of the bioreactor.

The governing equations of this system are:

- Fourier's law, which gives:

$$\Phi = \frac{\lambda S}{L} (T_h - T_c) \quad (\text{Eq. 38})$$

where Φ is the thermal flux in W or J·s⁻¹, S the cross section through which flows the thermal energy, L the length along which flows the thermal energy λ , the thermal conductivity in W·m⁻¹·K⁻¹, T_h the hotter temperature and T_c the colder temperature.

- Newton's law of cooling:

$$\Phi = hS(T_h - T_c) \quad (\text{Eq. 39})$$

where h is the convective transfer coefficient in W·m⁻²·K⁻¹

An equivalent electrical circuit can be established (Figure 54) considering that the difference of temperature is analog to a difference of potential, the heat flux is analog to the electrical current and the thermal resistances are analog to the electrical resistances, with:

$$R_{th,PMMA} = \frac{H}{\lambda_{PMMA} S} \quad (\text{Eq. 40})$$

$$R_{th,med} = \frac{H}{\lambda_{med} S} \quad (\text{Eq. 41})$$

$$R_{th,air} = \frac{1}{h_{air}S} \quad (\text{Eq. 42})$$

where $R_{th,PMMA}$ is the thermal resistivity of PMMA, $R_{th,med}$ of the medium and $R_{th,air}$ of the air.

The expression of the different temperatures of the model as a function of T_∞ (the temperature of the air) and T_i (temperature at mid height of the culture channel) can be simply derived using Ohm's law:

$$T_1 - T_\infty = \frac{(R_{th,med} + R_{th,PMMA} + R_{th,air})}{\left(\frac{R_{th,med}}{4} + R_{th,PMMA} + R_{th,air}\right)} (T_i - T_\infty) \quad (\text{Eq. 43})$$

$$T_2 - T_\infty = \frac{(R_{th,PMMA} + R_{th,air})}{\left(\frac{R_{th,med}}{4} + R_{th,PMMA} + R_{th,air}\right)} (T_i - T_\infty) \quad (\text{Eq. 44})$$

$$T_3 - T_\infty = \frac{R_{th,air}}{\left(\frac{R_{th,med}}{4} + 2R_{th,PMMA} + R_{th,air}\right)} (T_i - T_\infty) \quad (\text{Eq. 45})$$

$$T_s - T_\infty = \frac{(R_{th,med} + 2R_{th,PMMA} + R_{th,air})}{\left(\frac{R_{th,med}}{4} + R_{th,PMMA} + R_{th,air}\right)} (T_i - T_\infty) \quad (\text{Eq. 46})$$

Then:

$$T_1 = T_\infty + \frac{\left(\frac{H}{\lambda_{med}} + \frac{H}{\lambda_{PMMA}} + \frac{1}{h_{air}}\right)}{\left(\frac{H}{4\lambda_{med}} + \frac{H}{\lambda_{PMMA}} + \frac{1}{h_{air}}\right)} (T_i - T_\infty) \quad (\text{Eq. 47})$$

$$T_2 = T_\infty + \frac{\left(\frac{H}{\lambda_{PMMA}} + \frac{1}{h_{air}}\right)}{\left(\frac{H}{4\lambda_{med}} + \frac{H}{\lambda_{PMMA}} + \frac{1}{h_{air}}\right)} (T_i - T_\infty) \quad (\text{Eq. 48})$$

$$T_3 = T_\infty + \frac{\frac{1}{h_{air}}}{\left(\frac{H}{4\lambda_{med}} + \frac{H}{\lambda_{PMMA}} + \frac{1}{h_{air}}\right)} (T_i - T_\infty) \quad (\text{Eq. 49})$$

$$T_s = T_\infty + \frac{\left(\frac{H}{\lambda_{med}} + \frac{2H}{\lambda_{PMMA}} + \frac{1}{h_{air}}\right)}{\left(\frac{H}{4\lambda_{med}} + \frac{H}{\lambda_{PMMA}} + \frac{1}{h_{air}}\right)} (T_i - T_\infty) \quad (\text{Eq. 50})$$

Considering the following values:

$$\lambda_{med} = 0.62 \text{ W}\cdot\text{m}^{-1}\cdot\text{K}^{-2}[142], \lambda_{PMMA} = 0.18 \text{ W}\cdot\text{m}^{-1}\cdot\text{K}^{-2}[142], h_{air} = 20 \text{ W}\cdot\text{m}^{-2}\cdot\text{K}^{-2}[142]$$

$$H = 1 \text{ mm}, T_\infty = 295.15 \text{ K} (22^\circ\text{C}) \text{ and } T_i = 310.15 (37^\circ\text{C}).$$

We obtain:

$$T_s = 312.0 \text{ K} = 38.8^\circ\text{C}$$

$$T_1 = 310.5 \text{ K} = 37.3^\circ\text{C}$$

$$T_2 = 310.0 \text{ K} = 36.9^\circ\text{C}$$

$$T_3 = 308.6 \text{ K} = 35.4^\circ\text{C}$$

Appendix H

Thermal characterization of the cooling of the Cytoo™ chamber was performed by IR imaging (Flir A20). The Cytoo™ chamber was incubated for several hours in a 5 % CO₂ incubator at 37°C with culture medium inside. As soon as it was taken out from the incubator it was placed under the IR camera to follow its cooling over time. Figure 55 shows the variation of the Cytoo™ chamber temperature over time.

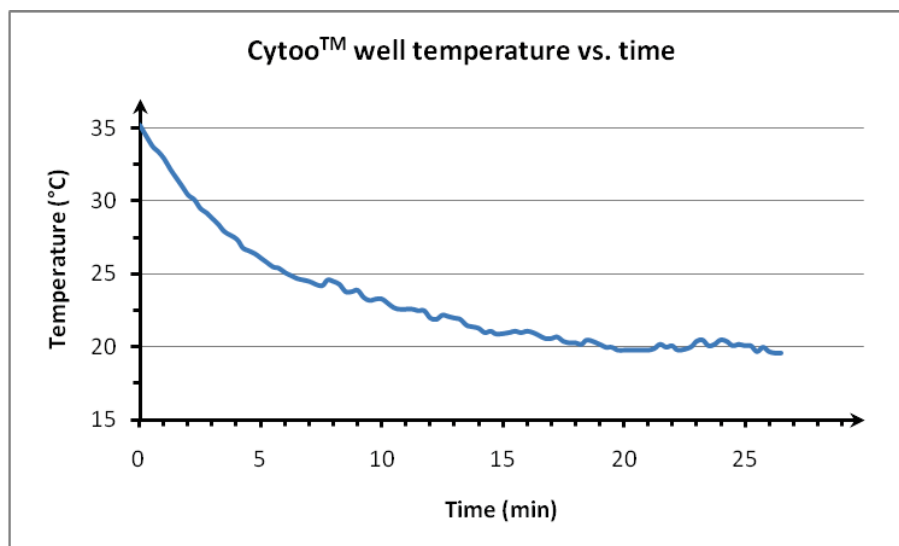


Figure 55. Variation of the Cytoo™ chamber temperature over time after incubation in a CO₂ incubator at 37°C.

The Cytoo™ chamber reaches the temperature of 30°C in about 4 min (1 min has to be added to account for the time to take the chamber of the cell culture room, bring it under the IR camera and start recording). In less than 20 min, the chamber reached the room temperature.

Appendix I

The protocol used for cell staining on microcarrier in section 4.2.2 is given here.

Cells grown on microcarriers were characterized by immunostaining of actin filaments after 4 days of culture. Cells adhered to the microcarriers were fixed for 20 min using 4% (v/v) paraformaldehyde (PFA) in Tris-buffered saline (TBS) solution, followed by 2 washes with phosphate-buffered saline solution supplemented with Mg^{2+} and CA^{2+} (PBS+). Then, the cells were permeabilized for 10 min with 0.5% Triton X-100 in TBS, followed by two 10-min washes with PBS+. Actin filaments were stained for 40 min with phalloidin tetramethylrhodamine B isothiocyanate (Jackson ImmunoResearch) diluted 1:300 in 0.1% (v/v) Tween-20 (Sigma) in TBS, followed by a 10-min wash with PBS+. Nuclei were counterstained for 5 min with Hoechst (Jackson ImmunoResearch) diluted 1:7000 in PBS+. A final 10-min wash was performed with PBS+. A Gene Frame[®] (ThermoFisher Scientific) was used to create a thin-height well (250 μ m) on a standard microscope glass slide. Stained cells adhered to microcarriers were transferred into this well, and a coverslip was mounted using the Gene Frame[®] with fluorescent mounting medium kit (Dako) and stored at 4°C before imaging. All reagents were purchased from Life Technologies™ unless stated otherwise.

The PC3 cell behavior during their growth on the microcarriers was investigated using a Leica TCS SP2 laser scanning confocal microscope with a 20x/0.5 NA objective. The PC3 cells were cultured as described in the “cell culture” section and imaged after 2 days of culture. Stained PC3 cells adhered to microcarriers were imaged using a Nikon Eclipse Ti spinning disk confocal microscope with a 40x/1.3 NA objective.

Bibliography

1. Freshney RI (2010) *Culture of Animal Cells: A Manual of Basic Technique and Specialized Applications*: John Wiley & Sons, Inc. 732 p.
2. Grossel SS (1984) *Riegel Handbook of Industrial Chemistry*, 8th Edition - Kent,Ja. *Chemical Engineering* 91: 127-129.
3. Barnett JA (2010) A history of research on yeasts 14:(1) medical yeasts part 2, *Cryptococcus neoformans*. *Yeast* 27: 875-904.
4. Thorpe TA (2007) History of plant tissue culture. *Molecular Biotechnology* 37: 169-180.
5. Rous P, Jones FS (1916) A Method for Obtaining Suspensions of Living Cells from the Fixed Tissues, and for the Plating out of Individual Cells. *J Exp Med* 23: 549-555.
6. Gey GO, Coffman WD, Kubicek MT (1952) Tissue Culture Studies of the Proliferative Capacity of Cervical Carcinoma and Normal Epithelium. *Cancer Research* 12: 264-265.
7. Cavalier-Smith T (2004) Only six kingdoms of life. *Proceedings of the Royal Society B-Biological Sciences* 271: 1251-1262.
8. Dean AC (1957) The adaptation of bacterial cultures during the lag phase in media containing new substrates or antibacterial agents. *Proc R Soc Lond B Biol Sci* 147: 247-257.
9. Davis PK, Ho A, Dowdy SF (2001) Biological methods for cell-cycle synchronization of mammalian cells. *Biotechniques* 30: 1322-1331.
10. Todaro GJ, Green H (1963) Quantitative Studies of Growth of Mouse Embryo Cells in Culture and Their Development into Established Lines. *Journal of Cell Biology* 17: 299-&.
11. Wang JD, Levin PA (2009) Metabolism, cell growth and the bacterial cell cycle. *Nat Rev Microbiol* 7: 822-827.
12. Norbury C, Nurse P (1992) Animal cell cycles and their control. *Annu Rev Biochem* 61: 441-470.
13. Cooper GM, Hausman RE (2006) *The Cell A Molecular Approach*: The American Society for Microbiology and Sinauer Associates Inc. 739 p.
14. Reid Y (2011) Characterization and Authentication of Cancer Cell Lines: An Overview. In: Cree IA, editor. *Cancer Cell Culture*. 2nd ed: Humana Press. pp. 35-43.
15. Hughes P, Marshall D, Reid Y, Parkes H, Gelber C (2007) The costs of using unauthenticated, over-passaged cell lines: how much more data do we need? *BioTechniques* 43: 575-586.
16. Stanley JF, Pye D, MacGregor A (1975) Comparison of doubling numbers attained by cultured animal cells with life span of species. *Nature* 255: 158-159.
17. Soldstein S (1974) Aging in vitro. Growth of cultured cells from the Galapagos tortoise. *Exp Cell Res* 83: 297-302.
18. Clark WR (1999) *A means to an End: The Biological Basis of Ageing and Death*: Oxford University Press, New York. 234 p.
19. Stephens C (2005) Senescence: even bacteria get old. *Curr Biol* 15: R308-310.
20. Cross LJ, Russell JE, Desai M (2011) Examining the genetic variation of reference microbial cultures used within food and environmental laboratories using fluorescent amplified fragment length polymorphism analysis. *FEMS Microbiol Lett* 321: 100-106.
21. Brunner D, Frank J, Appl H, Schoffl H, Pfaller W, et al. (2010) Serum-free cell culture: the serum-free media interactive online database. *ALTEX* 27: 53-62.
22. Mather JP, Roberts PE (1998) *Introduction to Cell and Tissue Culture: Theory and Technique; Techniques ICaMB*, editor: Plenum Press, New York. 241 p.
23. Fulda S, Gorman AM, Hori O, Samali A (2010) Cellular Stress Responses: Cell Survival and Cell Death. *International Journal of Cell Biology* 2010.

24. Kempner ME, Felder RA (2002) A Review of Cell Culture Automation. *Journal of the Association for Laboratory Automation* 7: 56-62.
25. Ho L, Lee ES, Humphrey AE (2003) Industrial Fermentation: Principles, Processes, and Products. In: Kent JA, editor. *Riegel's Handbook of Industrial Chemistry*: Springer US. pp. 963-1045.
26. Mirbach MJ, El Ali BM (2004) Industrial fermentation. In: Ali MF, El Ali BM, Speight JG, editors. *Handbook of industrial chemistry : organic chemicals*. New York: McGraw-Hill. pp. 679.
27. Ho L, Lee ES, Humphrey AE (2003) Industrial Cell culture: Principles, Processes, and Products. In: Kent JA, editor. *Riegel's Handbook of Industrial Chemistry*: Springer US. pp. 1046-1072.
28. Ruffoni B, Pistelli L, Bertoli A (2010) Plant cell cultures: bioreactors for industrial production. *Adv Exp Med Biol* 698: 203-221.
29. Bandaranayake AD, Almo SC (2014) Recent advances in mammalian protein production. *FEBS Letters* 588: 253-260.
30. Jinyou Z (2010) Mammalian Cell Culture for Biopharmaceutical Production. In: Baltz RH, Davies JE, Demain AL, editors. *Manual of Industrial Microbiology and Biotechnology*. 3rd ed: ASM Press. pp. 766.
31. Demain AL, Vaishnav P (2009) Production of recombinant proteins by microbes and higher organisms. *Biotechnol Adv* 27: 297-306.
32. Zhu J (2012) Mammalian cell protein expression for biopharmaceutical production. *Biotechnol Adv* 30: 1158-1170.
33. Nagels B, Weterings K, Callewaert N, Van Damme EJM (2012) Production of Plant Made Pharmaceuticals: From Plant Host to Functional Protein. *Critical Reviews in Plant Sciences* 31: 148-180.
34. Plasson C, Michel R, Lienard D, Saint-Jore-Dupas C, Sourrouille C, et al. (2009) Production of Recombinant Proteins in Suspension–Cultured Plant Cells. In: Faye L, Gomord V, editors. *Recombinant Proteins From Plants*: Humana Press. pp. 145-161.
35. Placzek MR, Chung IM, Macedo HM, Ismail S, Mortera Blanco T, et al. (2009) Stem cell bioprocessing: fundamentals and principles. *J R Soc Interface* 6: 209-232.
36. Backer MP, Metzger LS, Slaber PL, Nevitt KL, Boder GB (1988) Large-scale production of monoclonal antibodies in suspension culture. *Biotechnol Bioeng* 32: 993-1000.
37. Boze H, Moulin G, Galzy P (2008) Production of Microbial Biomass. In: Rehm H-J, Reed G, editors. *Biotechnology Set*. 2nd ed: Wiley-VCH Verlag GmbH. pp. 165-220.
38. Goudar CT (2012) Computer programs for modeling mammalian cell batch and fed-batch cultures using logistic equations. *Cytotechnology* 64: 465-475.
39. Birch JR, Flickinger MC (2009) Suspension Culture, Animal Cells. *Encyclopedia of Industrial Biotechnology*: John Wiley & Sons, Inc.
40. Deo YM, Mahadevan MD, Fuchs R (1996) Practical Considerations in Operation and Scale-up of Spin-Filter Based Bioreactors for Monoclonal Antibody Production. *Biotechnology Progress* 12: 57-64.
41. Freshney RI (1992) *Animal cell culture: a practical approach*: IRL Press at Oxford University Press. 329 p.
42. Rose S, Black T, Ramakrishnan D (2003) Mammalian cell culture: Process Development Considerations. In: Vinci VA, Parekh SR, editors. *Handbook of Industrial Cell Culture: Mammalian, Microbial and Plant Cells*. Totowa, NJ: Humana Press. pp. 548.
43. Warnock JN, Al-Rubeai M (2006) Bioreactor systems for the production of biopharmaceuticals from animal cells. *Biotechnol Appl Biochem* 45: 1-12.
44. Rodrigues ME, Costa AR, Henriques M, Azeredo J, Oliveira R (2010) Technological progresses in monoclonal antibody production systems. *Biotechnol Prog* 26: 332-351.

45. Huang TK, McDonald KA (2012) Bioreactor systems for in vitro production of foreign proteins using plant cell cultures. *Biotechnol Adv* 30: 398-409.
46. Jain E, Kumar A (2008) Upstream processes in antibody production: evaluation of critical parameters. *Biotechnol Adv* 26: 46-72.
47. Tissot S (2011) *OrbShake Bioreactors for Mammalian Cell Cultures: Engineering and Scale-up*. Lausanne, Switzerland: ÉCOLE POLYTECHNIQUE FÉDÉRALE DE LAUSANNE. 144 p.
48. Xu J, Ge X, Dolan MC (2011) Towards high-yield production of pharmaceutical proteins with plant cell suspension cultures. *Biotechnol Adv* 29: 278-299.
49. Shi Y, Ryu DD, Park SH (1992) Performance of mammalian cell culture bioreactor with a new impeller design. *Biotechnol Bioeng* 40: 260-270.
50. Xing Z, Kenty BM, Li ZJ, Lee SS (2009) Scale-up analysis for a CHO cell culture process in large-scale bioreactors. *Biotechnol Bioeng* 103: 733-746.
51. Li F, Vijayasankaran N, Shen AY, Kiss R, Amanullah A (2010) Cell culture processes for monoclonal antibody production. *MAbs* 2: 466-479.
52. Glindkamp A, Riechers D, Rehbock C, Hitzmann B, Scheper T, et al. (2009) Sensors in Disposable Bioreactors Status and Trends. In: Eibl R, Eibl D, editors. *Disposable bioreactors*. Springer ed. pp. 145-169.
53. Ozturk S, Hu WS (2005) *Cell Culture Technology for Pharmaceutical and Cell-Based Therapies*: Taylor & Francis.
54. Borys MC, Linzer DI, Papoutsakis ET (1993) Culture pH affects expression rates and glycosylation of recombinant mouse placental lactogen proteins by Chinese hamster ovary (CHO) cells. *Biotechnology (N Y)* 11: 720-724.
55. Jardon M, Garnier A (2003) pH, pCO₂, and temperature effect on R-adenovirus production. *Biotechnol Prog* 19: 202-208.
56. Griffiths B (2000) Scaling-up of animal cell cultures. In: Masters J, editor. *Animal Cell Culture: A Practical Approach*. 3rd ed: OUP Oxford. pp. 334.
57. Chalmers JJ (1994) Cells and bubbles in sparged bioreactors. *Cytotechnology* 15: 311-320.
58. Brecht R (2009) Disposable bioreactors: maturation into pharmaceutical glycoprotein manufacturing. *Adv Biochem Eng Biotechnol* 115: 1-31.
59. Eibl R, Eibl D (2009) Application of disposable bag bioreactors in tissue engineering and for the production of therapeutic agents. *Adv Biochem Eng Biotechnol* 112: 183-207.
60. Griffiths B (2001) Scale-up of suspension and anchorage-dependent animal cells. *Mol Biotechnol* 17: 225-238.
61. GE_Healthcare (2005) *Microcarrier cell culture: Principle and Methods*: GE Healthcare.
62. Liu N, Zang R, Yang S-T, Li Y (2014) Stem cell engineering in bioreactors for large-scale bioprocessing. *Engineering in Life Sciences* 14: 4-15.
63. Kaisermayer C (2007) Influence of microcarrier surface modification on adhesion and product formation of mammalian cells. Vienna, Austria: Universität für Bodenkultur.
64. Butler M (1996) *Animal Cell Culture and Technology: The Basics*: IRL Press at Oxford University Press. 114 p.
65. Micheletti M, Lye GJ (2006) Microscale bioprocess optimisation. *Curr Opin Biotechnol* 17: 611-618.
66. Neubauer P, Cruz N, Glauche F, Junne S, Knepper A, et al. (2013) Consistent development of bioprocesses from microliter cultures to the industrial scale. *Engineering in Life Sciences* 13: 224-238.
67. Hegab HM, Elmekawy A, Stakenborg T (2013) Review of microfluidic microbioreactor technology for high-throughput submerged microbiological cultivation. *Biomicrofluidics* 7: 21502.
68. Bareither R, Pollard D (2011) A review of advanced small-scale parallel bioreactor technology for accelerated process development: current state and future need. *Biotechnol Prog* 27: 2-14.

69. Kim BJ, Diao J, Shuler ML (2012) Mini-scale bioprocessing systems for highly parallel animal cell cultures. *Biotechnol Prog* 28: 595-607.
70. Sackmann EK, Fulton AL, Beebe DJ (2014) The present and future role of microfluidics in biomedical research. *Nature* 507: 181-189.
71. Whitesides GM (2006) The origins and the future of microfluidics. *Nature* 442: 368-373.
72. Squires TM, Quake SR (2005) Microfluidics: Fluid physics at the nanoliter scale. *Reviews of Modern Physics* 77: 977-1026.
73. Jingdong C, Di C, Yao X, Tao Y, Xiang C (2013) Progress of Microfluidics for Biology and Medicine. *Nano-Micro Letters* 5: 66-80.
74. Ren K, Zhou J, Wu H (2013) Materials for microfluidic chip fabrication. *Acc Chem Res* 46: 2396-2406.
75. Ren K, Chen Y, Wu H (2014) New materials for microfluidics in biology. *Curr Opin Biotechnol* 25: 78-85.
76. Mehling M, Tay S (2014) Microfluidic cell culture. *Curr Opin Biotechnol* 25: 95-102.
77. Harink B, Le Gac S, Truckenmuller R, van Blitterswijk C, Habibovic P (2013) Regeneration-on-a-chip? The perspectives on use of microfluidics in regenerative medicine. *Lab Chip* 13: 3512-3528.
78. Berthier E, Young EW, Beebe D (2012) Engineers are from PDMS-land, Biologists are from Polystyrenia. *Lab Chip* 12: 1224-1237.
79. Derda R, Tang SK, Laromaine A, Mosadegh B, Hong E, et al. (2011) Multizone paper platform for 3D cell cultures. *PLoS One* 6: e18940.
80. Alrifaiy A, Lindahl OA, Ramser K (2012) Polymer-Based Microfluidic Devices for Pharmacy, Biology and Tissue Engineering. *Polymers* 4: 1349-1398.
81. Mecomber JS, Stalcup AM, Hurd D, Halsall HB, Heineman WR, et al. (2006) Analytical performance of polymer-based microfluidic devices fabricated by computer numerical controlled machining. *Anal Chem* 78: 936-941.
82. Hecke M, Schomburg WK (2004) Review on micro molding of thermoplastic polymers. *Journal of Micromechanics and Microengineering* 14: R1.
83. Liu K, Fan ZH (2011) Thermoplastic microfluidic devices and their applications in protein and DNA analysis. *Analyst* 136: 1288-1297.
84. Tsao C-W, DeVoe D (2009) Bonding of thermoplastic polymer microfluidics. *Microfluidics and Nanofluidics* 6: 1-16.
85. Schultz J, Nardin M (2003) Theories and Mechanisms of Adhesion. In: Pizzi A, Mittal KL, editors. *Handbook of Adhesive Technology, Revised and Expanded*. 2nd ed: Taylor & Francis. pp. 53-69.
86. Pocius AV (2002) *Adhesion and Adhesives Technology: An Introduction*: Hanser.
87. Paguirigan AL, Beebe DJ (2009) From the cellular perspective: exploring differences in the cellular baseline in macroscale and microfluidic cultures. *Integr Biol (Camb)* 1: 182-195.
88. Zhang C, van Noort D (2011) Cells in Microfluidics. In: Lin B, editor. *Microfluidics*: Springer Berlin Heidelberg. pp. 295-321.
89. Tehranirokh M, Kouzani AZ, Francis PS, Kanwar JR (2013) Microfluidic devices for cell cultivation and proliferation. *Biomicrofluidics* 7: 51502.
90. Velve-Casquillas G, Le Berre M, Piel M, Tran PT (2010) Microfluidic tools for cell biological research. *Nano Today* 5: 28-47.
91. Gao D, Liu H, Jiang Y, Lin J-M (2012) Recent developments in microfluidic devices for in vitro cell culture for cell-biology research. *TrAC Trends in Analytical Chemistry* 35: 150-164.
92. Fidalgo LM, Maerkl SJ (2011) A software-programmable microfluidic device for automated biology. *Lab Chip* 11: 1612-1619.
93. Toh YC, Lim TC, Tai D, Xiao G, van Noort D, et al. (2009) A microfluidic 3D hepatocyte chip for drug toxicity testing. *Lab Chip* 9: 2026-2035.

94. Sugiura S, Edahiro J, Kikuchi K, Sumaru K, Kanamori T (2008) Pressure-driven perfusion culture microchamber array for a parallel drug cytotoxicity assay. *Biotechnol Bioeng* 100: 1156-1165.
95. Wu MH, Huang SB, Lee GB (2010) Microfluidic cell culture systems for drug research. *Lab Chip* 10: 939-956.
96. Benya PD, Shaffer JD (1982) Dedifferentiated chondrocytes reexpress the differentiated collagen phenotype when cultured in agarose gels. *Cell* 30: 215-224.
97. Marimuthu M, Kim S (2011) Microfluidic cell coculture methods for understanding cell biology, analyzing bio/pharmaceuticals, and developing tissue constructs. *Anal Biochem* 413: 81-89.
98. El-Ali J, Sorger PK, Jensen KF (2006) Cells on chips. *Nature* 442: 403-411.
99. Kim D, Wu X, Young AT, Haynes CL (2014) Microfluidics-Based in Vivo Mimetic Systems for the Study of Cellular Biology. *Accounts of Chemical Research* 47: 1165-1173.
100. Baudoin R, Griscom L, Prot JM, Legallais C, Leclerc E (2011) Behavior of HepG2/C3A cell cultures in a microfluidic bioreactor. *Biochemical Engineering Journal* 53: 172-181.
101. Gunther A, Yasotharan S, Vagaon A, Lochofsky C, Pinto S, et al. (2010) A microfluidic platform for probing small artery structure and function. *Lab Chip* 10: 2341-2349.
102. Grosberg A, Alford PW, McCain ML, Parker KK (2011) Ensembles of engineered cardiac tissues for physiological and pharmacological study: heart on a chip. *Lab Chip* 11: 4165-4173.
103. Nalayanda D, Puleo C, Fulton W, Sharpe L, Wang T-H, et al. (2009) An open-access microfluidic model for lung-specific functional studies at an air-liquid interface. *Biomedical Microdevices* 11: 1081-1089.
104. Ronco C, Davenport A, Gura V (2011) The future of the artificial kidney: moving towards wearable and miniaturized devices. *Nefrologia* 31: 9-16.
105. Wu MH, Huang SB, Cui Z, Lee GB (2008) A high throughput perfusion-based microbioreactor platform integrated with pneumatic micropumps for three-dimensional cell culture. *Biomed Microdevices* 10: 309-319.
106. Viravaidya K, Sin A, Shuler ML (2004) Development of a microscale cell culture analog to probe naphthalene toxicity. *Biotechnol Prog* 20: 316-323.
107. Meyvantsson I, Beebe DJ (2008) Cell culture models in microfluidic systems. *Annu Rev Anal Chem (Palo Alto Calif)* 1: 423-449.
108. Huh D, Hamilton GA, Ingber DE (2011) From 3D cell culture to organs-on-chips. *Trends in Cell Biology* 21: 745-754.
109. Hung PJ, Lee PJ, Sabouchi P, Lin R, Lee LP (2005) Continuous perfusion microfluidic cell culture array for high-throughput cell-based assays. *Biotechnology and Bioengineering* 89: 1-8.
110. Huh D, Matthews BD, Mammoto A, Montoya-Zavala M, Hsin HY, et al. (2010) Reconstituting organ-level lung functions on a chip. *Science* 328: 1662-1668.
111. Cheong R, Paliwal S, Levchenko A (2010) High-content screening in microfluidic devices. *Expert Opin Drug Discov* 5: 715-720.
112. Rosenfeld L, Lin T, Derda R, Tang SKY (2014) Review and analysis of performance metrics of droplet microfluidics systems. *Microfluidics and Nanofluidics* 16: 921-939.
113. Benien P, Swami A (2014) 3D tumor models: history, advances and future perspectives. *Future Oncol* 10: 1311-1327.
114. Schöpfer D, Stocks SM, Szita N, Lantz AE, Gernaey KV (2010) Development of a single-use microbioreactor for cultivation of microorganisms. *Chemical Engineering Journal* 160: 891-898.
115. Lee KS, Boccuzzi P, Sinskey AJ, Ram RJ (2011) Microfluidic chemostat and turbidostat with flow rate, oxygen, and temperature control for dynamic continuous culture. *Lab Chip* 11: 1730-1739.

116. Chan HF, Zhang Y, Ho Y-P, Chiu Y-L, Jung Y, et al. (2013) Rapid formation of multicellular spheroids in double-emulsion droplets with controllable microenvironment. *Sci Rep* 3.
117. Maharbiz MM, Holtz WJ, Howe RT, Keasling JD (2004) Microbioreactor arrays with parametric control for high-throughput experimentation. *Biotechnol Bioeng* 85: 376-381.
118. Schapper D (2010) *Continuous Culture Microbioreactors*. Lyngby: DTU, Denmark. 184 p.
119. Barbulovic-Nad I, Au SH, Wheeler AR (2010) A microfluidic platform for complete mammalian cell culture. *Lab Chip* 10: 1536-1542.
120. Zhang B, Kim MC, Thorsen T, Wang Z (2009) A self-contained microfluidic cell culture system. *Biomed Microdevices* 11: 1233-1237.
121. Keizer GD, Visser W, Vliem M, Figdor CG (1988) A monoclonal antibody (NKI-L16) directed against a unique epitope on the alpha-chain of human leukocyte function-associated antigen 1 induces homotypic cell-cell interactions. *J Immunol* 140: 1393-1400.
122. Sutradhar BC, Park J, Hong G, Choi SH, Kim G (2010) Effects of Trypsinization on Viability of Equine Chondrocytes in Cell Culture. *Pakistan Veterinary Journal* 30: 232-238.
123. Canavan HE, Cheng X, Graham DJ, Ratner BD, Castner DG (2005) Cell sheet detachment affects the extracellular matrix: a surface science study comparing thermal liftoff, enzymatic, and mechanical methods. *J Biomed Mater Res A* 75: 1-13.
124. Kwon KW, Choi SS, Lee SH, Kim B, Lee SN, et al. (2007) Label-free, microfluidic separation and enrichment of human breast cancer cells by adhesion difference. *Lab Chip* 7: 1461-1468.
125. Born C, Zhang Z, Al-Rubeai M, Thomas CR (1992) Estimation of disruption of animal cells by laminar shear stress. *Biotechnol Bioeng* 40: 1004-1010.
126. Wang H, Riha GM, Yan S, Li M, Chai H, et al. (2005) Shear stress induces endothelial differentiation from a murine embryonic mesenchymal progenitor cell line. *Arterioscler Thromb Vasc Biol* 25: 1817-1823.
127. Zheng Q, Iqbal SM, Wan Y (2013) Cell detachment: post-isolation challenges. *Biotechnol Adv* 31: 1664-1675.
128. Kim L, Toh YC, Voldman J, Yu H (2007) A practical guide to microfluidic perfusion culture of adherent mammalian cells. *Lab Chip* 7: 681-694.
129. Deen WM (1998) *Analysis of Transport Phenomena*: OUP USA.
130. Tilles AW, Baskaran H, Roy P, Yarmush ML, Toner M (2001) Effects of oxygenation and flow on the viability and function of rat hepatocytes cocultured in a microchannel flat-plate bioreactor. *Biotechnology and Bioengineering* 73: 379-389.
131. de Jong J, Lammertink RG, Wessling M (2006) Membranes and microfluidics: a review. *Lab Chip* 6: 1125-1139.
132. Thuenauer R, Rodriguez-Boulan E, Romer W (2014) Microfluidic approaches for epithelial cell layer culture and characterisation. *Analyst* 139: 3206-3218.
133. Zhou Y (2007) *Microfluidics Interfacing to Mass Spectrometry*: University of Maryland, College Park, USA.
134. Horwood RJ (1974) Towards a Better Understanding of Screen Print Thickness Control. 1: 129-136.
135. Ni M, Tong WH, Choudhury D, Rahim NAA, Iliescu C, et al. (2009) Cell Culture on MEMS Platforms: A Review. *International Journal of Molecular Sciences* 10: 5411-5441.
136. Brauker JH, Carbrendel VE, Martinson LA, Crudele J, Johnston WD, et al. (1995) Neovascularization of Synthetic Membranes Directed by Membrane Microarchitecture. *Journal of Biomedical Materials Research* 29: 1517-1524.
137. Kotzar G, Freas M, Abel P, Fleischman A, Roy S, et al. (2002) Evaluation of MEMS materials of construction for implantable medical devices. *Biomaterials* 23: 2737-2750.
138. Borovansky J, Riley PA (1989) Cyto-Toxicity of Zinc In Vitro. *Chemico-Biological Interactions* 69: 279-291.

139. Mishra AK, Ahluwalia JC (1984) Apparent molal volumes of amino acids, N-acetylamino acids, and peptides in aqueous solutions. *The Journal of Physical Chemistry* 88: 86-92.
140. Schmidt RJ, Chung LY, Andrews AM, Turner TD (1993) Toxicity of L-ascorbic acid to L929 fibroblast cultures: relevance to biocompatibility testing of materials for use in wound management. *J Biomed Mater Res* 27: 521-530.
141. Schapper D, Alam MN, Szita N, Eliasson Lantz A, Gernaey KV (2009) Application of microbioreactors in fermentation process development: a review. *Anal Bioanal Chem* 395: 679-695.
142. Petronis S, Stangegaard M, Christensen CB, Dufva M (2006) Transparent polymeric cell culture chip with integrated temperature control and uniform media perfusion. *BioTechniques* 40: 368-376.
143. Cheng JY, Yen MH, Kuo CT, Young TH (2008) A transparent cell-culture microchamber with a variably controlled concentration gradient generator and flow field rectifier. *Biomicrofluidics* 2: 24105.
144. Takeuchi M, Nakajima M, Fukuda T. Semi-closed microchip for probe manipulation and the target cell harvesting; 2009 12-17 May 2009. pp. 1838-1843.
145. Lin JL, Wu MH, Kuo CY, Lee KD, Shen YL (2010) Application of indium tin oxide (ITO)-based microheater chip with uniform thermal distribution for perfusion cell culture outside a cell incubator. *Biomed Microdevices* 12: 389-398.
146. Huang SB, Wang SS, Hsieh CH, Lin YC, Lai CS, et al. (2013) An integrated microfluidic cell culture system for high-throughput perfusion three-dimensional cell culture-based assays: effect of cell culture model on the results of chemosensitivity assays. *Lab Chip* 13: 1133-1143.
147. Schumacher K, Strehl R, de VU, Minuth WW (2002) Advanced technique for long term culture of epithelia in a continuous luminal-basal medium gradient. *Biomaterials* 23: 805-815.
148. Lepe-Zuniga JL, Zigler JS, Jr., Gery I (1987) Toxicity of light-exposed Hepes media. *J Immunol Methods* 103: 145.
149. Hung PJ, Lee PJ, Sabounchi P, Aghdam N, Lin R, et al. (2005) A novel high aspect ratio microfluidic design to provide a stable and uniform microenvironment for cell growth in a high throughput mammalian cell culture array. *Lab Chip* 5: 44-48.
150. Hochfeld WL (2006) *Producing Biomolecular Substances with Fermenters, Bioreactors and Biomolecular Synthesizers*: Taylor & Francis. 389 p.
151. Forry SP, Locascio LE (2011) On-chip CO₂ control for microfluidic cell culture. *Lab Chip* 11: 4041-4046.
152. Takano A, Ogawa T, Tanaka M, Futai N (2011) On-chip incubation system for long-term microfluidic cell culture. *Conf Proc IEEE Eng Med Biol Soc* 2011: 8404-8407.
153. Arechabala B, Coiffard C, Rivalland P, Coiffard LJM, Roeck-Holtzhauer YD (1999) Comparison of cytotoxicity of various surfactants tested on normal human fibroblast cultures using the neutral red test, MTT assay and LDH release. *Journal of Applied Toxicology* 19: 163-165.
154. Yu IF, Yu YH, Chen LY, Fan SK, Chou HY, et al. (2014) A portable microfluidic device for the rapid diagnosis of cancer metastatic potential which is programmable for temperature and CO₂. *Lab Chip* 14: 3621-3628.
155. Goh TK, Zhang ZY, Chen AK, Reuveny S, Choolani M, et al. (2013) Microcarrier culture for efficient expansion and osteogenic differentiation of human fetal mesenchymal stem cells. *Biores Open Access* 2: 84-97.
156. Tamura A, Kobayashi J, Yamato M, Okano T (2012) Temperature-responsive poly(N-isopropylacrylamide)-grafted microcarriers for large-scale non-invasive harvest of anchorage-dependent cells. *Biomaterials* 33: 3803-3812.

157. Bombera R, Leroy L, Livache T, Roupioz Y (2012) DNA-directed capture of primary cells from a complex mixture and controlled orthogonal release monitored by SPR imaging. *Biosens Bioelectron* 33: 10-16.
158. Rupperecht P, Gole L, Rieu JP, Vezy C, Ferrigno R, et al. (2012) A tapered channel microfluidic device for comprehensive cell adhesion analysis, using measurements of detachment kinetics and shear stress-dependent motion. *Biomicrofluidics* 6: 14107-1410712.
159. Zhu H, Yan J, Revzin A (2008) Catch and release cell sorting: electrochemical desorption of T-cells from antibody-modified microelectrodes. *Colloids Surf B Biointerfaces* 64: 260-268.
160. Higuchi A, Hamamura A, Shindo Y, Kitamura H, Yoon BO, et al. (2004) Photon-modulated changes of cell attachments on poly(spiropyran-co-methyl methacrylate) membranes. *Biomacromolecules* 5: 1770-1774.
161. Dou X-Q, Yang X-M, Li P, Zhang Z-G, Schonherr H, et al. (2012) Novel pH responsive hydrogels for controlled cell adhesion and triggered surface detachment. *Soft Matter* 8: 9539-9544.
162. Cole MA, Voelcker NH, Thissen H, Griesser HJ (2009) Stimuli-responsive interfaces and systems for the control of protein-surface and cell-surface interactions. *Biomaterials* 30: 1827-1850.
163. Brun-Graeppi AKAS, Richard C, Bessodes M, Scherman D, Merten O-W (2010) Thermo-responsive surfaces for cell culture and enzyme-free cell detachment. *Progress in Polymer Science* 35: 1311-1324.
164. Brun-Graeppi AK, Richard C, Bessodes M, Scherman D, Merten OW (2011) Cell microcarriers and microcapsules of stimuli-responsive polymers. *J Control Release* 149: 209-224.
165. da Silva RM, Mano JF, Reis RL (2007) Smart thermo-responsive coatings and surfaces for tissue engineering: switching cell-material boundaries. *Trends Biotechnol* 25: 577-583.
166. Holian O, Astumian RD, Lee RC, Reyes HM, Attar BM, et al. (1996) Protein kinase C activity is altered in HL60 cells exposed to 60 Hz AC electric fields. *Bioelectromagnetics* 17(): 504-513.
167. Docoslis A, Kalogerakis N, Behie L (1999) Dielectrophoretic forces can be safely used to retain viable cells in perfusion cultures of animal cells. *Cytotechnology* 30: 133-142.
168. Mone MJ, Volker M, Nikaido O, Mullenders LH, van Zeeland AA, et al. (2001) Local UV-induced DNA damage in cell nuclei results in local transcription inhibition. *EMBO Rep* 2: 1013-1017.
169. von Recum HA, Okano T, Kim SW, Bernstein PS (1999) Maintenance of retinoid metabolism in human retinal pigment epithelium cell culture. *Exp Eye Res* 69: 97-107.
170. Yamato M, Utsumi M, Kushida A, Konno C, Kikuchi A, et al. (2001) Thermo-responsive culture dishes allow the intact harvest of multilayered keratinocyte sheets without disperse by reducing temperature. *Tissue Eng* 7: 473-480.
171. Yang HS, Jeon O, Bhang SH, Lee S-H, Kinm B-S (2010) Suspension Culture of Mammalian Cells Using Thermosensitive Microcarrier That Allows Cell Detachment Without Proteolytic Enzyme Treatment. *Cell Transplantation* 19: 1123-1132.
172. Tamura A, Kobayashi J, Yamato M, Okano T (2012) Thermally responsive microcarriers with optimal poly(N-isopropylacrylamide) grafted density for facilitating cell adhesion/detachment in suspension culture. *Acta Biomater* 8: 3904-3913.
173. Wu C, Wang X (1998) Globule-to-Coil Transition of a Single Homopolymer Chain in Solution. *Physical Review Letters* 80: 4092-4094.
174. Furyk S, Zhang Y, Ortiz-Acosta D, Cremer PS, Bergbreiter DE (2006) Effects of end group polarity and molecular weight on the lower critical solution temperature of poly(N-isopropylacrylamide). *Journal of Polymer Science Part A: Polymer Chemistry* 44: 1492-1501.

175. Pei Y, Chen J, Yang L, Shi L, Tao Q, et al. (2004) The effect of pH on the LCST of poly(N-isopropylacrylamide) and poly(N-isopropylacrylamide-co-acrylic acid). *J Biomater Sci Polym Ed* 15: 585-594.
176. Zhang Y, Furyk S, Sagle LB, Cho Y, Bergbreiter DE, et al. (2007) Effects of Hofmeister Anions on the LCST of PNIPAM as a Function of Molecular Weight. *J Phys Chem C Nanomater Interfaces* 111: 8916-8924.
177. Rollason G, Davies JE, Sefton MV (1993) Preliminary report on cell culture on a thermally reversible copolymer. *Biomaterials* 14: 153-155.
178. Gong C, Gu Y, Xie Z, Xie X, Liu C, et al. (2008) [Synthesis and characterization of thermosensitive hydrogel based on PEG-PCL-PEG block copolymers]. *Sheng Wu Yi Xue Gong Cheng Xue Za Zhi* 25: 1121-1125.
179. Okano T, Yamada N, Okuhara M, Sakai H, Sakurai Y (1995) Mechanism of cell detachment from temperature-modulated, hydrophilic-hydrophobic polymer surfaces. *Biomaterials* 16: 297-303.
180. Halperin A, Kroger M (2012) Theoretical considerations on mechanisms of harvesting cells cultured on thermoresponsive polymer brushes. *Biomaterials* 33: 4975-4987.
181. Canavan HE, Graham DJ, Cheng X, Ratner BD, Castner DG (2006) Comparison of Native Extracellular Matrix with Adsorbed Protein Films Using Secondary Ion Mass Spectrometry†. *Langmuir* 23: 50-56.
182. Mias S, Sudor J, Camon H (2008) PNIPAM: a thermo-activated nano-material for use in optical devices. *Microsystem Technologies* 14: 691-695.
183. Schild HG (1992) Poly(N-isopropylacrylamide): experiment, theory and application. *Progress in Polymer Science* 17: 163-249.
184. Gong C, Qi T, Wei X, Qu Y, Wu Q, et al. (2013) Thermosensitive Polymeric Hydrogels As Drug Delivery Systems. *Curr Med Chem* 20: 79-94.
185. Yang J, Yamato M, Shimizu T, Sekine H, Ohashi K, et al. (2007) Reconstruction of functional tissues with cell sheet engineering. *Biomaterials* 28: 5033-5043.
186. Yamato M, Okuhara M, Karikusa F, Kikuchi A, Sakurai Y, et al. (1999) Signal transduction and cytoskeletal reorganization are required for cell detachment from cell culture surfaces grafted with a temperature-responsive polymer. *J Biomed Mater Res* 44: 44-52.
187. Xue C, Choi B-C, Choi S, Braun PV, Leckband DE (2012) Protein Adsorption Modes Determine Reversible Cell Attachment on Poly(N-isopropyl acrylamide) Brushes. *Advanced Functional Materials* 22: 2394-2401.
188. Mandal K, Balland M, Bureau L (2012) Thermoresponsive micropatterned substrates for single cell studies. *PLoS One* 7: e37548.
189. Kumashiro Y, Yamato M, Okano T (2010) Cell attachment-detachment control on temperature-responsive thin surfaces for novel tissue engineering. *Annals of Biomedical Engineering* 38: 1977-1988.
190. Nash ME, Healy D, Carroll WM, Elvira C, Rochev YA (2012) Cell and cell sheet recovery from pNIPAm coatings; motivation and history to present day approaches. *Journal of Materials Chemistry* 22: 19376-19389.
191. Mandal K, Balland M, Bureau L (2012) Thermoresponsive micropatterned substrates for single cell studies. *PloS one* 7: e37548.
192. Vinjimore Kesavan S, Allier CP, Navarro F, Mittler F, Chalmond B, et al. (2013) Lensless imaging system to quantify cell proliferation. *SPIE* 8587: 11.
193. van Engeland M, Nieland LJ, Ramaekers FC, Schutte B, Reutelingsperger CP (1998) Annexin V-affinity assay: a review on an apoptosis detection system based on phosphatidylserine exposure. *Cytometry* 31: 1-9.
194. Vermes I, Haanen C, Reutelingsperger C (2000) Flow cytometry of apoptotic cell death. *Journal of Immunological Methods* 243: 167-190.

195. Mias S, Sudor J, Camon H (2007) PNIPAM: a thermo-activated nano-material for use in optical devices. *Microsystem Technologies* 14: 747-751.
196. Schild HG (1992) Poly (N-Isopropylacrylamide) - Experiment, Theory and Application. *Progress in Polymer Science* 17: 163-249.
197. Gong C, Qi T, Wei X, Qu Y, Wu Q, et al. (2013) Thermosensitive Polymeric Hydrogels As Drug Delivery Systems. 79-94.
198. Yang J, Yamato M, Shimizu T, Sekine H, Ohashi K, et al. (2007) Reconstruction of functional tissues with cell sheet engineering. *Biomaterials* 28: 5033-5043.
199. Okano T, Yamada N, Okuhara M, Sakai H (1995) Mechanism of cell detachment from hydrophobic polymer surfaces. *Biomaterials* 16: 297-303.
200. Xue C, Choi B-C, Choi S, Braun PV, Leckband DE (2012) Protein Adsorption Modes Determine Reversible Cell Attachment on Poly(N-isopropyl acrylamide) Brushes. *Advanced Functional Materials* 22: 2394-2401.
201. Ernst O, Lieske A, Jager M, Lankenau A, Duschl C (2007) Control of cell detachment in a microfluidic device using a thermo-responsive copolymer on a gold substrate. *Lab Chip* 7: 1322-1329.
202. Nash ME, Healy D, Carroll WM, Elvira C, Rochev Ya (2012) Cell and cell sheet recovery from pNIPAm coatings; motivation and history to present day approaches. *Journal of Materials Chemistry* 22: 19376.
203. Malham IB, Bureau L (2010) Density effects on collapse, compression, and adhesion of thermoresponsive polymer brushes. *Langmuir* 26: 4762-4768.
204. Ishida N, Biggs S (2007) Direct Observation of the Phase Transition for a Poly(N-isopropylacrylamide) Layer Grafted onto a Solid Surface by AFM and QCM-D. *Langmuir* 23: 11083-11088.
205. Tu H, Heitzman CE, Braun PV (2004) Patterned Poly(N-isopropylacrylamide) Brushes on Silica Surfaces by Microcontact Printing Followed by Surface-Initiated Polymerization. *Langmuir* 20: 8313-8320.
206. Halperin A, Kröger M (2012) Theoretical considerations on mechanisms of harvesting cells cultured on thermoresponsive polymer brushes. *Biomaterials* 33: 4975-4987.
207. Kumashiro Y, Yamato M, Okano T (2010) Cell attachment-detachment control on temperature-responsive thin surfaces for novel tissue engineering. *Annals of Biomedical Engineering* 38: 1977-1988.
208. Canavan HE, Graham DJ, Cheng X, Ratner BD, Castner DG (2007) Comparison of native extracellular matrix with adsorbed protein films using secondary ion mass spectrometry. *Langmuir* 23: 50-56.
209. CellSeed UpCell: Temperature-responsive cell cultureware for "Cell-sheet" engineering.
210. Svajger U, Jeras M (2011) Optimal Dendritic Cell Differentiation in RPMI Media Requires the Absence of HEPES Buffer. *Immunological Investigations* 40: 413-426.
211. Lindskog U, Lundgren B, Billig D, Lindner E (1987) Alternatives for harvesting cells grown on microcarriers: effects on subsequent attachment and growth. *Dev Biol Stand* 66: 307-320.
212. Wang Y, Ouyang F (1999) Bead-to-bead transfer of Vero cells in microcarrier culture. *Bioprocess Engineering* 21: 211-213.
213. Ng SF, Rouse JJ, Sanderson FD, Eccleston GM (2012) The relevance of polymeric synthetic membranes in topical formulation assessment and drug diffusion study. *Arch Pharm Res* 35: 579-593.
214. Epstein N (1989) On tortuosity and the tortuosity factor in flow and diffusion through porous media. *Chemical Engineering Science* 44: 777-779
215. Beck RE, Schultz JS (1970) Hindered diffusion in microporous membranes with known pore geometry. *Science* 170: 1302-1305
216. Chantong A, Massoth FE (1983) Restrictive diffusion in aluminas. *AIChE J* 29: 725-731.

217. Renkin EM (1954) Filtration, diffusion and molecular sieving through porous cellulose membranes. *Gen Physiol J* 38: 225-243.
218. Satterfield CN, Colton CK (1973) Restricted diffusion in liquids within fine pores. *AIChE J* 19: 628
219. Inamdar NK, Griffith LG, Borenstein JT (2013) Chapter 6 - Transport Models for Three-Dimensional Cell Culture Systems. In: Bettinger C, Borenstein JT, Tao SL, editors. *Microfluidic Cell Culture Systems*. Oxford: William Andrew Publishing. pp. 137-172.
220. Vann JM, Goldman AJ, Szurek PF, Brooks BR (1995) Deoxyglucose uptake by mouse astrocytes: effects of temperature and retrovirus infection. *Neurochem Res* 20: 1013-1020.
221. Vaz CV, Alves MG, Marques R, Moreira PI, Oliveira PF, et al. (2012) Androgen-responsive and nonresponsive prostate cancer cells present a distinct glycolytic metabolism profile. *Int J Biochem Cell Biol* 44: 2077-2084.
222. Williams S-P, Flores-Mercado J, Port R, Bengtsson T (2012) Quantitation of glucose uptake in tumors by dynamic FDG-PET has less glucose bias and lower variability when adjusted for partial saturation of glucose transport. *EJNMMI Research* 2: 6.
223. Al-Shemmeri T (2012) *Engineering Fluid Mechanics*: Ventus Publishing ApS.

Abstract

Over the past six decades, cell culture has become a common practice. It is a major tool in biological research for the understanding of life science, such as the study of disease and the discovery of new drugs. It plays an important role in many industries since it is involved in the production of many food, cosmetic, and pharmaceutical products.

However, Research and the industry are now facing some limits and are expressing needs to be addressed. They are both associated with high costs due to a large consumption of resources (cells, reagents, qualified operators). More specifically, cell culture in research is characterized by low throughput of experiments, important variability and risk of contamination due to the recurrent manual operations performed by operators. Additionally, experiments are performed in static conditions and on models (2D cultures, animals...) which poorly resemble the human physiology. Industrial cell culture needs miniaturized systems that mimic the large-scale bioreactors and offer higher screening possibilities.

Microfluidic cell culture systems represent a promising tool to address the aforementioned issues and needs. The change of physical behaviors at the small-scale in microfluidic devices allow controlling temporally and spatially the cell microenvironment, unattainable with conventional cell culture methods. The level of automation and integration allows the substantial increase of the number of experience per system and considerable reduction of resource consumption. Thus, many small cellular 3D architectures grown under dynamic conditions and in high-throughput have been performed and have demonstrated their ability to quickly re-create more physiological environments. Regarding the industrial culture, miniaturized cultures have already shown their ability to reproduce the characteristics of the culture observed in macrobioreactors with higher screening capabilities.

In this framework, a benchtop microfluidic bioreactor, complying with the standard microfluidic platform and format used in the host laboratory, has been successfully fabricated to perform continuous cell cultures. Integrated solutions were developed to provide continuously the adequate conditions for cell proliferation (perfusion, thermal regulation...). Integrated cell harvest was also performed with the final goal to achieve long-term cell culture in the bioreactor.

The fabricated system proved to guarantee sterile conditions for cell cultures on a regular lab bench. Moreover, these cultures were achieved autonomously without requiring a cumbersome incubator. In these conditions, the bioreactor demonstrated the possibility to perform continuous cell cultures of various cell types during several days: insects cells were cultured during 5 days and mammalian cells during 3 days. Regarding the mammalian cell cultures performed, a breakthrough has been achieved compared to the cultures performed in microfluidic systems since microcarriers (diam.: 175 μm) were used as growth support.

Although microcarrier cell culture is routinely performed in the industry, no autonomous microfluidic culture system has addressed this type of culture yet. Such a miniaturization is a major step forward for bioprocess applications where the need to develop scaled-down bioreactors that mimic large-scale operation has been clearly identified to shorten and reduce the costs associated to bioproduct development.

Résumé

Au cours des six dernières décennies, la culture cellulaire est devenue une pratique courante. Elle est un outil majeur de la recherche biologique pour la compréhension du vivant, l'étude de maladies et la découverte de nouveaux médicaments. Elle représente un outil très répandu dans de nombreuses industries étant impliquées dans la production de produits alimentaires, cosmétiques et pharmaceutiques.

Cependant, les cultures cellulaires en recherche et en industrie sont aujourd'hui confrontées à des limites et soulèvent des besoins à satisfaire. Elles sont toutes deux associées à des coûts élevés du fait des ressources nécessaires (cellules, réactifs, opérateurs qualifiés). Plus précisément, la culture en recherche est caractérisée par le faible débit des expériences, une variabilité importante et un risque de contamination due à la répétition d'opérations manuelles. De plus, les expériences de culture sont effectuées dans des conditions statiques et sur des modèles (cultures 2D, animaux...) relativement éloignés de la physiologie humaine. La culture cellulaire industrielle, quant à elle, a besoin de systèmes miniaturisés qui miment les procédés des bioréacteurs à grande échelle et qui offrent des possibilités de criblage plus élevées.

Les systèmes de culture microfluidique représentent un outil prometteur pour résoudre ces problèmes et ces besoins. Le changement de comportement de la physique à petite échelle dans ces dispositifs permet de contrôler temporellement et spatialement le microenvironnement des cellules. Ce qui n'est pas possible avec des méthodes de culture classiques. Le degré d'automatisation et d'intégration permet une nette augmentation du nombre d'expériences par système et la réduction conséquente de la consommation de ressources. Ainsi, de nombreuses petites architectures 3D cellulaires cultivées dans des conditions dynamiques et à haut débit ont été réalisées et ont démontré leur capacité à recréer rapidement des environnements plus physiologiques. En ce qui concerne la culture industrielle, des cultures miniaturisées ont déjà montré leur capacité à reproduire les caractéristiques observées dans les macrobioreacteurs avec des possibilités de criblages élevées.

Dans ce contexte, un bioréacteur microfluidique de paillasse, se conformant aux formats standards utilisés dans le laboratoire d'accueil, a été fabriqué avec succès au cours de cette thèse pour effectuer des cultures cellulaires en continu. Des solutions intégrées ont été mises au point pour fournir de façon continue les conditions adéquates pour la prolifération cellulaire (perfusion, régulation de température...). Des études ont également été menées afin d'automatiser la récolte des cellules avec pour but final de cultiver ces cellules sur du long terme dans le bioréacteur.

Le système fabriqué garantit ainsi des conditions stériles pour les cultures sur un simple banc de laboratoire. En outre, ces cultures ont été réalisées de façon autonome sans utiliser un incubateur encombrant. Dans ces conditions, le bioréacteur permet de réaliser des cultures en continu de divers types cellulaires sur plusieurs jours: des cellules d'insectes ont été cultivées pendant 5 jours et des cellules de mammifère pendant 3 jours. En ce qui concerne les cultures de cellules de mammifère, une avancée majeure a été effectuée par rapport aux cultures réalisées dans les systèmes microfluidiques en utilisant comme support de culture des microporteurs (diam. : 175 μm).

Bien que la culture de cellules sur microporteurs soit réalisée en routine dans l'industrie, aucun système de culture microfluidique autonome n'a encore intégré ce type de culture. Ce genre de miniaturisation est une avancée majeure pour des applications en bioprocédés où il devrait permettre de raccourcir et réduire les coûts associés au développement de bioproduits.